

SPES

Satellite for Perlustration of Europa Surface

Ardiana Bushi, Giulia Brunelli, Luca Guglielmi, Riccardo Magnani, Yu Ou, Jiacheng Peng,
Alfonso Pisapia, Luca Pizzuto, Koushika Sri Lakshmi Srikanth, Alice Vendrame

A.Y. 2022-2023



SPACECRAFT SUBSYSTEMS AND SPACE MISSION DESIGN
Professor Prem Prasad Sundaramoorthy

Contents

List of Figures

List of Tables

1	Background and Motivation	1
2	Mission Objectives	2
2.1	Milestones	3
3	Work Breakdown Structure	4
4	Payload	5
4.1	Scientific Overview	5
4.2	Requirements	8
4.3	High Resolution Camera	10
4.4	Spectrometer	12
4.5	X-band Antenna	14
4.6	Mass and Power budget	16
5	Attitude Determination and Control Subsystem	17
5.1	Requirements	17
5.2	Estimation of the Disturbances	18
5.2.1	De-Tumbling	21
5.2.2	Angular Momentum Evaluation	21
5.3	Selection of the Reaction Wheel	22
5.3.1	Thrusters for Attitude De-Saturation	24
5.4	Selection of the Sensors	24
5.4.1	Sun Sensors	25
5.4.2	IMU	26
5.5	Mass and Power budget	27
6	Orbital Design	28
6.1	From Earth's surface to parking orbit	28
6.2	Interplanetary Journey	28
6.2.1	Hohmann Transfer Approach	29
6.2.2	Flyby Approach	31
6.3	Jupiter Orbit Reduction (JOR)	33
6.4	Multiple Flyby Concept	35
6.5	End Of Life (EOL)	37
6.6	Total Δv budget	38
6.7	Future Improvements	39
7	Communication	41
7.1	Requirements	41
7.2	Antennas	41
7.2.1	Radial Line Slot Antenna	41
7.2.2	Radial Line Slot Antenna with honeycomb structure	41
7.3	Parameters of HGAs	42

7.4	Links and Power budget	44
7.5	Earth Direction Variation and Off-Beam Loss	45
8	Thermal Control	46
8.1	Heat Sources	47
8.2	Requirements	48
8.3	Thermal Analysis	48
8.3.1	Results	50
8.3.2	Thermal Control of the Spectrometer	51
8.4	Temperature Sensor	52
8.5	Mass and Power Budget	52
9	Command and Data-Handling Systems	53
9.1	Requirements	54
9.2	On-Board Computer Selection	54
9.3	Software and Data Handling	57
9.3.1	Operation Modes	57
9.3.2	Software Architecture and Global Functions	58
9.3.3	Housekeeping Data Estimation	59
9.4	Failure Mitigation and Electronic Protection	59
9.4.1	Hardware Design for protection	60
9.4.2	Software Design for protection	61
9.5	Mass and Power Budget	61
9.6	Future Improvements	61
10	Electrical Power System (EPS)	62
10.1	Requirements	62
10.2	Power Budget	62
10.3	Power Generation	63
10.3.1	Solar Arrays	64
10.3.2	Fuel Cells	65
10.3.3	Radioisotope Thermoelectric Generators	65
10.3.4	Tradeoff and Choice of the RTG	67
10.3.5	e-MMRTG Power Degradation and Operational Modes	68
10.4	Power Distribution	69
10.5	Mass and Power Budget	69
11	Structures	70
11.1	Mission Requirements	70
11.2	Volume and Mass Budget	70
11.3	Spacecraft Design and Strength Properties	71
11.4	Materials Trade-off	72
11.5	Radiation Shielding	74
11.6	Selection of a S/C	75
12	Propulsion	78
12.1	Requirements	78
12.1.1	Launcher	78
12.1.2	Spacecraft	78

12.2 Launcher	79
12.3 Spacecraft	80
12.3.1 Tsiolkovsky Equation	81
12.3.2 Propulsion System Selection	81
12.3.3 Propellant Tank Selection	83
12.4 Results	84
13 Conclusions	85
13.1 Final Mass and Power budget	85
13.2 Compliance Check	85
13.3 Future Improvements	86
13.4 Considerations on the Design Process	88
14 References	89

List of Figures

1	Comparison between the liquid water content on Earth and the expected liquid water content beneath the surface of Europa [1].	1
2	Newly reprocessed image of Europa surface from the Galileo mission. Credit:NASA/JPL-Caltech/SETI insitute.	5
3	Simulated one-minute observation from the Ultraviolet spectrometer on Europa Clipper [2], with the excellent Signal-to-Noise ratio.	6
4	Simulated occultation observation from the Ultraviolet spectrometer on Europa Clipper [2].	6
5	A potential model of life underneath the Europa's surface [3].	7
6	Two smallsats cameras from Dragonfly Aerospace.	11
7	Three observation modes for the spectrometer. The sketch is from SPI-CAM and shows the different orientations and altitudes.	12
8	Schematic representation of the Doppler observable.	14
9	Decision flow for the choice of the antenna band.	15
10	X-Band Antenna from EnduroSat.	16
11	Total torque as a function of the displacement between C_p and C_m	20
12	Torques as a function of the distance to the surface of Europa.	20
13	RWP050 reaction wheel designed by Blue Canyons Technologies ([4]).	23
14	1N HPGP THRUSTER from Bradford ECAPS ([5]).	24
15	NFSS-411 by NewSpace Systems (NSS, [6]).	26
16	GS-IMU3000TA by Grand Stal Solutions Ltd ([7]).	27
17	Hohmann transfer to pass from Earth's orbit (1AU), to Jupiter's orbit (5.2AU).	29
18	Sketch showing the different interplanetary phases, from DSM, to Earth's flyby and Jupiter Orbit insertion.	31
19	Diagram illustrating the Jupiter Orbit Reduction phase: after JOI, two break maneuvers (in red) are needed to pass (using Hohmann transfer) from the bigger orbit (JOI orbit, in green) to the smaller orbit (Europa orbit, in blue).	34
20	Diagram showing the scientific orbit chosen to study Europa. Europa's orbit is shown in azure. The orange part is the Flyby phase, lasting 4 days. Closest approach is when the majority of data is gathered (Nadir, in red). The blue part is the Playback phase, lasting 10 days, when data will be sent back to Earth.	36
21	Diagram representing the EOL maneuver, performed via Hohmann transfer from an initial Europa orbit (in blue) to a final orbit that ends inside Jupiter's atmosphere (azure layer around Jupiter), were the atmospheric drag will eventually make SPES crash on the planet.	37
22	Antenna with honeycomb structure.	42
23	RF telecommunications capability (DDOR: Delta Differential One-way Range).	43
24	RF telecommunications characteristics.	43
25	Antenna gain and aperture efficiency of HGAs. Values for antenna gain were measured relative to coaxial cable input.	43
26	DSN stations compatible for Ka-band downlink.	44
27	Change rate of Earth's rotation.	45
28	Design process of the thermal control subsystem (based on [8]).	46

29	Sketch of heat sources.	47
30	Graphic representation of heating sources while flying around Europa. . .	50
31	MiSER by Sierra Nevada Corporation.	51
32	Series 44 Cryogenic Temperature Probe by Scientific Instruments. . . .	52
33	The final architecture of CDHs. On-board Computer connected with all subsystems architecture	53
34	The block diagram of GR740.	56
35	GR-VPX-GR740 design and architecture including Mezzanine board. . .	57
36	Power output as a function of the mission duration for different sources; taken from [9].	63
37	Structure of the e-MMRTG.	67
38	Power generated by the RTG as a function of the operational years. . . .	68
39	P60 PDU-200 from GOMspace.	69
40	S/C interior map.	73
41	S/C propellant and payload map.	74
42	Design of S/C as a hollow cylinder.	75
43	Images of the three engines taken into consideration for the trade-off. .	82
44	Hydrazine tank Model OST 31-1.	83
45	Specifics of the hydrazine tank Model OST 31-1.	84

List of Tables

1	Scientific requirements.	8
2	Subsystem's requirements.	9
3	Comparison between the two cameras. TRL is 8 for both of them.	11
4	Brief description and requirements for observation modes.	13
5	Main parameters for the spectrometer for SPES.	14
6	Main parameters of our antenna.	16
7	Mass and power budget of each payload instrument.	16
8	Requirements for the ADCS.	17
9	Absolute rating values for the main parameters.	22
10	Reaction wheels for attitude control. The first three are designed by NewSpace Systems ([10]), the last three are designed by Blue Canyons Technologies ([4]).	22
11	Total score for each wheel is weighted by the parameters of Table 9. The normalized one is given by the total score divided by the maximum score a wheel can obtain (270 for first 3, 210 for last 3).	23
12	Absolute rating values for the main parameters of a sun sensor.	25
13	Sun sensors for attitude control. The first is designed by RedWire ([11]), the second by CubeSpace ([12]), the fine sun sensor by Bradford Engineering ([13]) and the last two by NewSpace Systems ([6]).	25
14	Total score for each sun sensor is weighted by the parameters of Table 12. The normalized one is given by the total score divided by the maximum score a wheel can obtain (230 for the first 4, 180 for the last 2).	26
15	Mass and power budget of each instrument used for attitude.	27
16	Results showing the total $\Delta v_{\text{launcher},1}$ that should be provided by the launcher, to reach parking orbit and escape Earth's gravity.	30
17	Results showing the total $\Delta v_{\text{Hohmann}}$, computed using Eq. 15 that are meant to be provided by our spacecraft to pass from a 1AU orbit around the Sun (Earth's orbit) to a 5.2AU orbit around the Sun (Jupiter's orbit).	30
18	Results showing the total $\Delta v_{\text{launcher},2}$ that should be provided by the launcher, to reach parking orbit with altitude $h_{\text{park}} = 350$ km and afterwards to transfer to a coasting orbit with altitude $h_{\text{coast}} = 6564$ km, using Hohmann transfer.	32
19	Results showing the total Δv_{inter} needed for the interplanetary orbital phase. Gray rows indicate values that do not contribute to the final Δv budget. The value in the first row was computer using Eq. 20. All other values were taken from Juno [14] and Europa Clipper [15] papers.	33
20	Results showing the total $\Delta v_{\text{reduction}}$ that should be provided by the spacecraft, to reduce the orbit around Jupiter from $R_{\text{JOI}} = 912921$ km to $R_{\text{Eu}} = 671476$ km, using Hohmann transfer.	34
21	Characteristic of the elliptical flyby orbit chosen for the scientific phase of the mission.	36
22	Distances between Earth and spacecraft, in the case of closest (3.929AU) and furthest approach (6.473AU) between Earth and Jupiter.	37
23	Results showing the total Δv_{EOL} that should be provided by the spacecraft, to perform its disposal, crashing inside Jupiter's atmosphere.	38

24	Summary of the orbital maneuvers planned for SPES mission: for every maneuver we indicated the date in which they are planned to be performed. Gray rows are values that do not contribute to the total Δv budget, while green cells show total Δv required for a given orbital phase.	39
25	Total Δv budget for our spacecraft, with or without considering the End Of Life maneuver.	39
26	Additional maneuvers that we neglected. Both of them are referred to the Jupiter orbital reduction phase, treated in Section 6.3.	40
27	Temperature ranges for every instrument of each subsystem.	48
28	Equilibrium temperatures for the selected coatings; in red are shown the ones that exceed the limit for T_{max} , in blue the ones that exceed the limit for T_{min}	50
29	Main properties of MiSER radiator, from the data sheet [16].	51
30	Main properties of the sensor from the data sheet [17].	52
31	Mass and power budget of each instrument used for thermal control. *Heat pipes are not completely defined in terms of unit number.	52
32	CDHs requirements for hardware and software.	54
33	CDHs requirements from other subsystems.	54
34	A simple trade-off between microprocessor and micro-controller.	55
35	The OBC examples for several space missions.	55
36	Based on the power values provided in Table 45, two sub-modes are included in the nominal mode.	58
37	Working subsystems are marked with orange colors. OPS means opening with a strategy.	58
38	Summary of Radiation Protection values for GR740.	61
39	Mass and overall Power budget for CDHs subsystem.	61
40	Requirements of EPS.	62
41	Power requirements of the different instruments.	62
42	Power requirements of the different operational modes; we have taken into account the open with strategy subsystems. *The navigation subsystem is not treated in this report, but it should be taken into account for this mode.	63
43	Trade-off table of the different RTG models.	67
44	Values of the power generated by the RTG for some years after the launch.	68
45	The overall power consumption with different scientific instruments in operation.	68
46	Main characteristics of P60 PDU-200, from the datasheet [18].	69
47	Mass and power budget of each instrument for EPS.	69
48	List of requirements for structures subsystem.	70
49	Mass, size and volume for each subsystem.	70
50	Frequencies and stiffnesses for the launcher.	72
51	Trade-off between the different selected materials for the S/C.	72
52	Deviation from the centre of mass (COM) along the three axis x, y, z. . .	73
53	Comparison between different materials of the outer layer.	75
54	Comparison between different materials of the reflectors.	75
55	Dimensions of the hollow cylinder we used to model our spacecraft. . . .	76
56	Trade-off between different materials.	76
57	List of the structure requirements that have been satisfied.	77
58	List of the requirements for the launcher.	78

59	List of the requirements for the spacecraft.	79
60	Comparison between NASA's Space Launch System (SLS) and SpaceX's Falcon Heavy. Values are taken from the user's manuals of both of them [19], [20]. Pay attention: the success rate of SLS is given as 100%, but only one successful launch was performed.	80
61	Types of propellant and associated engine, with the specifics for each case.	82
62	Trade-off between different engines.	83
63	List of the requirements that will be satisfied.	84
64	Total mass budget for all subsystems, with the relative uncertainties. Propellant is not considered in the total.	85
65	Total power budget for all subsystems, with the relative uncertainties. . .	85

1 Background and Motivation

Water is one of the most abundant molecules in living cells and it is the most critical to life as we know it. The reason why we search for water on other planets is that it is one of the most essential resources for life's existence on Earth and it would play an important role in supporting the survival of humans on any other planet. Moreover, since we are at a critical point of water shortage, there have been many studies and actual missions over the years searching for water on other worlds beyond Earth.

We were able to identify some places in our solar system that could be promising as habitable environments. The missions related to the search for water beyond Earth known until now are directed to planet Mars and three of the moons of planet Jupiter. Between these astronomical objects, Jupiter's moon Europa is one of the most promising, since studies have shown strong evidence of an ocean of liquid water beneath its icy crust. It seems to be globally extended and includes more water than all of Earth's oceans combined.

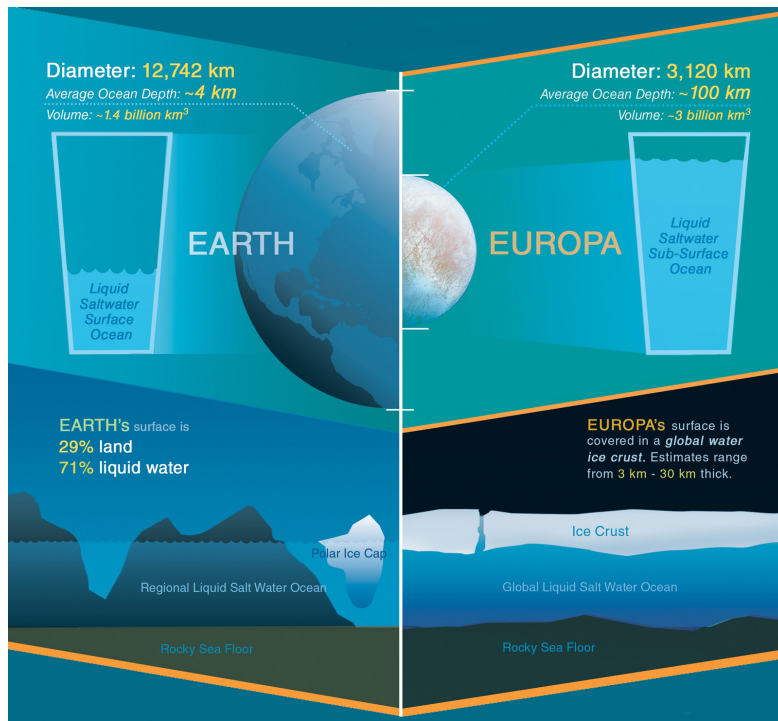


Figure 1: Comparison between the liquid water content on Earth and the expected liquid water content beneath the surface of Europa [1].

We are also looking for water on exoplanets, but the large distance does not allow any on-site research. A space mission to Europa will consist in a close study of the structure of the moon, its atmosphere composition and land morphology: one of the firsts of its kind.

2 Mission Objectives

The SPES (Satellite for Perlustration of Europa Surface) mission, consisting of a single spacecraft designed to withstand the temperature rise due to the Van Allen Belt and Jupiter's strong magnetic field, will be able to prove the existence of liquid water under Europa's surface with accurate coverage of the chosen points to detect plumes. While studying them, it will be also possible to build a complete map of the moon's geological and surface structure. Lastly, this is also the first mission designed to look for biological life forms in Europa by studying possible organic gas leaks, such as methane.

We came up with the following list of objectives, connecting the fields of astrobiology, geology, and hydrogeology through different detectors.

- **Plumes and study of the Ocean:** thanks to NASA's Galileo spacecraft in the past years and to the observations carried out by the Hubble Space Telescope ([21], [22]), it was possible to observe Europa very closely and to find the presence of powerful jets: these break through the moon's icy surface, reaching considerable heights. These jets are called plumes and they are an extremely powerful tool to exploit in order to study the moon and gather more information about the subsurface ocean that is thought to hide beneath the icy crust [23]. Since a mission to the surface of Europa has not been planned yet, a more complete and specific study of these plumes is the best way we have to better constrain the nature and properties of Europa's hidden ocean;
- **Search of biological forms and study of gas leaks:** we know there are some basic requirements to be fulfilled when looking for life in the universe, like a source of energy, complex chemistry, and a benign environment. We want to conduct this study on Europa because it satisfies all these conditions [24]; it has an external source of energy, the tidal flexing from Jupiter, which heats its interior and stops the ocean from freezing solid. Complex chemistry is present in the form of hydrogen peroxide, abundant on the surface, and especially as liquid water beneath the surface. In terms of a benign environment, while it is true that Europa's surface is blasted by radiation from Jupiter reducing the likelihood of developing life on the ground, we have to consider that the same radiation may create fuel for life in an ocean below the surface.

In the past, multiple missions focused on looking for water to determine the habitability of a planetary system, since water is the strongest element that can lead us to find signs of life in extraterrestrial environments. However, it is not the only one: indeed, the presence of living organisms, even in the simplest forms, can produce unmistakable signatures such as the emission of organic gasses (e.g., methane).

In this sense, our mission to Europa seeks to improve life search by looking for hints of this kind of organic emission [25], exploiting technologies that have been already developed and extensively tested to control anomalous gas leaks on Earth and even on Mars. In this way, we hope to obtain a more complete view of the potential causes of these emissions and possibly constrain a biological origin;

- **Geological structure and land morphology:** like our planet, Europa is thought to have an iron core, a rocky mantle, and an H₂O layer. There are two components of the latter, including a globally covered ice surface and a layer of liquid water or warm ice beneath it, which is currently still controversial at present. While data from various instruments on the Galileo spacecraft [26] indicate that a Europa ocean might exist, no conclusive proof has yet been found. More observations and detection are required to understand the physical state of the water layer beneath the surface of Europa. Observations in the past also showed that processes of refreezing, pressurization and fracture of ice are common on the surface, but still not well understood; usually, traces of these events can be seen through the presence of ridges on the surface. This can be exploited in our mission.

In particular, Europa is the smoothest object in the solar system known so far, lacking craters and large mountains due to the active and young ice crust on the surface. The special features are the linear, dark streaks crisscrossing the whole surface: these streaks are presumed to be produced by a few eruptions of warm ice, which will be tested with more detailed imaging from our mission.

Recent studies have also discovered the presence of ridges on Jupiter's moon surface, similar to the ones in mid-ocean. Europa appears covered in tectonic plates: a younger surface seems to have resurfaced actively, showing proof of subduction activity, as we observe on Earth [27]. Our mission can study the geological structure of the moon and discover the geological history behind it.

2.1 Milestones

1. **Time:** the time to finalize the whole mission will take almost 12 years, considering the planning of the project, the building of the spacecraft, and finally the launch. The journey will take approximately 5.5 years to arrive at our destination, considering the Earth flyby that we will need to reach Europa's orbit. The duration of the mission itself will be 2 years: indeed, we need a time range long enough to obtain constant monitoring of the surface activities and features (like gas leaks or plumes), but at the same time we will be limited by the strong radiation field that is present around Jupiter [28], that will make our mission inefficient in a short period of time;
2. **Cost:** the budget for this mission will be around 3 billion euros, which mostly depends on the scientific payload and duration of the mission that can be changed while building it;
3. **Expected results and goals:** the main goal of the mission will be to find signs of habitability of Europa, comprehending the search for water and organic signatures, like methane leaks from the surface. Moreover, it will also try to map in a more detailed way the structures and morphology of the icy crust of the moon. Our expectation is to obtain data more complete than ever about possible signs of life outside of our planet and to open up the possibilities for future missions, with rovers that can go deeper in these studies, as has been done on Mars.

3 Work Breakdown Structure

One of the key elements of project development is the Work Breakdown Structure (WBS), which consists in the division of the work that must be done for the realization of a certain project into logically-connected steps. Each person in the team will be in charge of doing one or more of the steps so that the responsibilities will be distributed within the group.

For the design of SPES, the team sub-division between the different space-segment sub-systems is the following:

- **Payload:** Luca Pizzuto, Jiacheng Peng, Yu Ou
- **ADCs:** Riccardo Magnani, Luca Pizzuto
- **Orbital Design:** Ardiana Bushi, Luca Guglielmi, Koushika Sri Lakshmi Srikanth
- **Communication:** Yu Ou
- **Thermal Control:** Giulia Brunelli, Riccardo Magnani
- **CDHs:** Ardiana Bushi, Jiacheng Peng
- **EPS:** Giulia Brunelli, Koushika Sri Lakshmi Srikanth
- **Structures:** Alfonso Pisapia, Alice Vendrame
- **Propulsion:** Luca Guglielmi, Alfonso Pisapia, Alice Vendrame

For this project, the ground segment and the Navigation subsystem will not be treated, but they can be developed in the future.

4 Payload

The payload is the combination of hardware and software on the spacecraft that will interact with the subject of the mission. This subsystem then is responsible for the selection of the instruments that will let us achieve our mission objectives. It consists of three instruments: a high-resolution imager, a spectrometer and an X-band antenna. In this chapter, we will present the final payload design as well as all the steps that have led to it, with a focus on the requirements to and from the other subsystems.

4.1 Scientific Overview

In order to understand the scientific requirements that the payload has to satisfy we investigated more deeply the features that we want to study.

One of the main goals of the mission is to get high-quality images of the surface of Europa and characterize the water vapour plumes that come out of it.



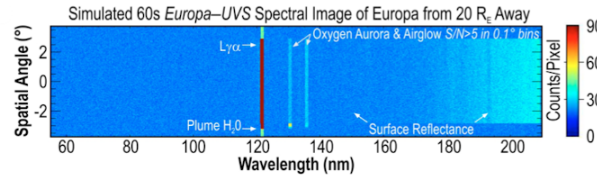
Figure 2: Newly reprocessed image of Europa surface from the Galileo mission.
Credit:NASA/JPL-Caltech/SETI insitute.

Europa's most striking surface features are a series of dark streaks crisscrossing the entire globe, called bands (visible in **Figure 2**). Close examination shows that the edges of Europa's crust on either side of the cracks have moved relative to each other. The larger bands are more than 20 km across, often with dark, diffuse outer edges, regular striations, and a central band of lighter material[29]. The images from the Galileo spacecraft have dramatically increased the amount of detail revealed in the bands, and this has led researchers to explore how the bands formed and how they have resurfaced Europa.

Plumes, instead, could be difficult to observe; they may be sporadic, small and thin. Europa's gravity, which is much stronger than on Enceladus, likely would keep these water plumes at altitudes below a few 100s km[30]. Scientists are very interested in these phenomena, not only because they are another confirmation of the presence of water beneath the surface, but also because the molecules that make them will get excited by solar flux and emit in the IR following vibrational de-excitation.

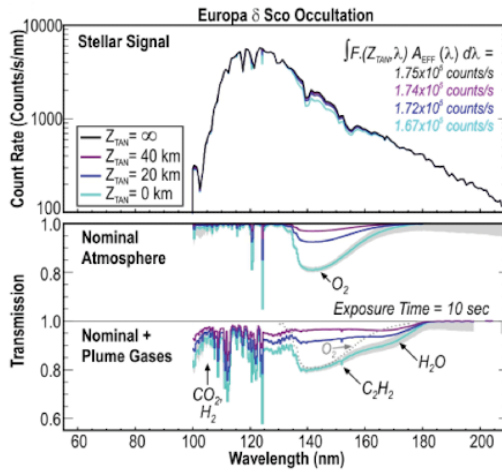
Our goals as Payload team are to obtain images of these features with a resolution never reached before and understand their composition, in order to stimulate breakthroughs in these research fields.

It is also important to study the surface features indicated by the atmosphere's spectral properties. The tenuous and thin [31] atmosphere on Europa includes several components which represent the surface composition, since the planet is embedded in the Jovian magnetospheric plasma bombarded by intense radiation that erodes the surface, launching molecules into a thin atmosphere which is expected to be linked with the surface compositions, such as H_2O , O_2 , H_2 . In terms of the physical mechanisms of the ejection from the surface, the primary one is electronic sputtering. The subsequent dissociation process can also create neutral O , H and OH . In addition, volatiles exist in Europa's atmosphere because of thermal desorption. SO_2 has been detected once by cyclotron waves [32]. CO_2 has not been detected yet but is expected as a contribution of the atmosphere [31]. Therefore, the observables are basically in the UV band including expected emission lines such as $OI1356/1304$ and $Lyman - \alpha$, as shown in **Figure 3**. Several absorption features can also be observed during stellar occultations due to the significant absorption cross sections in UV [2], as shown in **Figure 4**.



Excellent signal-to-noise ratios in Europa-UVS observations are expected despite the high radiation background.

Figure 3: Simulated one-minute observation from the Ultraviolet spectrometer on Europa Clipper [2], with the excellent Signal-to-Noise ratio.



Molecular and atomic species expected at Europa have significant absorption cross sections in the UV. Stellar occultations observed by Europa-UVS will provide a powerful means of detecting them.

Figure 4: Simulated occultation observation from the Ultraviolet spectrometer on Europa Clipper [2].

The organic components on Europa lack of study so far. They are usually related to the analysis of habitability as well as the fingerprints of life, hence it is worthwhile to detect the presence of organic molecules such as CH_4 , C_2H_2 and compounds such as hydrated salt both on the surface and the atmosphere. The main expected absorption features of organic components are in the infrared band. In **Figure 5** it is a potential of emergence of life on Europa an alkaline hydrothermal mound [3]. The organic signals are believed to be highly relevant to the bio-activities.

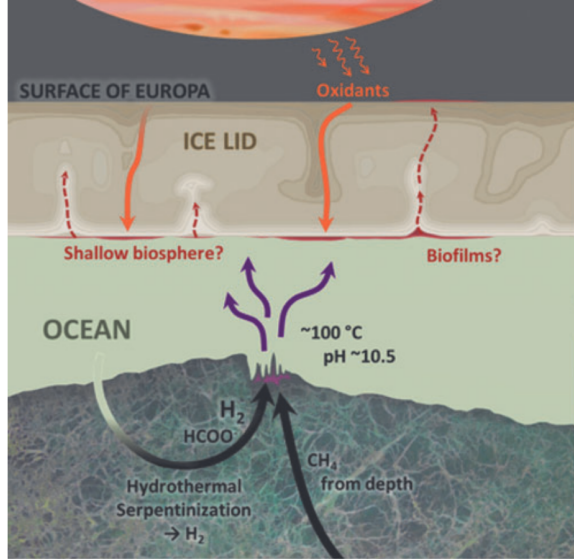


Figure 5: A potential model of life underneath the Europa's surface [3].

Last, but not least, SPES aims at studying the liquid water ocean that Europa hosts beneath the surface. The reason Europa has liquid water is because tides cause Europa's ice shell and interior to flex during the course of its orbit around Jupiter[33]. The heating is not enough to permit water to exist in liquid form on the frigid surface, but it should be sufficient to maintain a liquid water ocean beneath an outer ice shell. A huge confirmation of this theory is the existence of Europa's induced magnetic field, which can be produced only with the presence of some electrically conductive fluid in its interior, most likely a salty water ocean.

Our goal is to further investigate the features of the ocean, by estimating the *Tidal Love Number*, which represents how susceptible Europa is to tidal forces, which depends on its internal structure; Europa's flexing is determined by how much water the moon contains, how close water is to the surface, and other factors, like the thickness of the ice mantle. This mission will provide important results for scientists interested in this field.

4.2 Requirements

On the knowledge of the previous scientific overview, we identified the following scientific requirements:

Table 1: Scientific requirements.

ID	Requirement	Rationale	Instrument
PL.01	Being able to reach resolution of at least 5 m at 500 km	Capturing details of surface features	Camera
PL.02	Having at least 100 pictures each flyby	Sporadicity of plumes	Camera
PL.03	Having a SWATH of at least 20 km at 500 km	Getting the full width of a surface band	Camera
PL.04	Imaging over a wide spectral range (Visible and I.R)	Accounting for eclipse and excitation of water vapor molecules	Camera
PL.05	Establishing a 2 way-link with the ground	Study of gravity	Antenna
PL.06	Choosing the correct number of the antenna, and communication window	Avoiding interference with the communication antenna	Antenna
PL.07	Containing a wide wavelength range in infrared band which including both near-infrared and mid-infrared ($0.75 - 8 \mu\text{m}$)	Observation for potential organic signals	Spectrometer
PL.08	Containing UV band	Observation for atmospheric components	Spectrometer
PL.09	One instruments with the combination for both bands with a total mass less than 20kg	Limited Space and overall mass budget on the S/C	Spectrometer
PL.10	Minimizing cost, mass and power	Reducing requirements on other subsystems	All payload

In order to reach the resolution we want, we clearly need a powerful camera coupled with an orbital design that let us get close to the surface and achieve images in the range between 1000-50 km from the surface. Also, given the sporadicity of the plumes and the I.R emission that can follow from solar excitation, our camera must take multiple pictures with a range that covers both visible and N.I.R. For the antenna, we need to establish a 2-way link in order to get the Tidal Love number, and we need to choose the right number of antenna and design a communication strategy.

At the same time, we had to constantly communicate with the other subsystems and take into account the requirements coming from them (**Table 2**).

Table 2: Subsystem's requirements.

ID	Requirement	Subsystem
PL.OR	Acquiring data for a close approach time of 2 minutes	Orbits
PL.EPS	Keeping the power below 80 W	EPS
PL.STR	Geometry compatible with a cylindrical s/c	Structures
PL.CD	Data storage estimation	CDHs

According to the above requirements, we have to design a proper observation strategy that will allow us to get all the high resolution images and spectroscopy data that we want in a limited time, while keeping the power requirements below 80W. The geometry requirement has been easily satisfied, since the antenna is a low profile patched antenna, the spectrometer is small, and the camera has a cylindrical shape.

4.3 High Resolution Camera

To help us decide which camera could make for our case, we explored different options on the market considering the following criteria:

- **FOV and IFOV:** The FOV (Field of View) is the largest area that the imager can see at a set distance. The IFOV (Instantaneous Field of View) is the smallest detail within the FOV that can be detected or seen at a set distance. The FOV is given by the following equation:

$$\text{FOV} = 2 \arctan \left(\frac{D}{2f} \right) \quad (1)$$

where f is the focal length of the lens. For the IFOV, the formula is the same but we have to substitute the length of the image plane (D) with the pixel size (p):

$$\text{IFOV} = 2 \arctan \left(\frac{p}{2f} \right) \quad (2)$$

- **SWATH:** The SWATH is defined as the image on the surface, and enters in the FOV equation as D .
- **Ground Sample Distance (GSD):** The GSD is defined as the distance between the centers of two adjacent pixels measured on the ground. This metric is related to the camera focal length, the resolution of the camera sensor, and the camera's distance from the subject. A lower value of the GSD corresponds to higher spatial resolution, since smaller square translates to more detail within the image.
- **Spectral range:** The possibility of observing in a wide range of wavelengths is a fundamental scientific requirement (PL.04). An imager can produce images in two different modes: **Panchromatic (PAN)** and **MultiSpectral (MS)**. The former is obtained by using the total light energy in the visible spectrum in a single band, producing a single intensity value per pixel that is commonly visualized in a greyscale image. The latter is obtained by using multiple bands that give an image with higher spectral resolution, but lower spatial resolution. The goal is generally to combine the images via a process called multi-resolution fusion.
- **Mass, Size and Power requirements:** If it is true that the payload is the subsystem that actually "does the job" of achieving the mission objectives, we don't have to forget that it is always linked with the other subsystems, and thus trying to minimize mass, size and power requirements is always a wise choice.

Based on these parameters, we explored options on the market, and we found two imagers with good features, both produced by Dragonfly Aerospace: DragonEye[34] and Raptor[35].



Figure 6: Two smallsats cameras from Dragonfly Aerospace.

Both these cameras are able to satisfy the scientific requirements, so we confronted their parameters and opted for the best option. In **Table 3** we can see a direct comparison, which helped us in our decision making process.

Table 3: Comparison between the two cameras. TRL is 8 for both of them.

Parameter	DragonEye	Raptor
GSD at 500 km (m)	1.4(PAN)-2.8(MS)	0.7(PAN)-2.8(MS)
SWATH at 500 km (km)	22	11
Mass (kg)	17	45
Size (cm)	32x92	45x120
Power (W)	45-25	45-25
Spectral bands	PAN+6MS	PAN+6MS

As we can see the Raptor imager has better spatial resolution then DragonEye in PAN mode, but the same in MS mode. Also, the SWATH of DragonEye is 22 km, which is the typical width of the bands on the surface. Both the camera cover the visible-I.R range we are looking for, but actually, considering we will reach altitudes of around few 10 s of km from the surface, we wouldn't exploit at full capacity the higher resolution that Raptor brings to the table, since even a lower spatial resolution can get the job done at such ‘close’ distance. In addition, considering that Raptor is significantly heavier and bigger than DragonEye, we chose the latter as our payload camera.

We also decided the Operation Mode of DragonEye[36]: the imager will be shooting for few minutes in the altitude range between 1000 and 25 km from the surface of Europa, with exposure times varying from 0.005s to 10s, starting from longer exposures when being further from the features, and progressively reducing the exposures when the s/c will be closer to the moon. The number of bits per pixel is 24, we consider a shooting frequency of few seconds and we plan to take at least 100 pictures per flyby. Then, the expected approximated amount of data per flyby is:

$$\frac{\text{Bits}}{\text{Pixel}} \cdot \text{Size}_{\text{pic}} \cdot N_{\text{pic}} = 4.32 \cdot 10^{-1} \text{GB} \quad (3)$$

4.4 Spectrometer

The spectrometer (SPUR, spectrometer for ultraviolet and infrared band) combines both Ultraviolet band and infrared band. For the UV band, the wavelength range is from 100 to 320 nm which covers most important emission lines from the simulation, as for infrared band it covers from 0.8 to 5.0 μm . The instrument is expected to include both bands because of the light-weight requirement from the traveling, which is inspired by the design of SPICAM (The Spectroscopy for Investigation of Characteristics of the Atmosphere of Mars) instrument on Mars Express [37].

To comprehensively study the atmosphere and maximize the functions of the spectrometer, three observation modes are designed for observation in various altitudes and with different sources, as shown in **Table 4**. In Nadir mode, the spectrometer is maintained to the center of the planet. When the orbit altitude is high, the limb mode is active and the spectrometer will focus on the limb of the planet. Comparing with the nominal Nadir observation, limb observations can maximize the integrated emission and reduce the strong UV background of scattering solar light by the surface. It can also be used to study the upper atmosphere via airglow spectroscopy [37]. In the occultation mode, the spectrometer is either oriented either to the direction of a star or the sun observing for the spectrum modified by Europa's atmosphere, which activates when the eclipse starts. The sketch diagram for observation modes is presented in **Figure 7**.

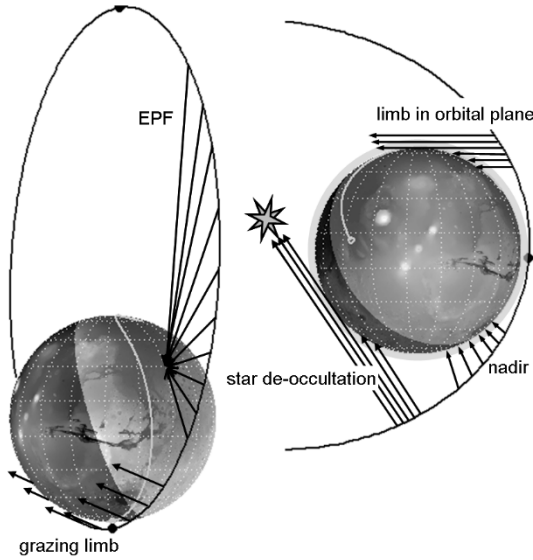


Figure 7: Three observation modes for the spectrometer. The sketch is from SPICAM and shows the different orientations and altitudes.

Table 4: Brief description and requirements for observation modes.

Mode Name	Goal	ADCs Requirement	Altitude Requirement	Working Band
Nadir	Observe for the spectra of Europa's atmosphere and surface in the center direction	+Z axis to the center of Europa	Nadir period for 4 hours	UV+IR
Limb	Observe the emission features from the upper atmosphere and detect UV airglows	fixed inertial attitude to the star		UV
Occultation	Observe the stellar spectra from the star or the sun to study the absorption features in occultation	fixed inertial attitude to the Sun		UV

In the Nadir mode, the background UV continuum from the surface can contaminate the spectrum as **Figure 3**, hence high spectral resolution and high SNR is necessary. To get the best SNR, the spectrometer is expected to work continuously in the Nadir period for around 4 hours. In terms of spectral resolution, at UV band it is designed as 0.50 nm/pix for pointed source ($\lambda/\Delta\lambda \simeq 440$) following the SPICAM's design[37], which is better than UV spectrometer on Europa's Clipper (0.6 nm/pix for pointed source, $\lambda/\Delta\lambda \simeq 220$ [38]). For the IR band it is 10 nm/pix as MISE on Europa's clipper.

Overall, considering three different modes, the spectrometer is expected to acquire data during the whole flyby period for 4 days. We take the estimation of spectroscopy data from the SPICAM with the maximum 300 Mbits/day (37.5 MB/day) [39], therefore in total 150 MB/flyby.

However, there is a conflict between the requirement of light weight and infrared wavelength coverage. In the light-weight design as SPICAM, the spectrometer uses acousto-optic tunable filters (AOTF) technology without slit and which only covers near-infrared band (1.0-1.7 μm) [37]. In missions to Europa, a wider wavelength range is strongly expected for the observation of water vapor absorption, hydrated salt and potential organic signals such as CH_4 . The CaF2 Dyson spectrometer is used in Europa Clipper [40] to reach such a wide wavelength coverage but the weight is significantly higher. We believe in the near future this problem can be solved with the state-to-art technology. The main parameters of the spectrometer are presented in **Table 5**.

Table 5: Main parameters for the spectrometer for SPES.

Parameter	Value
Wavelength Range (μm)	UV: 0.1 - 0.32 IR: 0.8 - 5.0
Spectral Resolution (nm/pixel)	UV: 0.50 IR: 10
Mass (kg)	4.85
Power (W)	25
Observation Duration (min)	5 - 60

4.5 X-band Antenna

In order to characterize the ocean beneath the surface, we decided to use multiple radio antennas (XAO, X-band antennas for ocean study) that will be used for the study of Europa's gravity field; as explained in the scientific overview, the gravity field strongly depends on the internal structure of Europa, and that's why by investigating this field we can gain significant knowledge. This is definitely the most complicated aspect of our mission, and our plan involves tasks that are usually carried on by the Navigation subsystem, so in this preliminary design phase we will limit to present how we plan to conduct this study, with focus on the instrumental side of the problem.

Our approach consists of exchanging a frequency coherent radio signals between the s/c and the ground, to study its Doppler shift. The size of the frequency shift depends on how fast the light source is moving relative to the observer. Ground controllers will know the frequency of the signal that is emitted from the spacecraft. However, when the spacecraft is moving away from (or towards) us, this frequency is being Doppler shifted to a different frequency. Computers will compare the received frequency with the emitted frequency to get the Doppler shift. A schematic representation is showed in **Figure 8**.

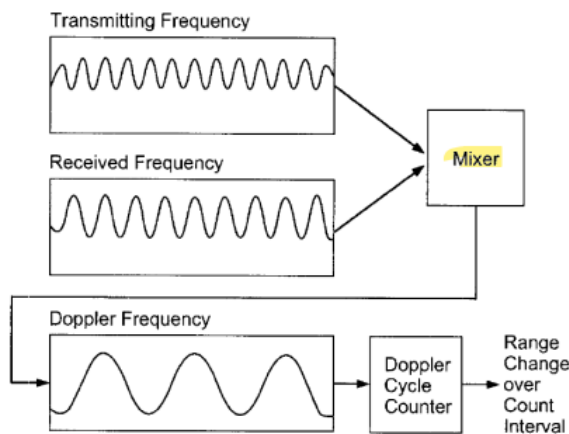


Figure 8: Schematic representation of the Doppler observable.

The mathematical formulation linking the frequency received with the frequency transmitted, is straightforward:

$$f_R = M_{s/c} \left(1 - \frac{\rho'}{c} \right) f_T \quad (4)$$

where ρ' is the derivative of the relative position between the antenna on ground and the s/c of mass $M_{s/c}$. Our goal is to model everything that can cause the change in position to the relative accuracy and attribute the rest to the ocean.

First we had to understand which frequency band is best suitable for our needs. We considered that:

- the higher the frequency, the greater the bandwidth, which leads to less congestion, higher speeds, higher traffic, and higher bit rates;
- with shorter wavelengths, the atmospheric absorption is higher, and the signal degrades with the presence of moisture and rain, diminishing the quality of communication, and increasing power requirements;
- with higher frequency, the size of the antenna decreases but offers a gain with a smaller aperture. This makes the pointing budget an issue;
- the cost of an antenna depends on the frequency: the higher, the more expensive;
- the choice is between X band or Ka band, we take S band out of the picture.

Our decision flow, showed in **Figure 9**, brought to the choice of an X-band antenna, rather than a Ka band antenna, since we don't need high data rates, we don't want to suffer from atmospheric influence and we want to recude the power, cost and accuracy requirements.

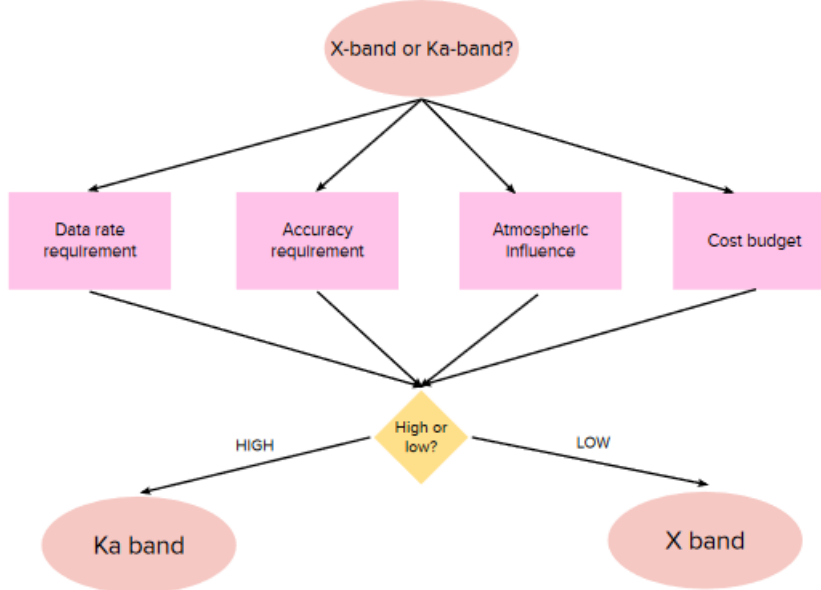


Figure 9: Decision flow for the choice of the antenna band.

With this result in mind, we explored different options available on the market, and selected the X-Band 2×2 Patch Array Antenna from EnduroSat, showed in **Figure 10**. Its main features are showed in a table.

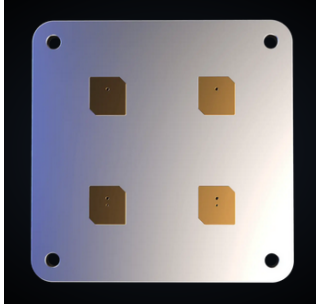


Figure 10: X-Band Antenna from EnduroSat.

Parameter	Value
Mass (g)	23.2
Power (W)	< 4W
Frequency (MHz)	8025 - 8400
HPBW (deg)	40
Gain (dBi)	12+
Polarization	RH circular

Table 6: Main parameters of our antenna.

Taking Europa Clipper as a reference, we need to include 5 antennas, and the link should be established before and after the closest approach to Europa, because during that time the s/c will have to point toward Europa to perform its science tasks. This means that the X-band antennas and the Camera will not be active in the same moment, and this will keep the power consumption below the limit of the requirement PL.EPS. Taking the paper “A possible new test of general relativity with Juno” of L. Iorio as a reference [41], we expect a typical range rate measurement $\Delta\rho'$, for a s/c orbiting Jupiter system, between $160\mu m$ and $280\mu m$ in the ± 3 hour window with respect to the closest approach. Juno’s radio science system enables range rate measurements accurate to $3 \cdot 10^{-6} m/s$ over timescales of 1000 s, but, since we will perform the study of the gravity field along with multiple other tasks, we don’t expect to reach such accurate measurements. In terms of expected relative velocity to the Earth, from one of the Juno Status Report of NASA [42], we expect a value of around 10.4 kilometers per second.

4.6 Mass and Power budget

Table 7: Mass and power budget of each payload instrument.

Instrument	Unit number	Mass (kg)	Power consumption (W)
Camera (DragonEye Imager)	1	17	45-25
Spectrometer (SPUR)	1	4.85	25
Antenna (XAO)	5	0.0232	<4W
TOTAL	7	21.966	70

The total mass of the payload is 21.966 kg, while the total power consumption, considering that the camera and the antenna will not be used at the same time, is 70 W at maximum, a value reached during the simultaneous activity of the imager and the spectrometer.

5 Attitude Determination and Control Subsystem

The meaning of the word attitude, or orientation, in spacecraft terminology is essentially “what is up and down”. However, the spacecraft is in the space and therefore the words “up and down” lose their meaning. Alternatively, the attitude is determined as the angular departure from some reference. The attitude information is a fundamental information for a spacecraft and is typically used to point the solar arrays toward the sun, point the high gain antenna toward the earth after deployment or acquisition of an attitude for a science payload. The goal of this subsystem are the following:

- Determination of the attitude: we must know where the s/c is pointing as a function of time;
- Control of the attitude: we must correct for internal and external torques in order to satisfy the pointing requirements of the payload and the high gain antenna.

In this section we will start from the requirements we have to satisfy, and then we will move to the computation of the torques and the choice of the proper actuators and sensors to carry on the Attitude Determination and Control Subsystem (ADCS) goals.

5.1 Requirements

Table 8: Requirements for the ADCS.

ID	Description	Subsystem
ADCS.1	Ensure a minimum pointing accuracy of 0.5 degrees for the camera	Payload
ADCS.2	Ensure a minimum pointing accuracy of 0.35 for the antenna	Communication
ADCS.3	Minimize the power requirements	EPS
ADCS.4	Provide the same attitude requirements during an eclipse	ADCS
ADCS.5	Counter the disturbance torques that act on the s/c even in the worst case scenario	ADCS
ADCS.6	Stabilize all 3 axis with no bias	ADCS
ADCS.7	Providing a mechanism for attitude desaturation if needed	ADCS
ADCS.8	Eliminate eventual tumbling motions after the deployment phase	Various subsystems

The requirements that the ADCS of the SPES mission has to satisfy are presented in **Table 8**. Since SPES won’t use solar panels, we have to account for the pointing requirements of the camera and antenna alone. The 0.5 degrees accuracy for the camera emerges considering that the typical height of a plume is 100 km, which from a distance of 500 km will result in a structure of 11.45 degrees; we clearly won’t observe a plume from side view, so we accounted for half of this value, and then applied the rule of thumb of around 1/10, coming up with 0.5 degrees.

The 0.35 degrees of accuracy required by the HGA is the precise value provided by the datasheet [43], but in the preliminary analysis we had to estimate it (following [44]). We did this by considering that, in general, the pointing accuracy is 1% of the beam-width (BW); for an antenna with 44.2 dBi of gain, the BW is 35.3 degrees, so the accuracy was estimated to be 0.35 degrees, which turned out to be the real value. We obviously want to minimize the cost, mass, and power requirements when possible, especially to guarantee the proper work of the RTG from EPS. We chose to stabilize all three axis instead of using spin because we want the optical instruments and antennas to point at desired targets without having to perform “despin” maneuvers. We also considered that we may operate in period of eclipse and that the disturbances won’t be constant, but they will depend on the distance from Europa and Jupiter, since we will perform flybys; we accounted for the worst case scenario, as we will present in the following section.

5.2 Estimation of the Disturbances

In this section, we determine the size of the disturbance torques the ADCS must tolerate. A disturbance is any undesirable or uncontrollable effect, a force or torque, vibration, structural distortion, or electrical anomaly, which produces a degradation in the performance of the s/c. There are two types of disturbances:

- **External:** the external disturbances result from the interaction between the s/c and the space environment. They may produce deformations and deflections which could alter the spacecraft geometric and mass distribution properties.
- **Internal:** internal mechanisms, sloshing of the fuel, flexible appendages and general mass movements are examples of internal sources of disturbances, that can affect the attitude of the s/c. In this preliminary analysis, we neglected those, because they are less impactful than the external ones.

Having an estimation of the total torque that the external disturbances provide is of fundamental importance for the choice of the components, actuators and sensors, that will make the ADCS counterbalance them. We computed the upper limits of the external torques, because the ADCS should be able to operate even in the worst case scenario. We considered:

- **Solar Radiation Pressure:** even if photons are massless, they carry momentum, and interacting with the s/c will engage in an exchange of momentum that can even produce a significant torque. This happens when there is a misalignment between the centre of solar pressure C_p , where the pressure imposed by the photons is applied, and the centre of mass of the spacecraft C_m . The formula is

$$T_{SRP} = \frac{F}{c} A_p (1 - q) (C_p - C_m) \quad (5)$$

where F is the solar flux, c the speed of light, A_p is the area exposed to the radiation and q is the reflectivity factor. Considering that the solar flux at the distance of Jupiter and Europa is 50 Wm^{-2} , we asked for the other values to the other subsystems and, assuming $(C_p - C_m) = 0.01 \text{ m}$, we found a value of $T_{SRP} = 2.71 \cdot 10^{-8} \text{ Nm}$;

- **Magnetic torque:** the coupling between a strong magnetic field and the residual magnetic dipole of the s/c, produced by onboard instruments and current-carrying wires, will induce a torque of

$$T_{\text{mag}} = \frac{M^2 B}{R^3} \quad (6)$$

Considering that Europa has a very weak induced magnetic field, the maximum effect will be due to the magnetic field of Jupiter, which has a dipole moment of $M = 1.5 \cdot 10^{20}$ Tm³. Considering a typical residual dipole B for the s/c and the minimum distance to Jupiter R , we found a value of $T_{\text{mag}} = 1.04 \cdot 10^{-7}$ Nm;

- **Gravity gradient:** Variations in the gravity force experienced by two opposite sides of the s/c will induce a torque which, close enough to Europa, can be significant. The formula is

$$T_{\text{gg}} = \frac{3\mu}{R^3} \mu_e \times I \mu_e \quad (7)$$

where μ is the gravitational parameter, μ_e is the unit vector toward nadir, R is the distance s/c-center of Europa, and I is the inertia matrix of the s/c. Assuming a cylindrical s/c of around 80 kg, as suggested by the structures subsystem, the maximum difference between the moments of inertia is 49.8 kg·m². Considering that the minimum distance to the surface of Europa will be 25 km, this torque will be dominated by Europa instead of Jupiter, and we found an upper limit of $T_{\text{gg}} = 1.20 \cdot 10^{-4}$ Nm;

- **Atmospheric drag:** The interaction between the atmosphere of Europa and the s/c will produce a torque, which strongly depends on the atmospheric density ρ , the square of the maximum orbital velocity v , the area of the s/c, the drag coefficient C_d and the displacement between the center of pressure and the center of mass

$$T_{\text{atm}} = \frac{1}{2} \rho C_d A_p v^2 (C_p - C_m) \quad (8)$$

The density of Europa is extremely rarefied, made mostly of Oxygen and still not well modeled. To have a reference value, we considered the surface pressure value of $0.1 \mu\text{Pa}$ and applied the ideal gas law to have a rough estimation on the maximum density of the atmosphere, which is around $3.04 \cdot 10^{-12}$ kg/m³. Assuming a typical C_d of 2.2 we found a maximum value of $T_{\text{atm}} = 6.87 \cdot 10^{-7}$ Nm.

Then, summing these values, we found an estimated maximum total torque of

$$T_{\text{gg}} + T_{\text{SRP}} + T_{\text{atm}} + T_{\text{mag}} = T_{\text{tot}} = 1.21 \cdot 10^{-4} \text{ Nm} \quad (9)$$

It's important to notice that this total torque is coming out assuming a displacement between C_p and C_m of 0.01 m. We wanted to make a more complete analysis, so we created a Python script to explore how the torques changes as a function of $(C_p - C_m)$, from 0.001 m to 1 m, with increments of 1 mm. The graphical results are shown in **Figure 11**.

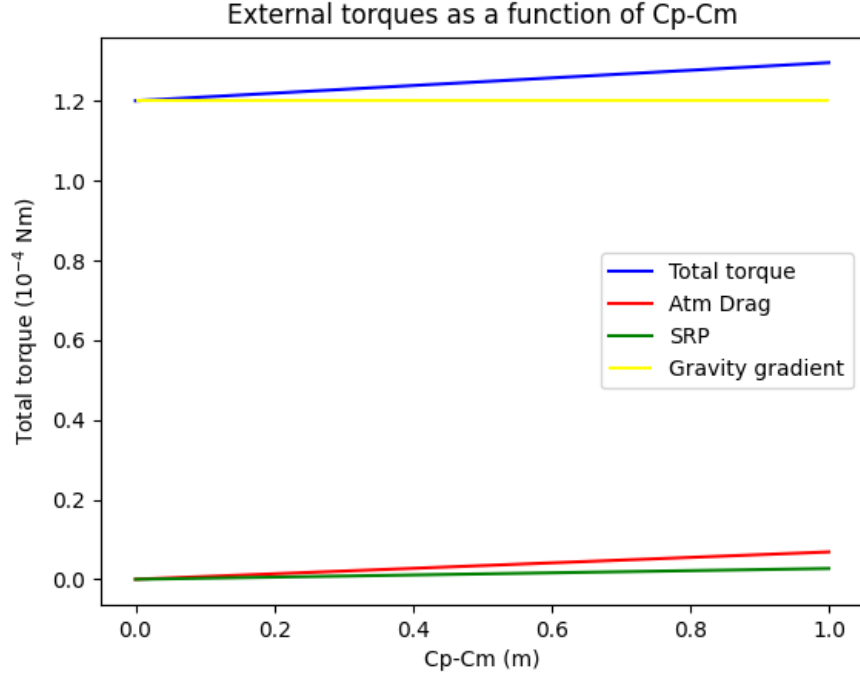


Figure 11: Total torque as a function of the displacement between C_p and C_m .

Only the SRP and the atmospheric drag torques are functions of $C_p - C_m$, but, in this worst case scenario analysis, they are different orders of magnitude smaller than the dominant torque, which is the gravity gradient one. For this reason, the difference in the total torque between the two extremes of assuming a very large and a very small displacement is negligible. Since T_{gg} is the dominant torque, we decided to explore more in depth its trend as a function of the distance to Europa, since we expect it to be dominant only at close distance. We then created another Python script to explore how the atmospheric drag torque and gravity gradient torque changes as a function of the distance to the surface (**Figure 12**).

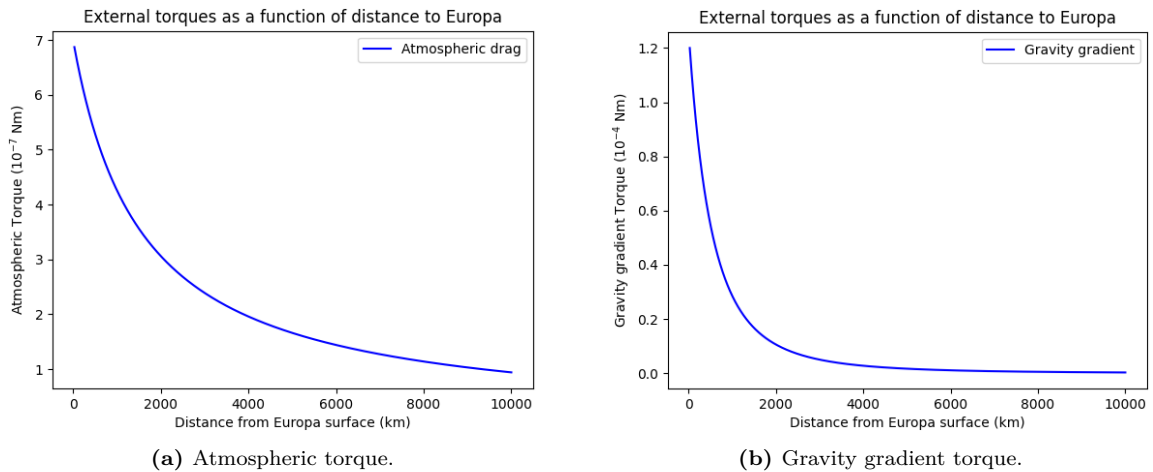


Figure 12: Torques as a function of the distance to the surface of Europa.

In the case of the atmospheric drag torque the plot serves just to show that getting further from Europa the torque gets smaller, because the velocity is decreasing; its physical meaning is not complete, because one should also consider that the atmospheric density would also decrease with increasing altitude, but since we don't have a model to describe it, we neglected this fact.

For the gravity gradient torque, however, we clearly see that it rapidly becomes less dominant with increasing altitude, until, at a distance from the surface of around 2000 km, it gets equal to almost 0. From this result, we concluded that we don't expect the worst-case scenario to dominate the entire mission duration; since we can survive this scenario, we can also design such that we suspend operations and nothing goes wrong during this time and then we revert to nominal operations after the phase passes. This might be a good way to further increase the efficiency of the mission in the next design phase.

5.2.1 De-Tumbling

In order to have a complete view of the torque that the actuators will have to control, we considered also the de-tumbling maneuver after the deployment of the s/c. To be as robust and safe as possible, we considered a maximum angular rate of 30 deg/s, which is the upper limit found on the launcher manual. Based on that, the needed time is found from the following equation

$$\Delta t = \frac{I}{T_{\text{ext}}} (\omega_f - \omega_i) \quad (10)$$

which, considering that we want to dissipate the entire angular velocity, the maximum principal inertia of the s/c $I = 129.6 \text{ kgm}^2$, and that previously derived total external torque T_{ext} acts in the same direction of rotation, we find a time of $565920s \approx 6.55\text{days}$. The required torque for the de-tumbling maneuver has been computed as

$$T_{\text{dtbl}} = SF \frac{h_{\text{dtbl}}}{\Delta t} = 2.4 \cdot 10^{-4} \text{ Nm} \quad (11)$$

where we assumed a safety factor SF of 2 and $h_{\text{dtbl}} = I\omega$.

5.2.2 Angular Momentum Evaluation

The de-tumbling torque has been added to the total external torque, in order to estimate the wheel momentum storage, useful to choose the right attitude actuators. We used the formula taken from [8]

$$h = (T_{\text{ext}} + T_{\text{dtbl}}) \frac{\text{Orbital period}}{4} (0.707) = 7.6 \text{ mNms} \quad (12)$$

We assumed an Orbital period of two minutes, because we made our computations in the closest approach scenario, which will last 2 minutes in total. As we showed previously, outside of this distance range the dominant torque, the gravity gradient torque, will rapidly goes to zero, leaving a total torque 3 orders of magnitude smaller. That's why we chose to re-scale the orbital period accordingly.

5.3 Selection of the Reaction Wheel

Based on the computed h , we selected a reaction wheel as main attitude actuator. Reaction or momentum wheels are called “storage momentum devices” as their operation is based on Newton’s third law: for every action there is an equal and opposite reaction. Hence, if the wheel is accelerated counterclockwise, it creates an internal torque on the spacecraft clockwise. The attitude of the s/c is controlled by the change in speed of the wheel; usually three or more reaction wheels are used on a s/c to provide full 3-axis attitude control and stability. We chose reaction wheels because they allow for high pointing accuracy, and they are power efficient, as no fuel is consumed. We explored different options available in the market, and to decide we followed this procedure:

1. Identification of the main parameters for a reaction wheel, and then absolute rating, attributing a score from 1 to 5 based on importance (**Table 9**);
2. Comparison of the performance of commercial wheels (**Table 10**);
3. Evaluation of every single wheel, taking into account that not all the data sheets are complete of all the information;
4. The wheel with the highest normalized score wins.

Table 9: Absolute rating values for the main parameters.

Parameters	Value
Mass (M)	4
Volume (Vol)	5
Power Consumption (PC)	5
Temperature (acceptance) (Temp)	4
Radiation TID (Rad)	2
Design Life (DL)	4
Momentum Capacity (Mom)	3

We gave maximum importance to the power consumption to account for the requirement ADCS.3, and we gave a mid score to the momentum capacity because our value of h is pretty low. We also considered the design life and the radiation TID, even though not all the wheels showed these parameters in their data sheet (**Table 10**).

Table 10: Reaction wheels for attitude control. The first three are designed by NewSpace Systems ([10]), the last three are designed by Blue Canyons Technologies ([4]).

Momentum wheel	M (kg)	Vol (cm ³)	PC (W)	T (°C)	Rad (krad)	DL (years)	Mom (Nms)
NRWA-T065	1.55	1902.42	<6	-10 to +45	10	>10	0.94
NRWA-T2	2.8	1687.5	<8	-10 to +58	10	>10	1.47
NRWA-T6	< 5	4410	<83	-20 to +60	20	>10	7.83
RWP050	0.24	84.1	<1	-	-	>5	0.050
RWP100	0.33	122.5	<1	-	-	>5	0.10
RWP500	0.75	459.8	<6	-	-	>10	0.50

Table 11: Total score for each wheel is weighted by the parameters of Table 9. The normalized one is given by the total score divided by the maximum score a wheel can obtain (270 for first 3, 210 for last 3).

Momentum wheel	Total score	Normalized score
NRWA-T065	195	0.722
NRWA-T2	190	0.704
NRWA-T6	151	0.559
RWP050	175	0.833
RWP100	169	0.805
RWP500	163	0.776

After this process we selected the reaction wheel RWP050 (**Figure 13**), because its momentum storage is sufficiently high, and its mass, volume and power requirements are the lowest.



Figure 13: RWP050 reaction wheel designed by Blue Canyons Technologies ([4]).

Choosing this reaction wheel means that 3 of those will be needed to stabilize all three axis, and they seem to be able to cover all the torques even in the worst case scenario. A common problem for wheels, though, is that over time it may build up enough stored momentum to exceed the maximum speed of a wheel, called saturation, which will need to be cancelled. That is why reaction wheel systems are supplemented with external attitude control mechanisms such as magnetorquers. In this preliminary design phase, it seems like saturation won't be reached, even in the worst case scenario and considering de-tumbling, but this is an unreal condition, since in real life there are also secular disturbances that can cause the wheel to drift toward saturation. We then selected an external torquer to perform the attitude de-saturation of the wheels, if needed. We couldn't choose magnetorquers due to the low and unmapped magnetic field of Europa, so we refold on thrusters.

5.3.1 Thrusters for Attitude De-Saturation

Even if from this preliminary analysis the necessity for attitude thrusters doesn't seem to arise, we wanted to add them in this design phase to avoid future problems. Chemical thrusters work by ejecting propellant to generate a thrust in the selected direction. They have advantages, because they can create torques on any axis, for any orbit and without altitude limitations, but they have also downsides, like the need for fuel, the general low impulse and toxicity. We selected a thruster that could minimize these disadvantages: 1N HPGP THRUSTER (**Figure 14**).

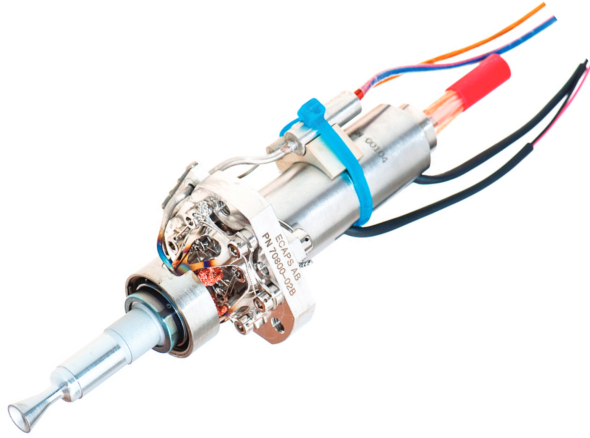


Figure 14: 1N HPGP THRUSTER from Bradford ECAPS ([5]).

Its propellant is based on ADN (Ammonium Di-Nitramide) which is easier to handle, less toxic and with increase performance with respect to Hydrazine. We preferred a chemical thruster over an electrical one, because we wanted to reduce the power requirements, and we want to be able to execute maneuvers faster.

5.4 Selection of the Sensors

To determine the attitude of satellite we will need both reference and inertial sensors. We have to choose them taking into account that:

1. The pointing accuracy from the payload should be below 0.5 degrees;
2. The pointing accuracy from the antenna must be 0.35 degrees;
3. We will use sun sensors and an IMU for three axis stabilization;
4. In order to detect the Sun's attitude in two directions, at least three coarse sun sensors are usually needed, unless a pyramid coarse sun sensor is used.

5.4.1 Sun Sensors

A sun sensor is a reference device that senses the direction of the Sun to measure its position or other light sources with respect to the sensor position. Sun presence sensors provide a binary output, indicating when the sun is within the sensor's field of view. Analog and digital sun sensors, in contrast, indicate the angle of the Sun by continuous and discrete signal outputs, respectively. Among all the reference sensors, sun sensor can satisfy our accuracy requirements with low costs (with respect to star trackers) and work in a more efficient way than magnetometers, which need a powerful magnetic field, or GPS (s/c is too far from Earth).

The Coarse Sun Sensor (CSS) delivers coarse information about the position of the Sun relative to the spacecraft. This information is used for coarse maneuvering of the spacecraft and to inform the spacecraft about the position of the Sun when it is in a safe mode of operation. To select the right sun sensor, we applied the same procedure used for the reaction wheel, but with different parameters (**Table 12**).

Table 12: Absolute rating values for the main parameters of a sun sensor.

Parameters	Value
Mass (M)	3
Volume (Vol)	3
Power Consumption (PC)	3
Accuracy (A)	5
Field of View (FOV)	4
Number of axis (N)	5

The accuracy and the FOV should be as high as possible. The number of axis on which the sun sensor acts is better to be larger than 1, because the more axis it stabilizes, the less sensors you need. After choosing 5 different sun sensors (**Table 13**), we evaluated them in order to find the best one (**Table 14**).

Table 13: Sun sensors for attitude control. The first is designed by RedWire ([11]), the second by CubeSpace ([12]), the fine sun sensor by Bradford Engineering ([13]) and the last two by NewSpace Systems ([6]).

Sun sensor	M (kg)	Vol (mm ³)	PC (W)	A (°)	FOV (°)	N
CSS Pyramid	0.13	89x89x43	0	±1 to ±5	360	2
Camera SS	0.03	42x18x23	0.2	0.2	170	2
FSS	0.375	108x108x53	<0.25	<0.3	138	2
NCSS	0.005	33x11x6	<0.05	<0.5	114	-
NFSS	0.03	34x40x20	<0.15	<0.1	136	-

Table 14: Total score for each sun sensor is weighted by the parameters of Table 12. The normalized one is given by the total score divided by the maximum score a wheel can obtain (230 for the first 4, 180 for the last 2).

Sun sensor	Total score	Normalized score
CSS Pyramid	170	0.739
Camera SS	173	0.752
FSS	142	0.617
NCSS	129	0.717
NFSS	135	0.754

The model we selected is NFSS-411 (**Figure 15**) which has low mass, volume and power consumption, coupled with very high accuracy. The front surface of NFSS-411 is a synthetic sapphire window with a reflective metal coating. In order to have a full sky coverage, 4 units are needed.



Figure 15: NFSS-411 by NewSpace Systems (NSS, [6]).

5.4.2 IMU

An inertial measurement unit (IMU) is an electronic device that measures and reports a body's specific force, angular rate, and sometimes the orientation of the body, using a combination of accelerometers and gyroscopes. IMUs are typically used to maneuver modern vehicles including satellites and landers. An inertial measurement unit works by detecting linear acceleration using one or more accelerometers and rotational rate using one or more gyroscopes. Typical configurations contain each of these elements per axis for each of the three principal axes: pitch, roll and yaw. A major disadvantage of using IMUs for navigation is that they typically suffer from accumulated error. Because the guidance system is continually integrating acceleration with respect to time to calculate velocity and position, any measurement errors, however small, are accumulated over time. One of these is the Angle Random Walk (ARW): it is the noise component perturbing the output of gyroscopes. Special filters are commonly used to reduce the noise in real-time.

The selected IMU is GS-IMU3000TA (**Figure 16**), made by three-Axis precision closed-Loop gyroscopes and three precision Quartz Pendulous accelerometers. It can operate in Navigation and Attitude mode with an excellent vibration and shock performance. With an ARW lower than $0.015^{\circ}/\text{h}^{0.5}$, it is affected by one of the best, and so lowest, noise in the market.



Figure 16: GS-IMU3000TA by Grand Stal Solutions Ltd ([7]).

5.5 Mass and Power budget

Table 15: Mass and power budget of each instrument used for attitude.

Instrument	Unit number	Mass (kg)	Power consumption (W)
Reaction wheel	3	0.72	<3
Thruster	6	0.38	-
Sun sensor	4	0.14	<0.6
IMU	1	1.9	12
TOTAL	14	6.9	23.4

6 Orbital Design

Several missions have been able to reach Jupiter in the past: Voyager 1 and 2, Galileo, Cassini and Juno. There are more planned missions in the upcoming years. The journey to Jupiter is far from being a simple problem and complexity grows exponentially if, we want to find a way to study one of its moons, in our case Europa.

Apart from the difficulties that a spacecraft would encounter to reach Jupiter orbit, it is well known that the environment around Jupiter is very extreme: its strong magnetosphere captures and accelerates ionized particles, creating radiation belts similar to Earth's Van Allen belts, but thousands of times stronger. Even a radiation hardened satellite would live just a few months orbiting close to the gaseous giant.

Our scientific orbits will have to take into account this problem and at the same time will have to allow us to reach all the requirements that our mission has in the study of Europa.

In the following sections, we report step by step the different phases in which SPES mission is divided, from the beginning to the end, giving particular importance to the different velocity increments Δv that will be required in each phase.

6.1 From Earth's surface to parking orbit

The first thing we studied is how much thrust is needed to take a launcher from Earth's surface up to a parking orbit with an altitude of $h_{park} = 350$ km. To give the total value of Δv_{park} , we had to sum four different contributes:

- Orbital velocity at parking orbit $v_{park} = \sqrt{\frac{\mu_E}{R_E + h_{park}}} = 7.697$ km/s;
- Variation in orbital potential energy (converted in velocity), that can be linearized in case of $h_{park} \ll R_E$

$$\Delta v_{pot} = \sqrt{\frac{\mu_E}{R_E}} \sqrt{2 - \frac{R_E}{R_E + h_{park}}} - \sqrt{\frac{\mu_E}{R_E + h_{park}}} \simeq \frac{h_{park}}{R_E} \sqrt{\frac{\mu_E}{R_E}} \quad (13)$$

In our case we obtained $\Delta v_{pot} = 0.41$ km/s;

- The variation in velocity needed to compensate the gravity loss $\Delta v_{grav} = 2.2$ km/s;
- The variation in velocity needed to compensate the drag loss $\Delta v_{drag} = 0.1$ km/s,

where μ_E is Earth's gravitational parameter, while R_E is Earth's radius.

As we can see, the main components to be considered are the orbital velocity and the gravity loss. Summing all the contributes listed above we found that, in order to reach a parking orbit with $h_{park} = 350$ km, we would need a velocity increment given by

$$\Delta v_{park} = 10.408 \text{ km/s.} \quad (14)$$

All this procedure was developed taking as a model [45].

6.2 Interplanetary Journey

From parking orbit, we needed to understand in which way we could escape Earth's gravity and start the interplanetary journey to reach Jupiter's orbit. At first, we tried

the simplest approach: doing a Hohmann transfer between Earth's orbit and Jupiter's orbit, but the value of Δv we found to do this maneuver was very high. Secondly, we tried instead an Earth flyby approach, taking as reference the Juno mission, to try to reduce the Δv .

6.2.1 Hohmann Transfer Approach

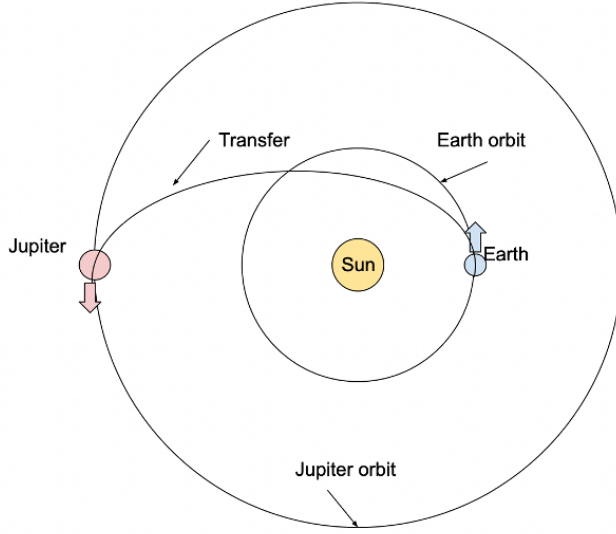


Figure 17: Hohmann transfer to pass from Earth's orbit (1AU), to Jupiter's orbit (5.2AU).

The simplest approach to pass from an original circular orbit to a circular orbit of a different size is to exploit the Hohmann transfer maneuver. It consists in two boosts: starting from the smaller circular orbit with radius R_1 , the first boost Δv_{H1} is given to enter an elliptical orbit, which semi-major axis is $a = (R_1 + R_2)/2$, while the second boost Δv_{H2} is given at the apoaxis of the ellipse, in order to enter in the bigger circular orbit, with radius R_2 . In case of an heliocentric transfer, the magnitude of the two boosts is given by Eq. 15.

$$\Delta v_{H1} = \sqrt{\mu_\odot \left(\frac{2}{R_1} - \frac{1}{a} \right)} - \sqrt{\frac{\mu_\odot}{R_1}} \quad \text{and} \quad \Delta v_{H2} = \sqrt{\frac{\mu_\odot}{R_2}} - \sqrt{\mu_\odot \left(\frac{2}{R_2} - \frac{1}{a} \right)} \quad (15)$$

The purpose was to pass from an initial orbit with radius $R_1 = 1\text{AU}$ (which corresponds to Earth's orbit around the Sun) to a final orbit with $R_2 = 5.2\text{AU}$ (which corresponds to Jupiter's orbit around the Sun, as shown in **Figure 17**). But before doing this computation, orbiting the Sun in a 1AU orbit coincides with having successfully escaped Earth's gravitational attraction. Starting from the parking orbit (see Section 6.1), the value of Δv_{escape} was computed subtracting the orbital velocity at an altitude h_{park} from the escape velocity at the same altitude, as shown in Eq. 16. In **Table 16**, the Δv values required to escape Earth's gravitational attraction are shown: those contributes are expected to be given by the launcher we will choose, that is not a strong assumption if we consider Falcon Heavy or SLS as launchers for our mission (see Section 12). The launch date we considered here is the same that will be taken into account in Section

6.2.2: this choice will be explained in the following.

$$\Delta v_{\text{escape}} = v_{\text{esc,park}} - v_{\text{park}} = \sqrt{\frac{2\mu_E}{R_E + h_{\text{park}}}} - \sqrt{\frac{\mu_E}{R_E + h_{\text{park}}}} = 3.19 \text{ km/s} \quad (16)$$

Table 16: Results showing the total $\Delta v_{\text{launcher},1}$ that should be provided by the launcher, to reach parking orbit and escape Earth's gravity.

Orbital maneuver	Δv (km/s)
Launch to parking (350 km)	10.408
Escape from parking	3.188
Total $\Delta v_{\text{launcher},1}$	13.596

After having escaped from Earth's gravity, the Hohmann transfer will be performed. Using Eq. 15, we obtained the results reported in **Table 17**. In our assumption, these two boosts needed to perform the transfer will be responsibility of the propulsion system of our spacecraft. The duration of the transfer was computed using the third Kepler's law, to find the orbital period of an ellipse with semi-major axis $a = (R_1 + R_2)/2$, and dividing it by 2, as shown in Eq. 17.

$$T_{\text{Hohmann}} = \pi \sqrt{\frac{a^3}{\mu_\odot}} \simeq 997 \text{ days} \quad (17)$$

Table 17: Results showing the total $\Delta v_{\text{Hohmann}}$, computed using Eq. 15 that are meant to be provided by our spacecraft to pass from a 1AU orbit around the Sun (Earth's orbit) to a 5.2AU orbit around the Sun (Jupiter's orbit).

Orbital maneuver	Δv (km/s)
Hohmann first thrust Δv_{H1}	8.793
Hohmann second thrust Δv_{H2}	5.643
Total $\Delta v_{\text{Hohmann}}$	14.436

In this case, the total Δv needed for Hohmann maneuvers is:

$$\Delta v_{\text{Hohmann}} = 14.436 \text{ km/s}. \quad (18)$$

This value is very high if it is meant to be provided just by the spacecraft, and also considering that here the maneuvers subsequent to Jupiter arrival are not taken into consideration yet: this gives a strong reason to exclude this method and to choose a better one to reduce the total Δv budget.

6.2.2 Flyby Approach

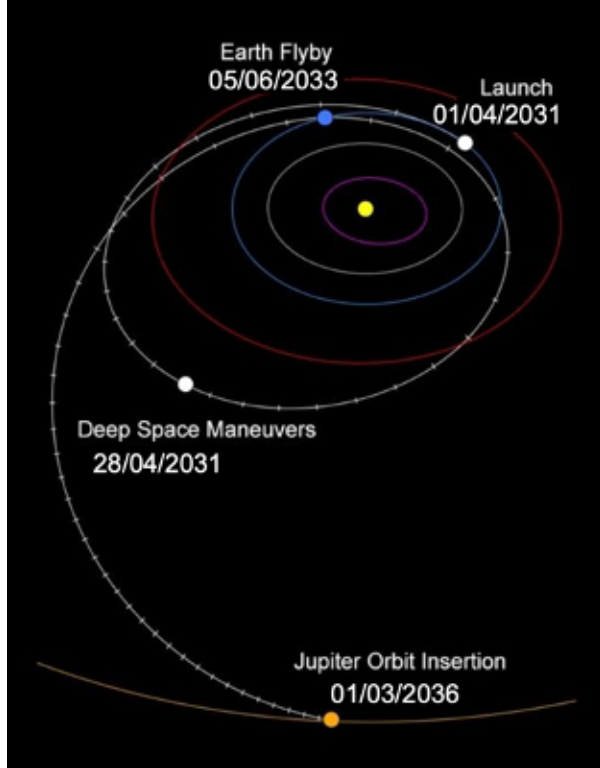


Figure 18: Sketch showing the different interplanetary phases, from DSM, to Earth’s flyby and Jupiter Orbit insertion.

After having verified that the value obtained with the interplanetary Hohmann transfer was too high, the approach was changed. A combination of patched conics method and gravity assist was used. Here the gravity assist is done with the departure planet itself (Earth). In the following of this section, in particular, Juno mission was taken as a strong reference [14].

To find a suitable launch window, we tried to find a date in which the phasing between Earth and Jupiter was similar to the one between them during Juno departure. Inspecting the JPL website¹, in which one can find the relative positions of planets on a specific date, we looked for a date in the upcoming years in which the relative position between Earth and Jupiter will be the same as it was on August 5, 2011 (the date of Juno launch [14]): this date was found to be on April 1, 2031, that was then chosen as the launch date for our mission. Starting from this date, and considering the duration of each phase of Juno mission, the dates at which all the different orbital maneuvers will have to be performed were calculated: these dates are reported in **Table 18** and **Table 19**.

The constraints regarding launch windows affect a lot the choice of the characteristic energy from pork chop plots. So, always using Juno as reference [42], we used a value of $C_3 = 30.8 \text{ km}^2 \text{ s}^{-2}$ for the *characteristic energy*, that is defined as the square of v_∞ and is also directly linked to the semi-major axis of the hyperbolic escape orbit a_∞ : all these relations are shown in Eq. 19.

$$C_3 = v_\infty^2 = \frac{\mu_E}{a_\infty}. \quad (19)$$

¹https://ssd.jpl.nasa.gov/tools/orbit_viewer.html

Doing reverse calculations we found $a_\infty = 12942$ km: this corresponds to an altitude from Earth's surface of ~ 6564 km. This was used as the altitude of the coasting orbit from which our interplanetary journey will start: to reach it from the parking orbit, a simple Hohmann transfer will be performed. So, with this second approach, the $\Delta v_{\text{launcher},2}$ (boost required from the launcher) is lower than before, and it is obtained by summing the velocity boost needed to reach a parking orbit with altitude $h_{\text{park}} = 350$ km and the one needed to perform the Hohmann transfer to a coasting orbit with altitude $h_{\text{coast}} = 6564$ km. The values of Δv related to this part are shown in **Table 18**. We decided not to go directly to the coasting orbit because we didn't know how the drag loss and gravity loss would have changed in this case, while having already a reference for the parking orbit at 350 km, we decided to keep that value as fixed, and to start from there.

Table 18: Results showing the total $\Delta v_{\text{launcher},2}$ that should be provided by the launcher, to reach parking orbit with altitude $h_{\text{park}} = 350$ km and afterwards to transfer to a coasting orbit with altitude $h_{\text{coast}} = 6564$ km, using Hohmann transfer.

Orbital maneuver	Δv (km/s)
Launch to parking (350 km)	10.408
From parking to coasting (6564 km)	2.092
Total $\Delta v_{\text{launcher},2}$	12.500

After having reached the coasting orbit, we had to compute the magnitude of the boost Δv_{hp} we needed to enter into the hyperbolic escape trajectory starting from the coasting orbit. This was done by subtracting the orbital velocity at coasting orbit v_{coast} from the velocity in the hyperbolic trajectory v_{hp} , computed as shown in Eq. 20.

$$\Delta v_{hp} = v_{hp} - v_{\text{coast}} = \sqrt{v_\infty^2 + \frac{2\mu_E}{a_\infty}} - \sqrt{\frac{\mu_E}{a_\infty}} = 4.06 \text{ km/s.} \quad (20)$$

In this way, our spacecraft was placed in an interplanetary trajectory escaping from Earth. But this hyperbolic trajectory would not have been enough to take our spacecraft to Jupiter. To solve this problem, we needed to introduce a so-called Deep Space Maneuver (DSM) to make our spacecraft head back to Earth and use it to gain extra-energy through an Earth's flyby. This is exactly what they did in Juno mission, apart from the fact that in that case they divided the DSM in two parts, because Juno's thrusters were not enough powerful to give a single boost; in our case instead we decided that the DSM would occur on April 28, 2032 and will provide a boost $\Delta v_{\text{DSM}} = 1.855$ km/s to our spacecraft, that will then go back towards Earth and will encounter it on June 5, 2033: it will pass at an altitude $h_{E,\text{flyby}} = 800$ km, and will use Earth's gravitational potential well as a slingshot to be able to gain a $\Delta v_{E,\text{flyby}} \sim 7$ km/s without using fuel. This will put the spacecraft on a much larger orbit that will eventually lead it to a distance of 5.2AU from the Sun, reaching Jupiter orbit on March 1, 2036.

At this point our spacecraft will have a velocity much larger than the velocity needed to enter in orbit around Jupiter: this is why we should provide some velocity decrement. We could do that simply using the spacecraft's thrusters, but this maneuver would be quite expensive in terms of propellant consumption. For the purpose of sparing some Δv , we could exploit one of the other moons of Jupiter, Ganymede (whose orbit around Jupiter is larger than Europa's) and use its gravitational attraction to do a flyby and obtain a velocity reduction with a magnitude $\Delta v_{Gan} \sim 0.4$ km/s (see [15] as a reference).

This will happen almost 12h before another maneuver, called Jupiter Orbit Insertion (JOI) maneuver, and will allow us lower the decrement needed to enter an orbit around Jupiter. In fact, the JOI will consist in a velocity decrement $\Delta v_{JOI} = 0.9$ km/s, that will put our spacecraft in a Jupiter orbit with a radius $R_{JOI} = 912921$ km.

The JOI is the maneuver that concludes the interplanetary transfer, since it will bound gravitationally our spacecraft to Jupiter. All the different steps of the interplanetary transfer, together with the values of Δv , are reported in **Table 19**. Apart from the first row (that we computed using Eq. 20), all other values of Δv are taken from the Juno paper [14] and Europa Clipper paper [15] references. The rows referring to Earth's flyby and Ganymede's flyby are reported with a grey background because for both of them no fuel consumption will be required, so we don't include them in the sum to calculate the Δv budget. Taken this into account, the total velocity budget needed for the whole interplanetary transfer is:

$$\Delta v_{inter} = 6.818 \text{ km/s}. \quad (21)$$

From this value, is quite evident how this flyby approach is much more convenient than the Hohmann transfer (see Eq. 18) in terms of Δv budget: in this way in fact we are able to spare ~ 7.6 km/s, that means more than half of the total Δv needed for Hohmann transfer.

Table 19: Results showing the total Δv_{inter} needed for the interplanetary orbital phase. Gray rows indicate values that do not contribute to the final Δv budget. The value in the first row was computer using Eq. 20. All other values were taken from Juno [14] and Europa Clipper [15] papers.

Orbital maneuver	Δv (km/s)
Inserting in hyperbolic orbit	4.063
DSM	1.855
Earth's flyby	~ 7
Ganymede flyby	~ 0.4
JOI (Jupiter orbit insertion)	0.9
Total Δv_{inter}	6.818

6.3 Jupiter Orbit Reduction (JOR)

As we said in Section 6.2.2, after performing JOI maneuver, SPES will effectively be in orbit around Jupiter. In reality this orbit would be a very elongated elliptical orbit, with a periaxis $R_{p,JOI} = 912921$ km and an apoaxis $R_{a,JOI} = 1.92 \cdot 10^7$ km. To simplify our treatment, we took as JOI reference orbit a circular orbit with a radius $R_{JOI} = R_{p,JOI}$. In theory, braking in the periaxis of the elliptical JOI orbit, we could effectively enter in this JOI circular orbit, so this is not an approximation but something that could be effectively achieved. Anyway, in our first approach we will neglect this transition and just assume that our spacecraft JOI orbit is circular from the beginning (further details about this phase are given in Section 6.7).

From this point our purpose is to get closer to Jupiter, and eventually reach the scientific orbit that our spacecraft will perform to gather all the data needed for our mission. Also in this case, we simplified our target to a circular one, with a radius $R_{Eu} = 671476$ km that coincides with the periaxis of our scientific (elliptical) orbit $R_{p,flyby}$ and is very

close to Europa's orbital radius.

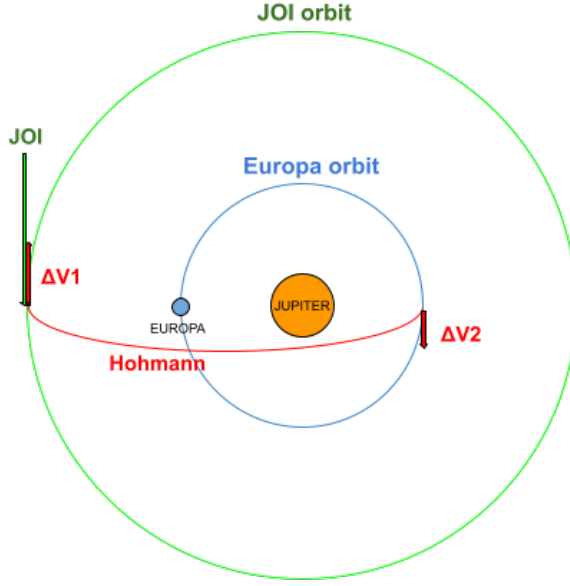


Figure 19: Diagram illustrating the Jupiter Orbit Reduction phase: after JOI, two break maneuvers (in red) are needed to pass (using Hohmann transfer) from the bigger orbit (JOI orbit, in green) to the smaller orbit (Europa orbit, in blue).

To transfer from the bigger circular orbit R_{JOI} to the smaller circular orbit R_{Eu} , we performed an Hohmann transfer in reverse, giving two breaks instead of two boost, in order to reduce the orbital radius, as shown in **Figure 19**. The formula we used are the same shown in Eq. 15, where we just inverted the signs. The results of this transfer are shown in **Table 20**. So the total change in velocity required by this orbital phase is:

$$|\Delta v_{reduction}| = 1.944 \text{ km/s.} \quad (22)$$

The duration of this transfer, calculated using Eq. 17, is $T_{reduction} \sim 2.28$ days.

Table 20: Results showing the total $\Delta v_{reduction}$ that should be provided by the spacecraft, to reduce the orbit around Jupiter from $R_{JOI} = 912921$ km to $R_{Eu} = 671476$ km, using Hohmann transfer.

Orbital maneuver	Δv (km/s)
From $R_{JOI} = 912921$ km to transfer ellipse	-0.935
From transfer ellipse to $R_{Eu} = 671476$ km	-1.009
Total $\Delta v_{reduction}$	-1.944

After reaching the circular orbit R_{Eu} , we should give another boost to our spacecraft to enter our final scientific (elliptical) orbit. Also in this case, we neglected this additional contribute, but a more detailed treatment is given in Section 6.7.

6.4 Multiple Flyby Concept

After having reached Europa, we had to consider the different possibilities we had to satisfy the scientific requirements of our mission.

The first thing we took into account was an Europa orbiter, but as is explained in [28], it is almost impossible to create a mission able to orbit Europa for a long time: in fact, as already mentioned in the beginning of Section 6, the intense magnetic field of Jupiter strongly accelerates ionized particles, creating zones of extremely high radiation reaching up to and even further than Europa's orbit. This means that a spacecraft constantly orbiting Europa would be continuously bombarded by this high radiation particles, and this means it would require a very thick and heavy shielding to survive: this would increase a lot the weight of the payload, translating in more propellant to launch and taking away mass that could be used for scientific instrumentation. In fact, having an heavier spacecraft would decrement the scientific payload mass because of the large increase in the amount of propellant needed to perform the orbital maneuvers needed to take an heavier spacecraft to Europa. Anyway, also a radiation-hardened spacecraft would be able to survive inside the harsh jovian environment just for few months, not enough to satisfy our scientific requirements.

This lead us to take into account a completely different approach, taking as strong reference the upcoming mission Europa Clipper [15], [28] and opting for a multiple flyby mission concept. This translates in a spacecraft that stays in a very large elliptical orbit around Jupiter, with an orbital period of several days, and quickly dips into the harsh radiation environment just for a small period of time, precisely when it is at the perijove of its orbit, and subsequently escapes from it, soon reaching larger distances where radiation is not a problem anymore. One could think that this fast encounter would not leave the time to gather enough data, but this is where the multiple flyby approach comes really into play: repeating the flyby orbit several times, we accumulate an observation time that will eventually match our scientific requests. This multiple flyby approach has different positive aspects:

- we pass only a limited amount of time inside Jupiter radiation environment, and this will allow our electronics to survive for a longer time even without a strong shielding;
- it allows us to divide the orbit in two main phases: flyby phase, where we effectively collect data, and playback phase, in which we are able to downlink data we gathered in the previous phase;
- this 2-phases split provides a margin to react (during playback phase) to any anomaly or discovery that could happen during the flyby phase;
- separating the data collection from the downlink allow us to use much more power in both these phases: during data collection we will be able to use high power instruments without simultaneously operating an high power telecom system, and viceversa;
- in theory, the possibility of changing orbital inclination in each orbit, would allow us to build-up a complex network of Europa flybys, obtaining an almost complete coverage of Europa's surface.

This multiple flyby design is extremely complicated and has a lot of parameters that need a much more detailed treatment that is out of the reach of this course. To simplify our

model, we took a standard and fixed flyby orbit, without changes in orbital inclination and in size: a sketch of this orbit is shown in **Figure 20**. The features of this orbit were chosen taken as a reference one of the several types of orbits that Europa Clipper is planning to perform [28].

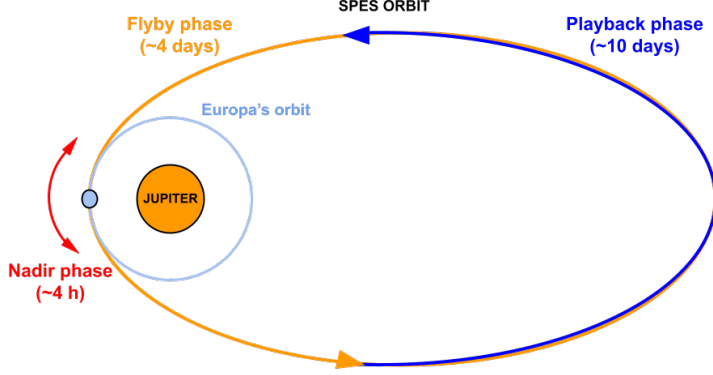


Figure 20: Diagram showing the scientific orbit chosen to study Europa. Europa's orbit is shown in azure. The orange part is the Flyby phase, lasting 4 days. Closest approach is when the majority of data is gathered (Nadir, in red). The blue part is the Playback phase, lasting 10 days, when data will be sent back to Earth.

Our scientific orbit will have a perijove radius $R_{p,flyby} = 671475.8$ km and eccentricity $e = 0.6$. It will have an orbital period $T_{flyby} = 14.2$ days, where the flyby phase will start approximately 2 days before and will end 2 days after the closest approach, that will happen at the perijove of the orbit, at an altitude $h_{close} = 25$ km from Europa's surface. During this phase, instruments will begin to prepare and make episodic observations of Europa, but the main data collection will happen in a 4h period around the closest approach including Nadir observartion by SPUR and image exposure by DragonEye Imager, called Nadir phase. The playback phase will instead last for approximately 10 days and will leave a great margin in time to send back to Earth all data gathered during flyby. The features of the flyby orbit are summarized in **Table 21**.

Table 21: Characteristic of the elliptical flyby orbit chosen for the scientific phase of the mission.

Characteristics of flyby orbit	
Perijove radius $R_{p,flyby}$ (km)	671475.8
Eccentricity	0.6
Period T_{flyby} (days)	14.2
Closest approach h_{close} (km)	25
Total number of flybys	50

This orbit will match quite well the requests we have from the different payload instruments regarding the altitude from Europa's surface and the observation time. We decided that our mission will consist of a total of 50 flybys of Europa, for a total duration of the scientific phase of $T_{science} = 720$ days.

Considering this model orbit, we computed the range of distances from Earth at which our spacecraft will be located both in the case of closest (3.929AU) and furthest approach (6.473AU) between Earth and Jupiter, shown in **Table 22**.

Table 22: Distances between Earth and spacecraft, in the case of closest (3.929AU) and furthest approach (6.473AU) between Earth and Jupiter.

Case	Earth - spacecraft distance (AU)
Closest approach	(3.92 ± 0.02)
Furthest approach	(6.47 ± 0.02)

These values will be useful for the Communication team; it is important to take into account that at furthest approach, Earth and Jupiter are in opposition with respect to the Sun, and this will make communication non-feasible.

It is clear that our treatment is still far from being detailed, since these kind of orbits would not be able to give a complete coverage of the surface of Europa, but it is useful to give a first idea of how we want to proceed. Moreover, a lot of orbital correction will be needed to maintain this kind of orbit, but inspecting [15] we were able to estimate a value for the change in velocity that would be needed during each flyby:

$$|\Delta v_{flyby,i}| = 0.005 \text{ km/s.} \quad (23)$$

This number is very small and, even if multiplied for 50 times, gives a negligible contribute to the total Δv budget.

6.5 End Of Life (EOL)

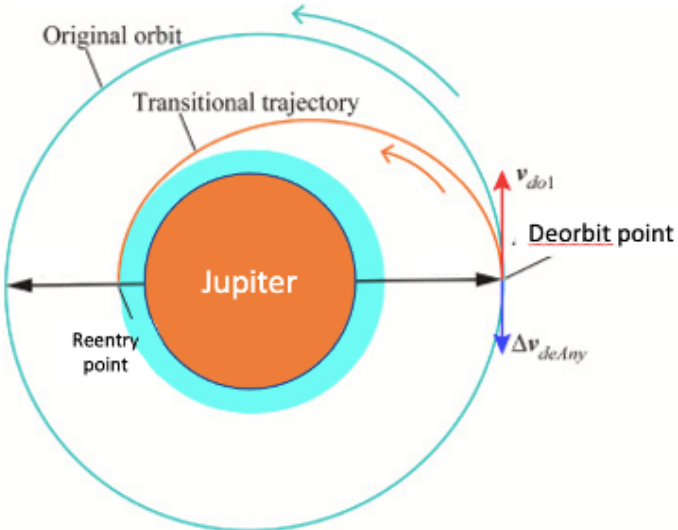


Figure 21: Diagram representing the EOL maneuver, performed via Hohmann transfer from an initial Europa orbit (in blue) to a final orbit that ends inside Jupiter's atmosphere (azure layer around Jupiter), were the atmospheric drag will eventually make SPES crash on the planet.

Since we are looking for a possible habitat on Europa we do not want to crash the spacecraft on one of the other moons of Jupiter because then we would have contaminated them. So for the spacecraft disposal, we chose Jupiter also because we wanted to prevent generating debris in space throughout our orbital lifetime. By using the reverse Hohmann transfer we decided to go from a radius of $R_{p,flyby} = 671476$ km (which is the radius of

Europa orbit) to the disposal radius, at an altitude $h_{disposal} = 10000$ km from Jupiter's surface, via the transfer ellipse as seen in **Figure 21**.

In **Table 23** we can see the Δv needed for going both from the radius or Europa orbit to the transfer ellipse and from the transfer ellipse to the disposal distance from Jupiter, and finally the total one. We arrive at Jupiter's atmosphere and we leave the spacecraft to be under the influence of the drag force, until it crashes on the planet. The total Δv is high, but could be improved by doing Ganymede flybys.

Table 23: Results showing the total Δv_{EOL} that should be provided by the spacecraft, to perform its disposal, crashing inside Jupiter's atmosphere.

Orbital maneuver	Δv (km/s)
From $R_{eu} = 671476$ km to transfer ellipse	-4.497
From transfer ellipse to $h_{disposal} = 10000$ km	-3.654
Total Δv_{EOL}	-7.348

6.6 Total Δv budget

As already mentioned at the beginning of this section, one of the main goals of the Orbital Design subsystem is to find an estimate of the total Δv required for the whole duration of our mission, differentiating between the ones that we want to be provided with the launcher and with the spacecraft. These values are really important cause other subsystems, like structure and propulsion, need them to accurately design the mission. To make things clearer, in **Table 24** we summarized all the different maneuvers required during our mission, indicating for each of them the dates on which we want them to be performed and the module of the Δv required by that specific maneuver.

The first section of the table refers to the launcher, and consists of the maneuver from launching to parking and the one from parking to coasting. This gives a total $\Delta v_{launcher,2} = 12.500$ km/s: based on the chosen launcher this value can either be reached or not.

For what concerns the spacecraft, we proceeded in order to obtain two different results:

- We summed the contribution from the interplanetary (Δv_{inter}) and from the orbit reduction ($\Delta v_{reduction}$) maneuvers, and then we summed to this value the 10% of it, to take into consideration both the contribute from all flybys ($\Delta v_{flyby,TOT}$, shown in **Table 24**) and from all the maneuvers we neglected; we didn't consider the contribution from the End Of Life in this approach Δv_{EOL} ;
- We repeated the same procedures, but adding the contribution of the End Of Life Δv_{EOL} .

The two values we obtained are shown in **Table 25**.

Table 24: Summary of the orbital maneuvers planned for SPES mission: for every maneuver we indicated the date in which they are planned to be performed. Gray rows are values that do not contribute to the total Δv budget, while green cells show total Δv required for a given orbital phase.

Orbital phase	Maneuver	Date	$ \Delta v $ (km/s)
Launch	Launch to parking	01/04/2031	10.408
	From parking to coasting	01/04/2031	2.092
	Total $\Delta v_{\text{launcher},2}$		12.500
Interplanetary	Inserting in hyperbolic orbit	01/04/2031	4.063
	DSM	28/04/2032	1.855
	Earth's flyby	05/06/2033	~ 7
	Ganymede's flyby	01/03/2036	~ 0.4
	JOI (Jupiter orbit insertion)	02/03/2036	0.9
Orbit reduction	Total Δv_{inter}		6.818
	From R_{JOI} to transfer ellipse	02/03/2036	0.935
Science phase	From transfer ellipse to R_{E_u}	05/03/2036	1.009
	Total $\Delta v_{\text{reduction}}$		1.944
	1^{st} flyby	05/03/2036	
EOL	50 th flyby	31/01/2038	
	$\Delta v_{\text{flyby,TOT}}$		0.250
	From R_{E_u} to transfer ellipse	13/02/2038	4.497
Total Δv_{EOL}	From transfer ellipse to h_{disposal}	14/02/2038	3.654
			7.348

It is quite clear that considering or not the End Of Life maneuvers changes a lot the total $\Delta v_{\text{spacecraft}}$, in fact it almost doubles the result. This result is not consistent, and we should be able to find an alternative maneuver for the disposal, in order to reduce the value of Δv_{EOL} to make it in line with the values obtained in the other maneuvers of the mission.

Table 25: Total Δv budget for our spacecraft, with or without considering the End Of Life maneuver.

$\Delta v_{\text{spacecraft}}$ (km/s)
Without Δv_{EOL}
With Δv_{EOL}

6.7 Future Improvements

Some future improvements for our SPES mission could be:

- The orbital design doesn't include a launch window period which should be considered for future developments.

- Studying how Ganymede flybys or any other flyby could reduce our total Δv budget, especially the disposal one, which we saw is high and affects the most our total result.
- Taking into consideration some of the maneuvers we neglected: for example, the maneuvers required to pass from an initially elliptical JOI orbit to the circular orbit considered in Section 6.3, and then also from the circular Europa orbit to the final elliptical orbit which will be used in the scientific part of our mission. The Δv needed for these maneuvers are shown in **Table 26**. The results obtained were quite high, nevertheless in this first order treatment we decided not to include them in the final Δv budget.
- Modeling the flyby orbits in a more accurate way (different sizes and inclinations), to obtain a complete mapping of Europa's surface.
- Developing a precise study of the phasing between Earth and Jupiter, to properly choose the best date for SPES launch.
- Computing the Deep Space Maneuver (DSM) calculations in a more rigorous way.

Table 26: Additional maneuvers that we neglected. Both of them are referred to the Jupiter orbital reduction phase, treated in Section 6.3.

Orbital maneuver	Δv (km/s)	Date
From elliptical JOI to circular JOI	-4.497	02/03/2036
From circular R_{Eu} to flyby orbit	3.654	05/03/2036

7 Communication

This part summarizes the Ka-band capability of SPES and its contribution to Europa flyby activity.

Compared to the X-band, the implementation of the Ka-band is four times more effective, because it increases the directivity of the downlink beam, which theoretically can increase the downlink data rate when assuming the same physical antenna size. The problem is that the telecommunication link of the Ka-band is highly affected by weather conditions (e.g. clouds, wind) at the receiving ground station on Earth.

In this mission, we plan to use two antennas (both of them weighing just 1.16 kg) to send 0.432 GB of data per flyby through the Ka-band. In case the Ka-band is not efficient because of bad weather conditions at the ground stations on Earth, we could always use the X-band signal to send back the data.

7.1 Requirements

According to the design of Payload, we have to send 0.432 GB of data back to the Earth within 10 days, for each flyby. Since the total number of flybys planned by the orbital team is 50, the total amount of data from the payload during the whole mission will be 21.6 GB.

The SPES flyby orbit of Europa is divided into two phases, as explained in Section 6.4: the antennas are expected to send data back to Earth during the so-called Playback phase, which lasts 10 days. During these orbits, the closest distance between Earth and the spacecraft will be 3.9 AU, as explained in **Table 22** and shown in **Figure 20**.

7.2 Antennas

7.2.1 Radial Line Slot Antenna

We show a photo in **Figure 22a** and a structural diagram of a radial line slot antenna, which is used as the mounted high-gain planar antenna of SPES. The two circular conductive plates are simply inserted through the dielectric and constitute a radial line, and input a signal transmitted as a radio wave to the antenna by a coaxial line provided at its centre. Radio waves powered from a coaxial line are radiated from the slot, a number of narrow windows drilled in the upper circular conductor plate, to the outside while propagating through the radial line as cylindrical waves outward [46].

In the telecommunications sector, the radio wave whose direction of the electric field rotates with time (called as the circular polarized wave) is suitable in that the satellite can communicate stably even though its position changes. Setting two orthogonal linear slots staggered by 1/4 of wavelength (called the slot pair), circularly polarized wave will occur like the principle that circular motion occurs by applying a single vibration of the phase difference of 90 degrees to the X-axis and Y-axis [46].

7.2.2 Radial Line Slot Antenna with honeycomb structure

In order to reduce the weight of the radial line slot antenna for the satellite, a radial line was achieved with the honeycomb structure shown in **Figure 22b** [46].

Firstly, we used the X-band antenna at 8.4 GHz. In the actual antenna, the waveguide forms a honeycomb structure, and thousands of slot pair is provided spirally on a circular conductor plate [46].

The honeycomb core is made from a material called Quartz, for which the transmission loss is small. It was revealed in the experiment that the transmission loss of the waveguide of the honeycomb structure was only 0.03 dB per cm. The antenna with a diameter of 92 cm is as light as only 1.16 kg, the gain is 35.9 dBi and the efficiency of the antenna is 58.7%.

Then we used the Ka-band antenna at 32.0 GHz. First, we measured the electromagnetic field distribution in the waveguide by the honeycomb core of the 1/4 inch period like the case of the X-band antenna. This was thought to result from the wavelength at 32.0 GHz decreased to 9.37 mm, and the period of the honeycomb core is too large in 1/4 inch (6.35mm). Therefore, the period of the honeycomb core was reduced to 1/8 inch (3.17mm). However, at that time, Nomex (R) what is larger transmission loss as compared to Quartz was only available as the honeycomb core material of 1/8 inch period. Therefore, the transmission loss of the waveguide of the honeycomb structure raised to 0.16dB per 1cm. Although we were able to achieve the gain of 44.6dB in the antenna with a diameter of 90cm, there was also the loss of 3.7dB [46].

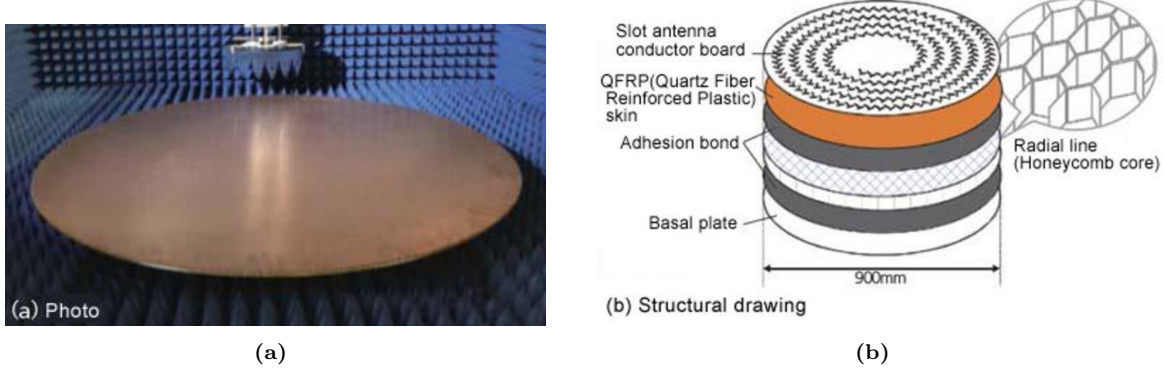


Figure 22: Antenna with honeycomb structure.

7.3 Parameters of HGAs

To obtain the data of the Payload during the mission, we have to take into account the distance of the spacecraft between the spacecraft and the Earth, which is expected to be in the range of 3.9 AU — 6.5 AU. Data downlink from SPES is realized using two high gain antennas (HGAs) which are designated to X-band (8GHz) downlink and Ka-band (32GHz) downlink respectively.

Ka-band telecommunications for deep space missions were initiated by the National Aeronautics and Space Administration (NASA) in the 1990s by Mars Observer, Mars Global Surveyor, Deep Space 1, and Mars Reconnaissance Orbiter [47]. Including more recent activities by Cassini and Kepler missions, NASA's continuous statistical analysis of Ka-band telecommunication over Deep Space Network's (DSN) tracking stations at all three tracking sites (Goldstone, Madrid, Canberra) derived a baseline recommendation for a Ka-band link margin for flight projects [48]-[49]. However, difficulties in the practical application have been also reported [47]-[50].

As shown in **Figures 23, 24, 25**, one of the major updates in SPES is the addition of Ka-band downlink capability including HGA designated to Ka-band. Ka-band transmission signal is generated by converting the frequency of the X-band transmission signal

generated from only one of the X-band transponders [47]. Downlink bitrates for both X/Ka bands have a common range from 8bps to 32Kbps which is restricted by data handling unit designed to be used commonly for both X and Ka-band downlinks. Also, the above bit-rate range fulfils SPES's mission requirement based on a link budget analysis. Detailed RF telecommunication capability and characteristics of SPES are shown respectively in the tables below, taken from [51].

Terms	Contents
X-band	TT&C (Coherent Xup/Xdown) 7GHz uplink, 8GHz downlink 8bps to 32Kbps
Ka-band	Telemetry (Coherent Xup/Kadown) 32GHz downlink 8bps to 32Kbps
Ranging	Transparent Regenerative
DDOR	X band DDOR* supported Ka band DDOR* supported
Transponder	2 X-band Transponders (XTRP) <ul style="list-style-type: none"> Only XTRP1 capable of DOR tone generation X-band transmission signal from XTRP1 can only be converted in terms of frequency to generate Ka-band transmission signal
Antenna	1 X-HGA 1 Ka-HGA

Figure 23: RF telecommunications capability (DDOR: Delta Differential One-way Range).

Channel	Signal	Data/Chip Rate	Modulation and Modulation index	Subcarrier/Tone Frequency	Notes
X-Band Uplink	Command	15.625bps, 125bps, 1000bps	0.3rad ~ 1.4rad	16.0kHz (Sine Wave)	BCH Code
	Ranging Signal	{Subcarrier Freq.}/4 cps		{Uplink Freq.}/2 ¹⁴ Hz (Sine Wave)	Configuration for JAXA Stations
	Ranging Tone	-		516.6kHz (Square Wave)	Configuration for NASA/DSN Stations
X/Ka-Band Downlink	Telemetry	2 ⁿ bps (n=3,4,5.....,10)	0.3rad ~ 1.5rad (0.05rad pitch) PM	8.192kHz (Square Wave)	Concatenated Code (with interleaving)
		2 ⁿ bps (n=11,12,13.....,15)		262.144kHz (Square Wave)	
	Ranging Signal	{Subcarrier Freq.}/4 cps		{Uplink Freq.}/2 ¹⁴ Hz (Sine Wave)	Configuration for JAXA Stations
	Ranging Tone	-		516.6kHz (Square Wave)	Configuration for NASA/DSN Stations
DDOR Tone	-		0.3rad, 0.55rad	0.5Fo, 2.0Fo	Differential Doppler One-way Ranging

Figure 24: RF telecommunications characteristics.

Antenna	Gain* [dBi]	Efficiency [%]	Antenna Type
KaHGA	44.2	27.6	Radial line slot antenna with honeycomb
XHGA	35.3	51.3	waveguide

Figure 25: Antenna gain and aperture efficiency of HGAs. Values for antenna gain were measured relative to coaxial cable input.

Ka-band downlink is established with the aid of NASA's DSN tracking stations located in each deep space communications complex (DSCC) at Canberra (CDSCC), Goldstone

(GDSCC), and Madrid (MDSCC). Also, SPES has a framework of cooperation with ESA's deep space tracking stations (Cebreros, Malarugue) which equips the Ka-band reception facility. This paper covers Ka-band operation results using DSN stations, and therefore, DSN stations compatible with SPES Ka-band downlink are summarized on **Figure 26**, taken from [51].

Site (Complex)	Tracking Stations	Notes
Goldstone (GDSCC)	DSS-25 DSS-26	34m-BWG ¹³⁾
Madrid (MDSCC)	DSS-54 DSS-55	34m-BWG ¹³⁾
Canberra (CDSCC)	DSS-34 DSS-35 DSS-36	34m-BWG ¹³⁾

Figure 26: DSN stations compatible for Ka-band downlink.

7.4 Links and Power budget

Link budget equations are given as follows:

$$\frac{C}{N_0} = P_{TX} + L_{FTX} + G_{ATX} + L_{APTX} + L_d + L_f + L_{RA} + L_V + G_{ARX} + L_A + L_{FRX} + L_{APRX} - T_{op} - k_0 \quad (24)$$

where:

- C/N_0 : the Signal Reception Level over Noise Density [dBHz]
- P_{TX} : TX Power [dBm]
- L_{FTX} : TX Line Loss [dB]
- G_{ATX} : Antenna Gain [dBi]
- L_{APTX} : TX Off Pointing Loss [dB]
- L_d : Free Space Loss [dB]
- L_f : Polarization Loss [dB]
- L_{RA} : Precipitation Loss [dB]
- L_V : Other Loss [dB]
- G_{ARX} : RX Antenna Gain [dBi]
- L_A : Atmospheric Attenuation Loss [dB]
- L_{FRX} : RX Line Loss [dB]
- L_{APRX} : RX Off Pointing Loss [dB]
- T_{op} : System Noise Temperature [dBK]
- k_0 : Boltzmann Constant (-198.6) [dBm/K/Hz]

In this calculation, the following assumptions are made: nominal spacecraft parameters (TX power = 43.9 [dBm], TX line loss = -1.2 [dB], TX antenna Gain=43.7 [dBi]) at nominal operational conditions are selected.

7.5 Earth Direction Variation and Off-Beam Loss

As shown in **Figure 27**, the change rate of Earth's direction varies from 0.73 deg/day to 1.06 deg/day. When assuming 8 hours tracking pass, since the target attitude epoch of the daily attitude manoeuvre is set to the centre of the Ka-band downlink tracking pass, the previous value corresponds to approximately 0.12 deg and 0.18 deg of maximum off-beam angle expected at AOS and LOS of the tracking pass [51]. Since these off-beam angles correspond to 0.5 dB and 1.0 dB off-beam loss for Ka-HGA, adding another Earth pointing attitude manoeuvre during the tracking pass may save more than 0.5 dB off-beam loss depending on the orbital geometry [51].

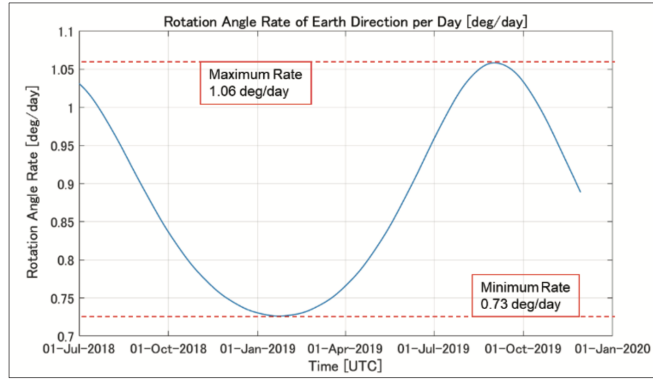


Figure 27: Change rate of Earth's rotation.

8 Thermal Control

The thermal control subsystem is responsible for keeping the temperature of the space-craft in the range defined by its instruments, in order to make them all operate without malfunctions, and to minimize the components' deformations that can occur due to thermal expansion. The first goal can be achieved with two opposite methods:

- **Passive control:** devices that don't need a power supply, such as surface finishes or radiators. They are relatively easy to design and build, reliable and cheap, but they are less flexible, they can have limited performances and, on average, they have larger areas;
- **Active control:** devices that need a power supply, such as heaters or coolers. When compared to passive devices, they usually have better performances and they are more flexible because they can be designed to satisfy specific requirements, however, they are more complex to design and build, less reliable and more expensive.

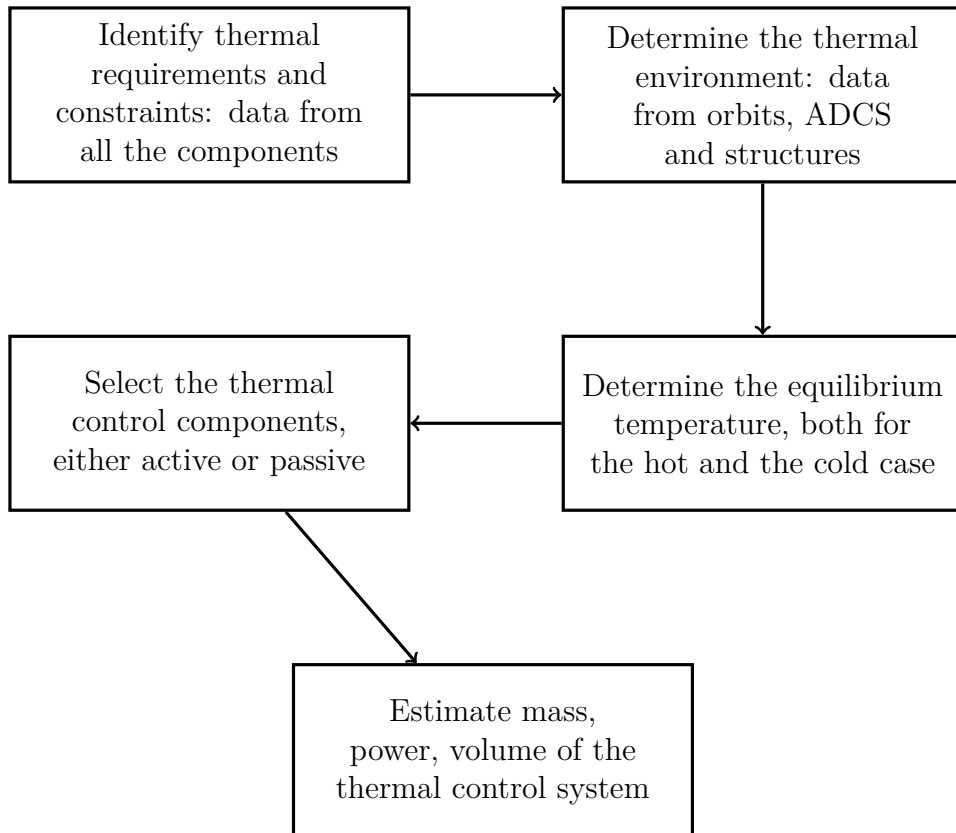


Figure 28: Design process of the thermal control subsystem (based on [8]).

8.1 Heat Sources

When considering a spacecraft travelling in space, since there can be no convection, the only way for it to exchange heat is via radiation or conduction. The latter is considered mainly for internal heat exchanges between the different interfaces of the spacecraft, while radiation is the dominant mechanism for the external exchanges. There can be several sources of heating in space, as we can see from **Figure 29**. The most important ones are:

- a) **Sun irradiance** (J_{sun}): the Sun is one of the main sources of heating when dealing with thermal control. The amount of heat absorbed by the spacecraft depends on the solar flux, which is determined by the distance to the Sun, the surface area viewing the Sun, and the solar absorptivity of that surface [52]. The value of J_{sun} can change during the year, but we will take into account an average value.
- b) **Albedo** (J_a) from nearby planets or moons: it is the fraction of incident sunlight that is reflected by the surface of the planet. The albedo can be easily estimated as $J_a = aJ_{sun}$, where a is the albedo coefficient. More accurate computations would require taking into account the visibility factor F , which is a function of the inclination angle of the spacecraft with respect to the incoming radiation and it is usually between 0 and 1, but in the present work, we will assume it as 1 to simplify the computations.
- c) **Infrared radiation** (J_{IR}) from nearby planets or moons: every planet emits a certain amount of radiation in the infrared band, due to the fact that we can associate them an infrared temperature from the Stefan-Boltzmann law. That infrared radiation is strongly dependent on the altitude of the spacecraft with respect to the surface of the planet, following the law:

$$J_{IR} = \left(\frac{R_{planet}}{R_{planet} + h} \right)^2 \sigma T_{planet}^4 \quad (25)$$

- d) **Internal heating** (P): all instruments, when operating, also produce heat that can change the temperature of the spacecraft. We can take into account this effect if the efficiency η of the instrument is provided: $(1-\eta)$ times the power consumption is transformed into heat.

The heat depends on the flux, the area which absorbs or emits and the coefficient of absorptivity α or emissivity ε , which are defined by the material that the surface exposed to the radiation is made of:

- emitted heat $Q_e = \sigma T^4 \varepsilon A_e$;
- solar heat $Q_{sun} = J_{sun} \alpha A_a$;
- albedo heat $Q_{alb} = J_{alb} \alpha A_a$;
- infrared heat $Q_{IR} = J_{IR} \varepsilon A_a$
($\alpha = \varepsilon$ in IR band);
- internal heat: $Q_{int} = P$.

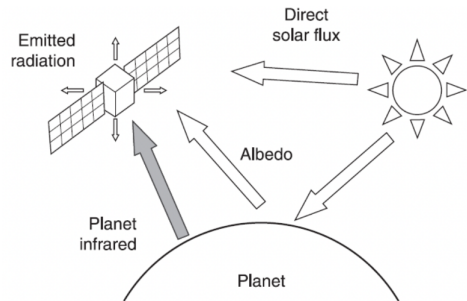


Figure 29: Sketch of heat sources.

8.2 Requirements

Thermal control subsystem must:

- keep all the components within their operational range during the activities;
- keep all the components within their survival range when they are not operating;
- work for the whole mission lifetime;
- prefer passive components over the active ones.

Table 27: Temperature ranges for every instrument of each subsystem.

Subsystem	Instrument	Phase	T_{min} (K)	T_{max} (K)
PAYLOAD	Camera	Operating	283	303
		Survival	253	343
	Spectrometer		<194 (best at 100 K)	
		Design	153	373
	X Antenna	Acceptance	148	378
		Qualification	143	383
EPS	PDU		238	358
CDHS	Microprocessor		233	398
			273	343
ADCS	Sun sensor		248	343
		IMU	228	333
			218	343
COMMS	Antenna	Operating	243	303
		Non-operating	243	318

The lower limit for the temperature range of the spacecraft is defined by the highest T_{min} , 283 K in this case, while the upper limit is defined by the lowest T_{max} , 303 K. This range is completely defined by the camera and must be kept for the whole spacecraft to correctly operate. We decided to treat the spectrometer separately since it must operate below 194 K and this value is way out of range with respect to the other instruments. The solution for its thermal control is discussed in Section 8.3.2.

8.3 Thermal Analysis

For the thermal analysis of SPES, we adopted a single-node model to simplify the treatment. This means we only take into account how the spacecraft and its instruments interact with the environment, ignoring the thermal behaviour of the internal interfaces and all the possible thermal gradients that could be present. With this, it's possible to find the average equilibrium temperature of the spacecraft in different situations, such as the cold case and hot case. To improve the accuracy of the thermal control, one could proceed with a higher-order analysis to include all the components that have been ignored.

To determine the equilibrium temperature of the spacecraft one must consider all the heat sources that can influence it and balance the emitted and absorbed radiation:

$$Q_e = Q_{abs} \quad \longrightarrow \quad Q_e = Q_{sun} + Q_{alb} + Q_{IR} + Q_{int} \quad (26)$$

(26) changes depending on the environmental conditions: one must discriminate between hot case and cold case. In the first one, all the sources (direct flux from the Sun, albedo and infrared radiation from the planet or moon, internal heating) must be considered; in the latter, the spacecraft doesn't receive the direct flux from the Sun and it's eclipsed by the planet it is orbiting around, meaning we only include the internal heating of the instruments (because they are on even during eclipses) and the infrared radiation. For SPES, since the planned duration of the journey to Europa is around five years, we decided to divide the thermal analysis of the travel phase, itself sub-divided into the fly-by phase around Earth and the approach of Jupiter, and the one related to the proper mission around Europa. For the travel phase around Earth, (26) becomes

$$\varepsilon\sigma T^4 A_e = (J_{Sun,Earth} + J_{a,Earth})\alpha A_a + J_{IR,Earth}\varepsilon A_a + P \quad (27)$$

for the hot case, and

$$\varepsilon\sigma T^4 A_e = J_{IR,Earth}\varepsilon A_a + P \quad (28)$$

for the cold case. Earth's important parameters, such as the albedo factor, the infrared temperature and the solar flux, have been recovered from NASA fact sheet [53], while the distance from the surface ($d_E \simeq 6622$ km) has been provided by the Orbital Design team. Instead, for the phase when the spacecraft approaches Jupiter, (26) becomes

$$\varepsilon\sigma T^4 A_e = (J_{Sun,Jup} + J_{a,Jup})\alpha A_a + J_{IR,Jup}\varepsilon A_a + P \quad (29)$$

in the hot case, and

$$\varepsilon\sigma T^4 A_e = J_{IR,Jup}\varepsilon A_a + P \quad (30)$$

in the cold case. As in the previous case, the important parameters have been recovered from NASA fact sheet [54] (the temperature was obtained from [55] because the value of the fact sheet wasn't updated), while the distance from the surface ($d_J \simeq 599327.4$ km) has been provided by the Orbital Design team.

When the spacecraft starts doing fly-bys around Europa, there is also Jupiter's influence on the thermal balance. (26) becomes

$$\varepsilon\sigma T^4 A_e = (J_{Sun,Jup} + J_{a,Europe} + J_{a,Jup})\alpha A_a + (J_{IR,Jup} + J_{IR,Europe})\varepsilon A_a + P \quad (31)$$

for the hot case (**Figure 30a**), and

$$\varepsilon\sigma T^4 A_e = J_{IR,Europe}\varepsilon A_a + P \quad (32)$$

for the cold case (**Figure 30b**). Europa's parameters have been recovered from NASA fact sheet [56] and from [57]. We considered an altitude of the spacecraft of 25 km with respect to the surface, provided by the Orbital Design team.

For all the computations, the internal heating P was approximated as the one of the RTG only, since it provides around 1.6 kW of dissipated power (section 10.3.4), which is much higher than the one of all the other instruments put together.

For what concerns the absorbing and emitting areas, given the shape and dimensions of the spacecraft decide by the Structures team, we assumed as A_e the total area of the structure ($A_e = 2\pi r^2 + 2\pi rh$) and for A_a we considered one of the two bases of the cylinder because the area is bigger than its lateral surface ($A_a = \pi r^2$).

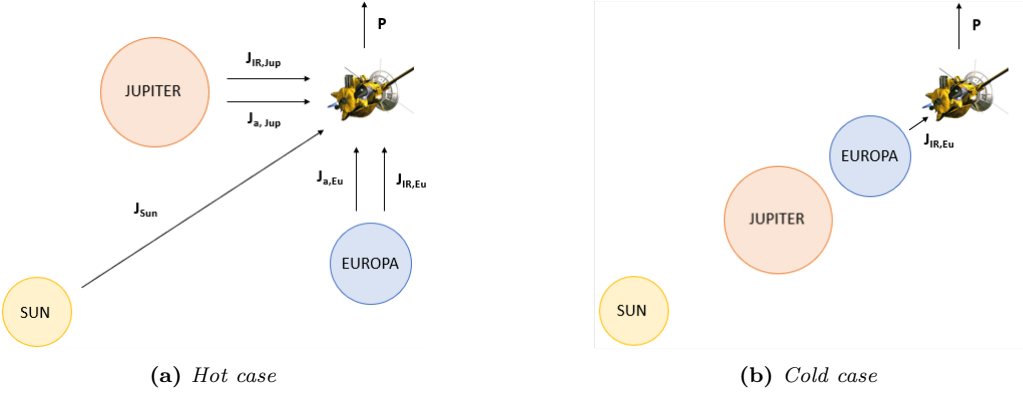


Figure 30: Graphic representation of heating sources while flying around Europa.

8.3.1 Results

The results of previous computations are reported in **Table 28**. We have chosen four coatings to cover our spacecraft, one black paint, one white paint and two metallic coatings, to understand what could be the best solution. The values of absorptivity and emissivity were taken from NASA's reference table [58].

Table 28: Equilibrium temperatures for the selected coatings; in red are shown the ones that exceed the limit for T_{max} , in blue the ones that exceed the limit for T_{min} .

(a) T_{eq} with black paint.

Pyramil black on Be-Cu ($\alpha = 0.92$, $\varepsilon = 0.72$)			
	TRAVEL	EUROPA	
	Earth	Jupiter	$h=25\text{ km}$
HOT (K)	332.97	198.69	205.53
COLD (K)	192.30	181.97	182.60

(b) T_{eq} with white paint.

SW white F8W2030 ($\alpha = 0.39$, $\varepsilon = 0.82$)			
	TRAVEL	EUROPA	
	Earth	Jupiter	$h=25\text{ km}$
HOT (K)	269.82	183.55	187.26
COLD (K)	187.42	176.16	176.85

(c) T_{eq} with stainless steel coating.

Stainless steel machine rolled ($\alpha = 0.39$, $\varepsilon = 0.11$)			
	TRAVEL	EUROPA	
	Earth	Jupiter	$h=25\text{ km}$
HOT (K)	440.78	303.16	308.38
COLD (K)	293.66	290.95	291.10

(d) T_{eq} with titanium coating.

Titanium ($\alpha = 0.52$, $\varepsilon = 0.12$)			
	TRAVEL	EUROPA	
	Earth	Jupiter	$h=25\text{ km}$
HOT (K)	457.71	300.32	306.81
COLD (K)	287.58	284.69	284.85

As we can see from **Tables 28a** and **28b**, both black and white paints are not suitable for our mission, since they provide too low temperatures compared to our required range. From now on, we will exclude them from our analysis.

In the case of the two metallic coatings, the temperatures are always inside the requirements. The hot-case value for Europa, actually, doesn't satisfy them, but this is not an issue: since we are only providing a first-order analysis, all the values we have found are affected by moderate uncertainties. If this problem is present also after a second-order analysis, then it must be corrected and a possible way could be to use, for example, thermal straps to transfer the excessive heat from the camera and the antenna (that both have a maximum operating temperature 303 K) towards other instruments that can handle slightly higher temperatures. Another problem that must be faced by the thermal control system, for both titanium and stainless steel coatings, is the hot-case temperature during the fly-by phase around Earth. This value is outside of the survival temperature range of all the instruments, given by 273-318 K (**Table 27**): even if the instruments are switched off, the temperature would be too high for survival. A possible solution can be Titanium water heat pipes, a passive thermal control system which works at 400 K and weighs around 0.73 kg (see [59]). Since these pipes are in the developing phase, we don't have enough data yet to do a complete thermal analysis, but for sure their final aim matches ours since they will dissipate power in the order of kW.

8.3.2 Thermal Control of the Spectrometer

As indicated in **Table 27**, the spectrometer must be kept at temperatures lower than 194 K, with the best performances at 100 K. These temperatures are much higher than the chosen operational range and the instrument must be cooled down. For reasons of power requirements and reliability, we decided to use a passive component to keep the spectrometer in its operational range and, in particular, we chose a radiator. Radiators are typically used for cooling detectors, cooling electronics, and thermal shielding, they are cheap and they can have small volumes. The model we chose is Miniature Satellite Energy-Regulating (MiSER) (**Figure 31**), which is a flat and small radiator (**Table 29**).

Dimensions (cm ³)	88.65
Radiator mass (g)	120
Life cycles (tested)	> 10 ⁵
Operating temperatures (°C)	-130 to +100
Maximum power dissipated (W)	12

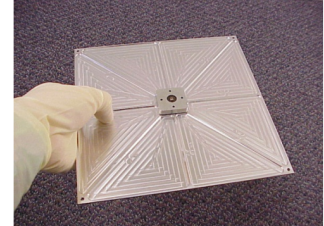


Table 29: Main properties of MiSER radiator, from the data sheet [16].

Figure 31: MiSER by Sierra Nevada Corporation.

We computed the range of power that the radiator should dissipate by using the equation

$$P_{diss} = \sigma\epsilon A_{spec}(T_{S/C}^4 - T_{spec}^4) \quad (33)$$

where $T_{spec}=100$ K. We considered the two components of the spectrometer, the DPU and SU, separately and then added the contributions to find the total value. For A_{spec} we considered the largest area for both components. The computations have been carried out for the stainless steel and the titanium coatings only, and to determine a range of power that must be dissipated, we considered the highest and the lowest temperatures of **Tables 28c** and **28d**. The result for the stainless steel coating is $5.06 \text{ W} \leq P_{diss} \leq 26.96 \text{ W}$. This means, in the worst-case scenario, we need three MiSER radiators to cool the spectrometer down. For titanium, instead, we found $5.05 \text{ W} \leq P_{diss} \leq 34.21 \text{ W}$: also in this case, three radiators are required.

8.4 Temperature Sensor

An additional component of the thermal control system is the temperature sensor, which is needed to track the temperature of every component and communicate to the onboard computer. These sensors are active components, but since they consume a small amount of power (of the order of mW or lower) they can be neglected for the power budget. The model chosen for SPES is Series 44 Cryogenic Temperature Probe (**Figure 32**), which is a temperature sensor with a very small power requirement (**Table 30**).

Table 30: Main properties of the sensor from the data sheet [17].

Operating temperatures (°C)	-40 to 200
Resistance (Ω)	200 ± 1.0
Operating current (mA)	1
Temperature accuracy (°C)	±1.28
Required power (W)	0.065



Figure 32: Series 44 Cryogenic Temperature Probe by Scientific Instruments.

8.5 Mass and Power Budget

Table 31: Mass and power budget of each instrument used for thermal control.

*Heat pipes are not completely defined in terms of unit number.

Instrument	Unit number	Mass (kg)	Power consumption (W)
Radiator	3	0.36	-
Temperature sensor	1	<0.15	-
Heat pipes*	1	0.73	-
TOTAL	5	1.24	-

9 Command and Data-Handling Systems

Command and data handling subsystem (CDHs) is responsible for performing onboard operations and controlling all internal communication between different subsystems. The design of CDHs is generally divided into three sections, hardware, software, and electronic protection. The foremost design for hardware is on-board computer (OBC). OS Architecture and functioning, operation modes, housekeeping data calculation, and memory estimation are included in software design. In particular, electronic protection needs to be discussed in both hardware and software.

In **Figure 33** the global architecture of SPES OBC is presented. The whole subsystems include external memory and all other subsystems connect to the OBC directly. The reasons will be discussed later in the paper.

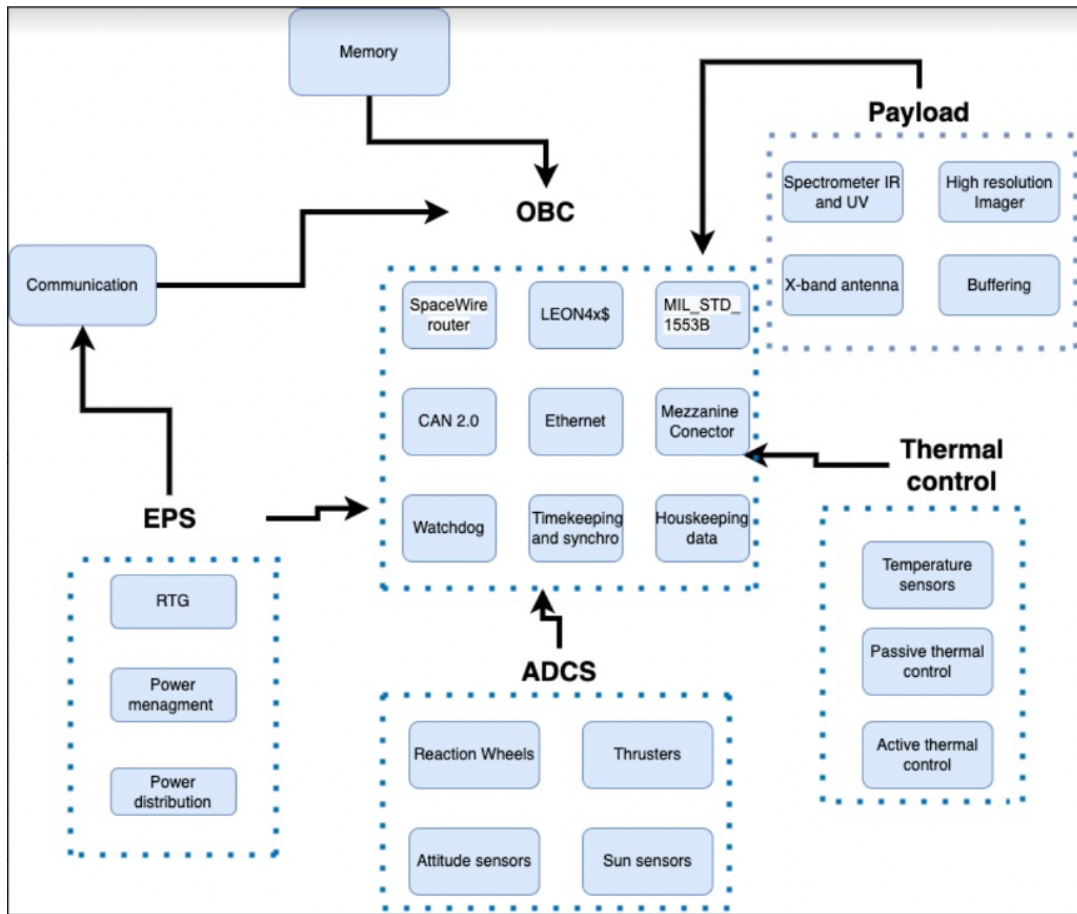


Figure 33: The final architecture of CDHs. On-board Computer connected with all subsystems architecture

9.1 Requirements

In **Table 32** and **Table 33** we present the requirements for the components inside CDHs subsystem and also the requirements from other subsystems.

Table 32: CDHs requirements for hardware and software.

ID	Requirement	Rationale	Component
PL.01	Strong parallel computation capability, multi-core processing expected	Complexity of the task processing during the mission	OBC
PL.02	Relatively low power consumption, acceptable value no more than 10W	Limited power supply and the expectation of technology development from the older OBC	OBC
PL.03	Strong radiation protection ability with TID threshold > 100k rad	The space environment of Europa which is embedded inside the Jovian magnetospheric plasma	Circuit and Software

Table 33: CDHs requirements from other subsystems.

ID	Requirement	Rationale	Subsystem
PL.EPS	Different modes inside nominal mode which allow instruments working alternatively	Limited power supply but long lifetime expectation	EPS
PL.ADC	Task processing from ADCs system for attitude control	Integrated processing with high efficiency	ADCs
PL.Pa	MIL-1553 bus and other multiple types of interface connections	Different instruments can use different connections	Payload

9.2 On-Board Computer Selection

As the heart of the CDHs system, OBC (On-Board Computer) runs all software for on-board operation control, as well as receiving, interpreting, and executing the operation commands from the ground station. The selection requirements for OBC are to be efficient, small, lightweight, and easy to integrate with all of the other subsystems. Generally, OBC can be a micro-controller or multi-core/single-core microprocessor. A simple comparison between two types of OBC is shown in **Table 34**. Since the task processing of Europa missions is complicated including observation control, energy control, altitude control, etc., SPES uses a multi-core microprocessor instead of several micro-controllers. Moreover, with the development of technology, the power consumption and total mass of microprocessors have been significantly reduced. In the case of GR740, the overall power

consumption is around 1.8W and the GR740 is 1.2 kg, which is much less compared to other microprocessors.

Following the JUICE missions to Europa (**Table 35**), LEON-4 processor, as the latest applicable version from LEON chip family developed by ESA, is selected for our mission due to its low power consumption and strong computation processing ability [60]. Therefore, most operation tasks will be sent and handled directly by the OBC without using particular micro-controllers in other subsystems such as ADCs, in order to reduce the mass and power consumption.

Table 34: A simple trade-off between microprocessor and micro-controller.

	Microprocessor	Microcontroller
Processing capability (Computation Power)	The fastest general computing platform; good at arithmetic operations and logic operations	Weaker than microprocessors in general; cannot handle multiple tasks
Power Consumption	1.8W for GR740	<1W
Size and Weight	Heavier in general (1.2kg for GR740)	Light
Memory and Peripherals	Requires external work memory and data bus controllers	Memory integrated
Cost	More expensive than microcontrollers in general	As expensive as the components featured in the chip

Table 35: The OBC examples for several space missions.

Examples of Onboard Computers

Spacecraft	Type	Environment	Launch Year	Onboard Computer
International Space Station	Space Station	LEO	1998	Intel 386 (rad-hard)
Spirit & Opportunity	Rover	Mars surface	2003	BAE RAD6000
Delfi-C3 & Delfi-n3Xt	CubeSats	LEO	2008 & 2013	MSP430
GOCE	Satellite	LEO	2009	ERC 32
JUICE	Satellite	Jupiter Moon	2020	LEON 2
Ariane 6	Launch Vehicle	LEO/GEO	2020	LEON 3 (?)

GR740 is the selected OBC that will be used on the SPES spacecraft. It is a 4-core microprocessor ASIC device based on the LEON4-FT processor core and the European Next Generation Microprocessor (NGMP) architecture designed by Cobham Gaisler[60]. It has a radiation-hardened circuit design and integrates a SpaceWire router with four internal ports and eight external ports with multiple interfaces (Ethernet, PCI, MIL-1553, etc.). The block diagram for this microprocessor is presented in **Figure 34**. In terms of the development board, the chosen one is GR-VPX-GR740, its specifics can be found in ref.[61]. It has been designed to support the development and fast prototyping of systems based on GR740, the selected quad-core 32-bit fault-tolerant LEON4FT SPARC V8 processor. In addition, it has a high-performance Single-Board Computer for use within OpenVPX and SpaceVPX environments. The board is developed to be used as a Switch Module in the OpenVPX architecture based on ANSI/VITA 65.0-2017. It can also be ordered as a factory-configured variant with the backplane interface designed as a Switch and Controller Module providing some of the features of the SpaceVPX architecture specified in the Draft ANSI/VITA 78.00-2015. Therefore, the board offers two factory-configured variants, which the difference is related to the pinout of the P1 connector for the Control Plane also backplane type:

- GR-VPX-GR740-OX: OpenVPX, as per Switch Slot Profile SLT6- SWH-16U20F-10.4.2, compatible with backplane BKP6-CEN05-11.2.5.
- GR-VPX-GR740-SX: SpaceVPX, as per Switch and Controller Slot Profile SLT6- SWC- 16T12F12U-10.4.1, compatible to backplane BKP6-CEN9-11.2.5 (not validated in a backplane).

SpaceVPX is chosen because the failure tolerance is significantly improved from Open-VPX and its primary goal is to cost-effectively remove bandwidth as a constrain for future space systems. The design and the architecture of GR-VPX-GR740 are shown in **Figure 35a** and **Figure 35b**.

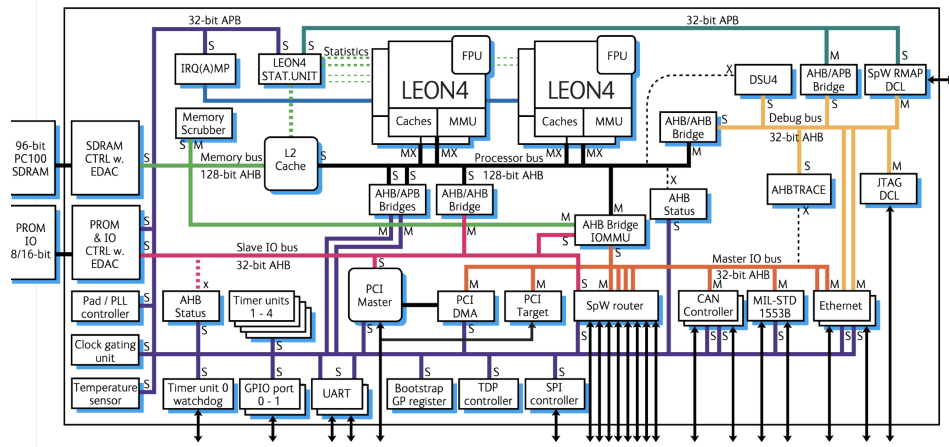
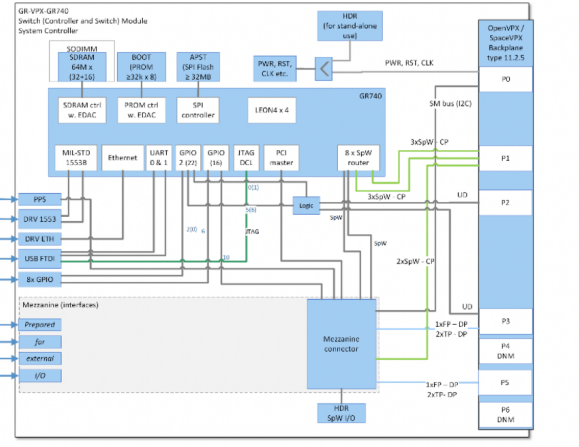


Figure 34: The block diagram of GR740.



(a) GR-VPX-GR740 design



(b) GR-VPX-GR740 architecture with OpenVPX and SpaceVPX backplane type

Figure 35: GR-VPX-GR740 design and architecture including Mezzanine board.

9.3 Software and Data Handling

9.3.1 Operation Modes

Before discussing the global functions of the software the operation modes for OBC should be designed first. In SPES mission, six different operation modes are included so far to allow the spacecraft to work properly in a variety of situations. Operation modes can be adjusted in the future based on further requirements from other subsystems.

- Nominal (N): Standard operations are implemented including thermal control, attitude monitoring, housekeeping data processing, and communication with other subsystems;
- Safe (S): All other subsystems will be shut down smoothly except EPS. The computer will then try to recover again based on the EPS data and/or FDIR report;
- Thrift (T): Energy saving when the energy supply or propulsion is at a low level.
- Traveling (R): When the spacecraft is in travelling to Europa, the payload is shut down in order to save energy. Data from navigation and ADCs will be transferred and handled by OBC in priority;
- Data Downlink (DD): The OBC sends the data stored through the communication system to the ground station;
- Failure Detection, isolation, and Recovery (FDIR): OBC will try to detect soft failures in subsystems such as data bus lockup or anomalous behavior of the software. Then it will try to recover or isolate the subsystem.

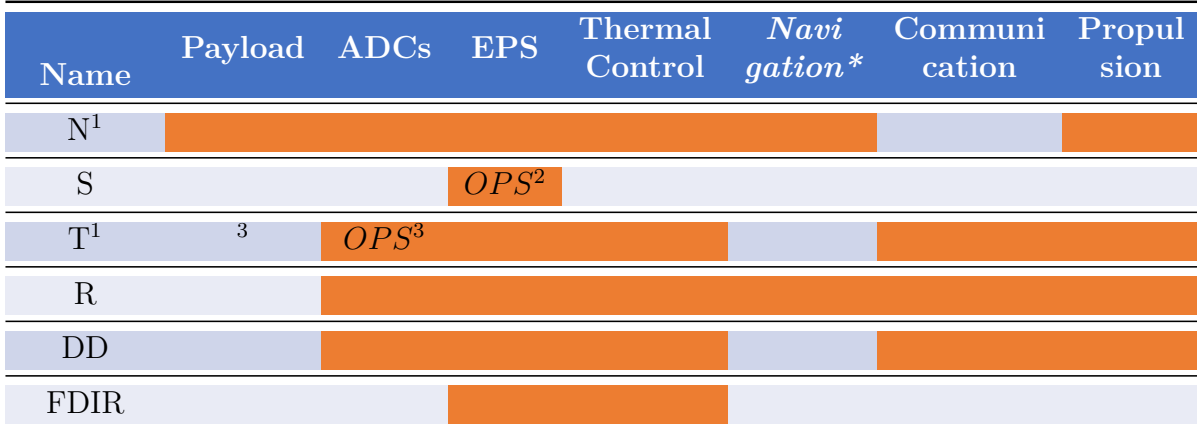
In each mode, different subsystems are active as shown in **Table 37**. Comments represented by the superscripts on this table are described below:

- 1 The power supply can maintain at this level for around one year and a half. Following the graceful degradation strategy, scientific instruments SPUR and DragonEye camera are expected to turn on and work alternatively after the power supply decreases to 118.315 W, which means only one instrument is active in one flyby. Therefore, the nominal mode can include two sub-modes that are active for different power ranges, as shown in **Table 36**;
- 2 In safe mode, EPS only supplies the On-board Computer;
- 3 For the payload in Thrift mode, OBC will shut down the camera at first due to the high power consumption as described in **Table 36**, then the spectrometer, then the radio antenna. After closing the radio antenna XAO, ADCs stops responding to the requirement from the payload but continue to respond to communication requirements.

Table 36: Based on the power values provided in Table 45, two sub-modes are included in the nominal mode.

Name	Power Condition	Opening Scientific Instrument
N0	>118.315 W	SPUR + Dragon Eye + XAO all instruments acquire data during flyby
N1	93.315 - 118.315 W	SPUR and DragonEye work alternately, XAO keep working
T	<93.315 W	DragonEye shut down, change to Thrift mode

Table 37: Working subsystems are marked with orange colors. OPS means opening with a strategy.



9.3.2 Software Architecture and Global Functions

The operating system (OS) for On-board system is based on Linux due to its high flexibility for programming. The software running on-board is expected to follow two partitioning functions as Europa's Clipper [62]: time partitioning and space partitioning. Space partitioning handles the division of memory into isolated activities that enhance the execution robustness of critical software functions without interruptions by lower-priority activities.

Meanwhile, time partitioning running for the OS can schedule multiple threads and processes in order to enhance the predictability of the software execution over time. Besides, the on-board software is expected to include primary functions as follows:

- Mode changing for the subsystems;
- Payload data compression and storage;
- Housekeeping data calculation, interpretation, and storage;
- Attitude calculation, monitoring, and changing;
- Radiation level monitoring and FDIR.

9.3.3 Housekeeping Data Estimation

The OBC also sends packets of housekeeping data to the ground station. Housekeeping data is calculated by adding all information from all subsystems which want to send information to Earth by downlink. Housekeeping data is given by

$$\text{Housekeeping data} = \text{Parameters} \times \frac{\text{measurements}}{\text{second}} \times \frac{\text{bits}}{\text{measurement}} \times \text{measurement duration}$$

where the parameters can be the number of sensors or batteries of each subsystem that operate in a certain frequency described by Hz/s (in the equation is the measurements per second) and by bits representatives (bits measurements). The measurement duration is 24 hours a day in terms of seconds. Then by summing together the Housekeeping data (in bits per day) and the Payload data (in bits per day) which was calculated by the three different instruments, the summation will be divided by the time when we want to send data on Earth. Based on the [62] the downlink communication window is during the Playback phase, which is approximately 10 days. In this way we obtain the *Total data rate* in bits per second sent to earth. From two instruments of the payload (DragonEye Imager and SPUR), we had 864Mb/day for the camera and 300Mb/day for the spectrometer that wanted to send data to Earth. So taking the 10 percent of the summation of both we get housekeeping data of 116Mb/day . The total data rate send to Earth then is 1280Mb/day and to get bits/s we should divide it by how many times per day and for how many seconds we want to communicate these to Earth.

In addition, it's still not clear to decide the amount of radio data, but it could be a very small contribution in the total data. We temporally neglect the data from the antenna and provide this value as a rough estimation of the housekeeping data.

9.4 Failure Mitigation and Electronic Protection

The main failures for spacecraft are:

- Software bugs and electrical design flaws: These errors are human errors.
- Radiation impact and damage: The error is caused by the impact of high energy plasma from space, and is the major problem to deal with in electronic protection.
- Mechanical damage: This error can result in extreme vibrations in launch or impact by a micrometeorite or other objects.

- Thermal-electrical and thermal-mechanical stress: These effects that can damage instruments and electronics are the result of an overwhelming thermal environment in space.

In particular, radiation effect can be roughly classified into three types: charging, ionization and single event effects, different strategy need to be applied for each type of effect:

- Charging: A build-up of electrons can occur at the time of prevention for the flow of electrons by the insulator. This is referred to as charging and can create an extra voltage potential resulting in biasing of transistors. This issue can be avoided with a good grounding of the body.
- Ionization: The ionization effect is a cumulative effect, which means it can become a vital problem for spacecraft after several years of working. Ionization occurs when the atoms or molecules within the electronics lose or gain an electron as a result of impact with a radiation particle from such as cosmic rays or the solar wind. A strong shielding structure and radiation-hardened technology for circuits are the main methods to prevent ionization damage. The measurement to quantify ionization is the total ionization dose (TID), which can be expressed by the absorbed radiation dose of the material (unit: rad).
- Single event effects (SEEs): The effect occurs immediately after the impact of high-energy particles. SEE can cause a logic change in software and then result in a permanent bit-flip for memory or software. In addition, the releasing energy from the impacting particle can also cause a short circuit. Hence special software and operation mode for detection are needed.

Radiation damage, software bugs and electrical design flaws are highly relevant to CDHs subsystem. Therefore, it is crucial to have a few designs both for hardware and software to prevent, mitigate or address the failures.

9.4.1 Hardware Design for protection

Four methods are discussed in SPES mission, redundancy and radiation harden for circuits, timekeeping instrument for OBC and shielding for the whole structure.

1. Redundancy: The whole hardware system consists of two strings as for redundancy, a prime and a backup. Each string includes the same onboard computer, external memory, and other components.
2. Timekeeping Instrument: Use of clock multipliers to create the system clock, memory interface clock, and the SpaceWire transmitter clock. So in GR740 we have a clock multiplexing.
3. Shielding: Proper shielding can significantly reduce TID and extend the lifetime of electronics. The selection of shielding material and thickness is done by the structure subsystem.
4. Radiation-hardened technology: As the state-of-the-art radiation-hardened ASIC technology in Europa, C65SPACE technology is selected in GR740 as it has been

tested in various radiation impact situations. Overall, The C65SPACE technology is immune to single event latch-up up to LET (linear energy transfer) 125 MeV·cm²/mg, has a high tolerance for TID up to 300 krad, and includes both SEU/SET hardened and non-hardened logic. The overall SEE error rate is below 1×10^{-5} events/device/day for typical orbits such as LEO and GEO, as shown in **Table 38**. The complete radiation protection report can be found in the manual of GR740 radiation summary [63].

Table 38: Summary of Radiation Protection values for GR740.

Radiation Effect	Protection Threshold
Overall SEE	1×10^{-5} events/device/day
SEL (Latch-up)	125 MeV·cm ² /mg
TID	300 krad

9.4.2 Software Design for protection

1. PLL Watchdog Timer which is internal and is clocked by the SYS-CLK input clock;
2. FDIR mode and special software: As designed in the operation mode, FDIR mode runs after the failure happens for detection, isolation, and recovery. To monitor the radiation impact level in space, Cobham Gaisler's SEU32 and GRMON2 test software are used in GR740 for radiation measurement and testing.

9.5 Mass and Power Budget

The overall mass and power budget for CDHs subsystems are in **Table 39**.

Table 39: Mass and overall Power budget for CDHs subsystem.

Instrument	Mass	Power consumption
GR-VPX-GR740	1.2 kg	~30 W

9.6 Future Improvements

Some future improvements for the Command and Data-handling Systems which are mostly related also to the other subsystems data are:

1. After all the payload data from three instruments are calculated, we can take the 10% of the Payload Data rate and assign it to the Housekeeping Data. After that, we will be able to sum them together for the total data rate;
2. Data Storage and Memory calculation will also be accomplished in the future, after the accurate data amount calculation from other subsystems and considering the performance degradation of storage materials.

The improvements will also be discussed later at Sec.13.3.

10 Electrical Power System (EPS)

The Electrical Power System, one of the key subsystems for a spacecraft, must be able to support the activity of the spacecraft for the whole duration of the mission by generating power and distributing it between all the subsystems that require power to function. In the following sections, the different power sources will be analysed and compared in order to find an optimal solution for the complete mission to Europa including disposal.

10.1 Requirements

As for the other subsystems, some requirements must be imposed (**Table 40**).

Table 40: Requirements of EPS.

ID	Description
EPS.1	Continuously provide power for the whole mission lifetime
EPS.2	Adapt to the different operational modes of the spacecraft
EPS.3	Minimize the mass and the volume of the power source

These are the basic requirements which must be satisfied by the chosen power system.

10.2 Power Budget

Every subsystem can be composed of different devices and they all have different power consumption. **Table 41** shows the complete list of all the instruments and the relative power consumption.

Table 41: Power requirements of the different instruments.

Subsystem	Instrument	Power (W)
PAYLOAD	Camera	45 (images), 25 (readout)
	Spectrometer	25
	X-band antenna	5
CDHS	On-board computer	30
ADCS	Wheel	1
	Sun sensor	0.15
	IMU	12
EPS	PDU	0.165
COMMS	Antennas	25

SPES has different operational modes, as explained in Section 9.3.1. Every mode, then, has its own power budget that is given by the sum of all the subsystems (or instruments) that operates during the mode.

Table 42: Power requirements of the different operational modes; we have taken into account the open with strategy subsystems.

*The navigation subsystem is not treated in this report, but it should be taken into account for this mode.

Operational mode	Power requirement (W)
NOMINAL (N)	118.315
SAFE (S)	30 - 30.165
THRIFT (T)	55.165 - 68.315
DATA DOWNLINK (DD)	68.315
TRAVEL (R)	68.315*
FAILURE DETECTION, ISOLATION AND RECOVERY (FDIR)	30.165

During Nominal mode the power requirement is high because all the subsystems, except communication, are operating during that period. Taking this power as the minimum power required for our mission we proceed in selecting the power source.

10.3 Power Generation

There are three main ways to provide power to a spacecraft: solar arrays, fuel cells and radioisotope thermoelectric generators.

The Sun is the most abundantly used renewable energy source by humans on Earth and it is also extensively used in space missions reducing the complete dependence on batteries. However, solar arrays cannot work during eclipses, often they need to be coupled to batteries that can store and give power to the spacecraft when solar panels are off. Solar arrays can also be inefficient for deep space missions as the irradiance of the sun decreases and external factors (like sandstorms from the planet) can damage the panels. In these circumstances, other sources like RTGs and fuel cells are used.

There are several factors that affect the choice of the power source, such as the mission duration, the amount of power needed, the distance from the Sun and others. In **Figure 36**, the power output of different power sources based on mission duration can be understood.

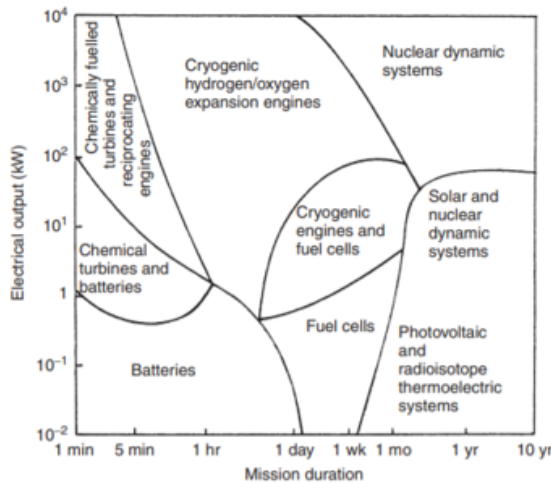


Figure 36: Power output as a function of the mission duration for different sources; taken from [9].

10.3.1 Solar Arrays

There are several space missions to Jupiter that have used or are currently using solar panels, such as *Juno* or *Europa Clipper*, even if the solar irradiance at the distance of Jupiter ($J_{\text{sun}} \simeq 50 \text{ W/m}^2$) is significantly lower than at the distance of Earth ($J_{\text{sun}} \simeq 1370 \text{ W/m}^2$).

Taking this into consideration, a rough computation was performed to find the size and weight of the solar panels needed for our mission. The assumptions made are as the following:

- we consider a spacecraft in a circular orbit around Jupiter at the same distance as Europa ($d \simeq 670900 \text{ km}$);
- we can approximate the geometry as a two-body problem (small angles of inclination of both Jupiter's [54] and Europa's orbits [56]);
- the power required during daytime is the same as during eclipses and it is equal to the highest power requirement of **Table 42** ($P_d = P_e = 118 \text{ W}$);
- the total mission lifetime, including the journey to Europa, is 10 years;
- the degradation of the solar panels is 5% per every year;
- we neglect the effect of the inclination angle of the spacecraft;
- the adopted values for the solar panel efficiencies are 82% for daytime and 85% for storage.

The orbital period of the spacecraft is:

$$\mathcal{T} = 2\pi\sqrt{\frac{d^3}{\mu}} \simeq 3.55 \text{ days}$$

where $\mu = 1.267 \cdot 10^8 \text{ km}^3/\text{s}^2$. The result is equal to the orbital period of Europa and this is consistent with our assumptions. Then, from the reference value of the eclipse time at the distance of Europa [64], we computed the daytime t_d .

The solar panels chosen for the computation are High-Efficiency Silicon rigid panels, with a specific power of 58.5 W/kg and an area per power of 4.45 m²/kW (measured for Earth's solar irradiance).

To find the power generated by the solar array without considering the degradation we used the following equation:

$$P_{sa}t_d = \frac{P_dt_d}{\eta_d} + \frac{P_et_e}{\eta_e} \quad (34)$$

The result is $P_{sa} \simeq 150 \text{ W}$. Including the effect of the 5% degradation for each year of the mission, the power becomes $P_{sa,deg} \simeq 251 \text{ W}$.

First, we computed the size and weight of the panels with Earth's values of specific power and area per power, and then we re-scaled them considering the different values of the solar irradiance.

The final results are $A = 30.6 \text{ m}^2$ and $m = 117.5 \text{ kg}$. These values must be compared to the typical characteristics of RTGs and fuel cells to determine what is the best option for our mission.

10.3.2 Fuel Cells

Fuel cells are an alternative to batteries. Hydrogen is the most common fuel, but it can be tricky to store because it's very light and must be pressurized to be stored in a small space.

Fuel cells generate electricity through the reaction between the fuel (hydrogen) and oxygen, provided there is an external source of energy that helps the reaction. The reactants are kept separate by a polymer membrane, called the electrolyte, and only protons produced by hydrogen can cross it. Electrons, instead, flow from the anode electrode into an electric circuit and then they end up with oxygen. Hydrogen protons pass to the other side, they react with oxygen and electrons generating water in a controlled way. In the end, we produce electric energy, heat, and water as a residual.

Even though fuel cells seem to be the best green choice that can be made since they produce only water, complications arise with size. To support a 10-year mission the volume and the weight of the fuel needed would be much larger than the ones of other sources. So this power source was excluded for our mission.

10.3.3 Radioisotope Thermoelectric Generators

Considering the estimated mission duration of SPES and looking at **Figure 36**, we decided that an RTG would be the best choice for our mission. The property of the half-life period of radioactive elements makes it a good choice to use it for longer missions.

This choice was confirmed by the average values of the mass (between 40 and 60 kg) and the volume of typical RTGs used in other missions. Moreover, RTGs don't have particular requirements on the operating temperature and this is convenient when designing deep-space missions.

The main problem with choosing nuclear power as the source is the high amount of dissipated heat. The current efficiencies of the different RTG models are below 10%, implying that most of the heat produced with radioactive decay is just dissipated in the environment instead of being converted into electrical power. However, when considering a deep-space mission, this wasted heat could be helpful to warm up the instruments if the equilibrium temperature of the spacecraft is too low compared to the requirements.

Taking the reference from missions like *Cassini*, *Voyager* and *New Horizons* etc., the choice of the model was carried out.

The most important choice regards the radioactive isotope that will be used as fuel. The two general rules that should be followed are:

- The radioactive element should have a high half-life period (the half-life period is inversely proportional to the amount of energy released per time);
- Alpha decays are better than beta decays as alpha decays produce 10 times more energy than that of beta decays and also can be easily absorbed and transformed into thermal radiation.

Taking the above-mentioned considerations, plutonium-238 was chosen as the radioactive element. The most important models that employ Pu-238 are the Multi-Hundred Watt RTG, the General-Purpose Heat Source RTG, and the Multi-Mission RTG.

The packaging of fuel is as important as the selection of radioactive elements because different packaging of fuel has different efficiency. For example, compared to the 24 pressed Pu-238 oxide spheres of MHW RTG, the GPHS RTG has better packaging as it contains cylindrical plutonium pellets.

Seebeck Effect helps in converting the heat released during radioactive decay into electricity using thermocouples and this forms the basic working principle of RTGs. This should also be remembered during the selection of RTG. As an example, MHW and GPHS RTGs use silicon-germanium thermocouples to convert the heat into electricity.

Moving to the newest RTG models:

- **MMRTG and e-MMRTG** The currently in-use model of RTG is the Multi-Mission Radioisotope Thermoelectric Generator (MMRTG), developed by NASA and Jet Propulsion Laboratory, which has been chosen to power *Curiosity* and *Perseverance* rovers on Mars.

MMRTGs, since Silicon-Germanium thermocouples are not produced anymore, employ either Lead telluride (PbTe) or Germanium telluride/Silver Antimony telluride (TAGS) thermocouples and, for the packing of plutonium, they use 8 GPHS modules. They are designed to survive both in deep space and inside planetary atmospheres and their lifetime is around 17 years, 3 years of fueled storage before launch and 14 years of mission [65].

MMRTGs, however, are able to deliver 110 W of power at the beginning of life and they have an efficiency of around 6%. For these reasons, in the last ten-twenty years, NASA and JPL (along with other partners) have been developing the enhanced Multi-Mission Radioisotope Thermoelectric Generator (e-MMRTG). This power source uses skutterudite (SKD), a mineral of cobalt arsenide (CoAs_3), thermocouples that are able to rise the efficiency to 8% while keeping the same volume, mass and interfaces of the MMRTG [66].

e-MMRTGs have not been used yet, but they will probably be ready by 2022-23.

- **ASRG** The Advanced Stirling Radioisotope Generator (ASRG) has the main advantage of not employing thermocouples to generate power. An ASRG produces electricity by a triple energy transformation: it first turns the thermal energy from the hot radioisotope fuel into the high-speed kinetic motion of a small piston and its companion displacer. In turn, this magnetized piston oscillates back and forth through a coil of wire, thereby generating a flow of electrical energy (using a property of physics known as Faraday's Law) [67]. Thanks to this process, ASRGs are able to use less plutonium with respect to previous RTGs and, consequently, produce power with much higher efficiency (of the order of 25%).

Like the MMRTG and e-MMRTG, the ASRG is designed to work both in deep space and inside planetary atmospheres, and more than one unit can be used for the same mission. This kind of power source, however, will not be ready before 2028.

10.3.4 Tradeoff and Choice of the RTG

Table 43: Trade-off table of the different RTG models.

	MHW	GPHS	MMRTG	e-MMRTG	ASRG
Packing	Pressed spheres	GPHS modules	GPHS modules	GPHS modules	GPHS modules
Thermocouples	Si-Ge	Si-Ge	PbTe or TAGS	SKD	-
Total mass (kg)	37.7	57	45	43	32
Pu mass (kg)	4.5	7.8	4.8	4.8	1.2
Power, BOL (W)	470	300	110	145	130
E_{spec} (W/kg)	4.2	5.2	2.8	3.6	6.4-7.4
Lifetime (yr)	48	13	14	17	>17
Efficiency, BOL	6.5%	6.5-7%	6%	8%	25%
Not in use due to Si-Ge thermocouples not being produced anymore		Currently used		Should be ready by 2022	In future

Due to the non-production of Si-Ge thermocouples, we excluded the MHW and the GPHS, even if they have high specific power and power at the beginning of life. The first choice for SPES was the MMRTG but, considering the power at the beginning-of-life of 110 W and its decrease for each year (at the end-of-life it provides around 60-70 W) and comparing it to the power requirements of **Table 42**, we found out it was not enough to support the activities of the mission. In the end, we decided to use the enhanced MMRTG, even though it has not been used for a mission yet: it can provide more power also at the end-of-life (around 90 W, as reported in the datasheet [68]), it has better specific power and it has a slightly lower mass when compared to the MMRTG.

The dimensions of the e-MMRTG (**Figure 37**) are the same as the MMRTG: 64 centimetres in diameter (fin-tip to fin-tip) by 66 centimetres tall [65].

The efficiency of e-MMRTG is around 8% at the beginning of life thus the power that is dissipated into heat is $P_{diss} \simeq 1.6$ kW and it must be taken into account in the thermal analysis of the spacecraft (refer to Section 8.3).

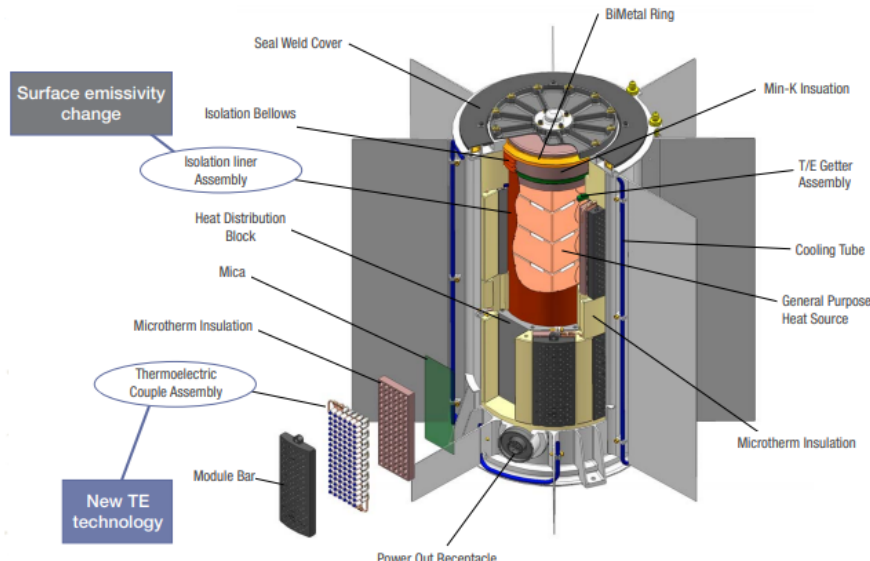


Figure 37: Structure of the e-MMRTG.

10.3.5 e-MMRTG Power Degradation and Operational Modes

As previously explained, the e-MMRTG generated power decreases as a function of time: from the 145 W peak at the beginning of life, after 14 years of operations it drops to 90 W. Given these values, we were able to find how much the power degrades for every year:

$$x_{deg} = 1 - \sqrt[14]{\frac{90}{145}} \simeq 3.349\%$$

Once this value was obtained, we computed how much power the RTG can deliver after every year and the results are reported in **Table 44** and plotted in **Figure 38**.

Table 44: Values of the power generated by the RTG for some years after the launch.

Year	1	5	6	7	8	9	10	11	12	13
Power (W)	140.14	122.29	118.195	114.237	110.41	106.71	103.14	99.68	96.35	93.12

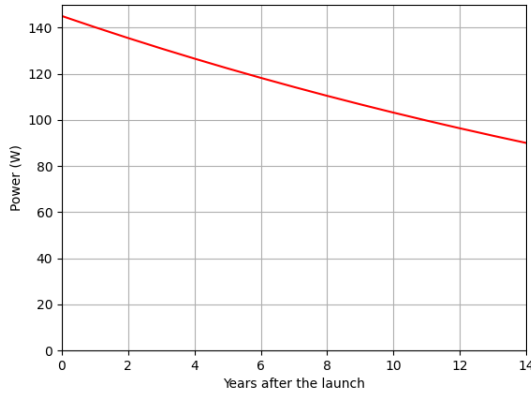


Figure 38: Power generated by the RTG as a function of the operational years.

As **Table 44** shows, after 6-7 years from the launch (1-2 years after reaching Europa), the power becomes lower than the requirement for the Nominal mode. To overcome this problem, two Nominal sub-modes, N0 and N1, have been designed with the help of the CDHs team; the details are shown in **Table 36**.

To determine the power ranges of the two sub-modes, we have computed the power consumption in the Nominal mode considering different combinations of switched-on payload instruments (**Table 45**).

Table 45: The overall power consumption with different scientific instruments in operation.

Description	Power consumption (W)
Only the camera and the X-band antenna are operating	93.315
Only the spectrometer and the antenna are operating	73.315
Only the X-band antenna is operating	48.315

10.4 Power Distribution

The EPS should also find a way to distribute the power of the source between the different subsystems, depending on when they are switched on or off.

P60 PDU-200 from GOMspace has been chosen as the power distribution unit for our mission. It has 3 output voltage switches of 3.3 V, 5V and 8V; it is built around GOMspace modular technology, allowing numerous configurations of modules to be implemented on a motherboard, saving significant volume. The standard configuration of P60 includes 1 motherboard, 1 Array Conditioning Unit (ACU) module (6 channels), and 1 PDU module (9 channels). They are used for nanosatellites but, due to the mass and size of our payload, rescaling this PDU for our mission might not be important.



Figure 39: P60 PDU-200 from GOMspace.

Table 46: Main characteristics of P60 PDU-200, from the datasheet [18].

Power consumption (mW)	165
Output voltages (V)	3.3, 5, 8 12, 18, 24 (optional)
Mass (g)	57
Size (mm)	65.6 × 40.1 × 4.7
Operational temperature (°C)	-35 to +85

10.5 Mass and Power Budget

Table 47: Mass and power budget of each instrument for EPS.

Instrument	Unit number	Mass (kg)	Power consumption (W)
RTG	1	43	-
PDU	1	$57 \cdot 10^{-3}$	0.165
TOTAL	2	43.057	0.165

11 Structures

11.1 Mission Requirements

The Structures subsystem is focused on providing a spacecraft structure which can envelope all the necessary instrumentation and technology of the other subsystems. The spacecraft selection was made following a series of specific criteria listed below.

Table 48: List of requirements for structures subsystem.

ID	REQUIREMENT	DESCRIPTION
ST.01	Structural Integrity	Design which avoids structure failing and is aware of static and dynamical loads on the S/C. The required natural frequency given by the launcher was 25 Hz in the axial direction and 10 Hz in the lateral direction, and this was used as minimum value.
ST.02	Operating environment	The spacecraft is a protected environment for all subsystems, guaranteeing radiation and debris protection. Material selection required a minimum of 10 krads protection for the entire duration of the mission.
ST.03	Alignment	Center of gravity is in the middle of the spacecraft, guaranteeing balance to the entire structure.
ST.04	Accessibility	Any component of the structure is as much as possible easily accessible for eventual maintenance.
ST.05	Interface with launcher	Ensuring that the satellite and rocket remains securely connected during launch and that the payload is placed in orbit with precision.

11.2 Volume and Mass Budget

A detailed table with all the elements composing the spacecraft is provided in **Table 49**. For each component, mass and volume were researched to calculate the final mass budget required by the mission.

Table 49: Mass, size and volume for each subsystem.

Subsystem	Elements	Mass (kg)	Sizes (cm)	Volumes (cm ³)
PAYLOAD	Spectrometer	4.85	40x20x20	16000
	Imager	18	32x92 (cylinder)	2944
	X-band antenna	0.023	200x200	
COMMUNICATION	X-band high gain antenna	1.16	92 (diameter)	9966
	Ka-band high gain antenna	1.16	92 (diameter)	9966
EPS	Generator	45.5	64x64x66	270336
	Power Distribution Unit	0.0057	NG	NG
THERMAL CONTROL	3x Radiators	0.036	0.2x0.2x0.01	0.006
ATTITUDE	3x Wheels	0.72	5.8x5.8x2.2	74
	4x Sensors	0.12	3.4x4x2	27
CDHS	OBC	1.2	0.05x2.9x2.9	0.4
PROPELLION	Engine	4.5	0.5x0.5x0.5	0.2

The total mass of the payload without fuel (in this case, propellant tanks) is around 78 kg with a volume of 0.5 m³. A preliminary disposition of instruments and electronic components was made considering the ST.03 (centre of gravity requirement).

11.3 Spacecraft Design and Strength Properties

The ST.01 requirement is integrity, which is first achieved avoiding structure failure due to vibrations during take-off. The launch is the moment of maximum stress for the spacecraft and it sets the maximum stress for the rocket. To calculate the thickness of the walls of the S/C we required the natural frequency of our structure to be higher or equal to the launcher's one.

$$f_{axial} = 0.250 \sqrt{\frac{(\pi r^2)E}{Mh}} \quad (35)$$

$$f_{lat} = 0.560 \sqrt{\frac{E(2\pi rh)}{Mh^3}} \quad (36)$$

where E is the Young modulus, r the radius of the S/C, M the S/C mass , h the height of the S/C. The natural frequency, also known as eigenfrequency, is the frequency at which a system tends to oscillate in the absence of any driving force. To avoid resonance with the launcher, this frequency is required to be higher for the S/C. Resonance describes the phenomenon of increased amplitude that occurs when the frequency of an applied periodic force (or a Fourier component of it) is equal or close to the natural frequency of the system on which it acts. When an oscillating force is applied at a resonant frequency of a dynamic system, the system will oscillate at a higher amplitude than when the same force is applied at other, non-resonant frequencies. Resonance can be dangerous in spacecraft architecture and must be avoided if possible.

The next step is considering design loads when sizing the structure: the launch phase is when the largest loads occur. First, we considered the dynamical stress loads in axial and lateral directions:

$$L_x = J_Q g_x M \quad (37)$$

$$L_y = J_Q g_y M \quad (38)$$

where J is flight qualification load factor , g are max acceleration on axial and lateral direction, M is S/C mass. The stiffness is derived from natural frequency as:

$$\sigma_{axial} = 2\pi M f_{axial} \quad (39)$$

$$\sigma_{lat} = 2\pi M f_{lat} \quad (40)$$

where M is S/C mass and f are natural frequency of the launcher. Our goal is a stiffness greater than the launcher's, considering stress loads is then also calculated as:

$$\sigma_{axial} = \frac{EAM}{h} \quad (41)$$

$$\sigma_{lat} = \frac{EMr^2}{h} \quad (42)$$

where E is Young modulus, A is S/C area, M is S/C mass, r is S/C radius and h is S/C height. Secondly, we considered buckling: we want to prevent this effect to happen on our structure. The critical stress at which buckling will occur is:

$$\frac{\sigma_c}{E} = 9 \left(\frac{t}{r} \right)^{1.6} + 0.16 \left(\frac{t}{h} \right)^{1.3} \quad (43)$$

where A is S/C area, M is S/C mass, r is S/C radius, g are max accelerations on axial and lateral direction and h is S/C height. Considering the maximum stress we can have on our S/C as:

$$\sigma_{tot} = \frac{g_y M h r}{2\pi r h} + \frac{g_x M}{\pi r^2} \quad (44)$$

The goal is then to have greater critical buckling stress with respect to maximum stress.

$$\sigma_c > \sigma_{tot} \quad (45)$$

In the end, the structure mass for each case was calculated:

$$M_{struc} = \rho(\pi D t)h \quad (46)$$

where p is structure density, D is diameter of S/C, h is S/C height and t is thickness of S/C walls.

11.4 Materials Trade-off

A first selection of materials was done considering Aluminum 6061 and 7075, Magnesium A2 and ZK. The two were chosen due to their very low density with respect to volume, and also for precedent mission results (especially aluminium, used in mostly S/C for scientific purposes). For each of them, wall thickness, stress loads and maximum/critical stress were calculated (**Table 51**). The necessary values of stiffness and natural frequency of the launcher are listed in **Table 50**.

Table 50: Frequencies and stiffnesses for the launcher.

Axial frequency (Hz)	25
Lateral frequency (Hz)	10
Axial stiffness	14848.4
Lateral stiffness	5903.2

Table 51: Trade-off between the different selected materials for the S/C.

Material	Aluminium6061	Aluminium7075	MagnesiumA2	MagnesiumZK
E(GPa)	68	71	45	45
Max axial acc (g)	2.5	2.5	2.5	2.5
Max lateral acc (g)	0.9	0.9	0.9	0.9
Qualification load	1.1	1.1	1.1	1.1
Ultimate stress	1.2	1.2	1.2	1.2
Density (kg/m ³)	2700	2800	1700	1700
Wall thickness, axial (m)	4·10 ⁻⁴	4·10 ⁻⁴	6·10 ⁻⁴	6·10 ⁻⁴
Wall thickness, lateral (m)	1.2·10 ⁻⁵	1.6·10 ⁻⁵	1.7·10 ⁻⁵	·10 ⁻⁵
Structure mass (kg)	20.8	20.7	19.8	19.8
Load, axial (N)	2551.4	2551.4	2551.4	2551.4
Load, lateral (N)	918.5	918.5	918.5	918.5
Axial stiffness	43334	45214.4	28670.1	28670.1
Lateral stiffness	9166.3	9505.8	5771.4	5771.4
Critical buckling stress (MPa)	1.36·10 ⁶	1.33·10 ⁶	1.70·10 ⁶	1.70·10 ⁶
Maximum stress	36.8	36.8	36.8	36.8

The wall thickness selected in both cases was the axial one since it is higher. There is a small difference in resulting mass for structure design for the four materials (in all scenarios, the value is around 20 kg). One positive side is that all cases show higher critical stress with respect to the maximum stress on S/C.

Another essential aspect to consider is the internal organization of the S/C: weight balance needs to be reached. To calculate the centre of mass position we used:

$$x_{CM} = \frac{\sum_{k=1}^N m_k x_k}{\sum_{k=1}^N m_k} \quad (47)$$

$$y_{CM} = \frac{\sum_{k=1}^N m_k y_k}{\sum_{k=1}^N m_k} \quad (48)$$

$$z_{CM} = \frac{\sum_{k=1}^N m_k z_k}{\sum_{k=1}^N m_k} \quad (49)$$

A map of the interior of the S/C was made considering the weight and volume of each component (**Figure 40**).

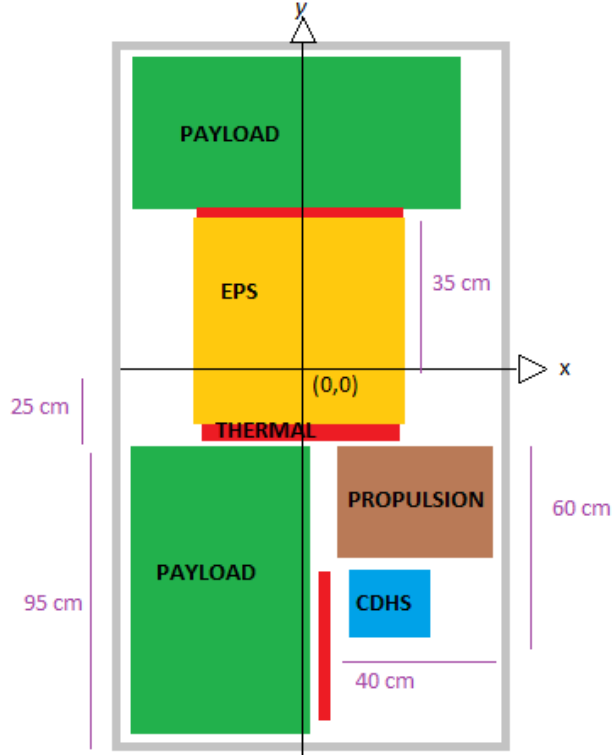


Figure 40: S/C interior map.

This led to the final deviations from the centre of mass, which is located in the middle of the S/C (**Table 52**).

Table 52: Deviation from the centre of mass (COM) along the three axis x, y, z.

Axis	Deviation from COM
x	-8.98
y	4.27
z	Negligible

As we can see, it will be necessary to balance with additional extra weight on the x and y-axis (on the z-axis it is negligible).

An important consideration to remember are the propellant tanks: volume and mass of the tanks, due to the fact that EOL is still to be analysed, are not considered in this map. In case, due to the long travel to Jupiter and the high mass of fuel, the storage will be located under the payload:

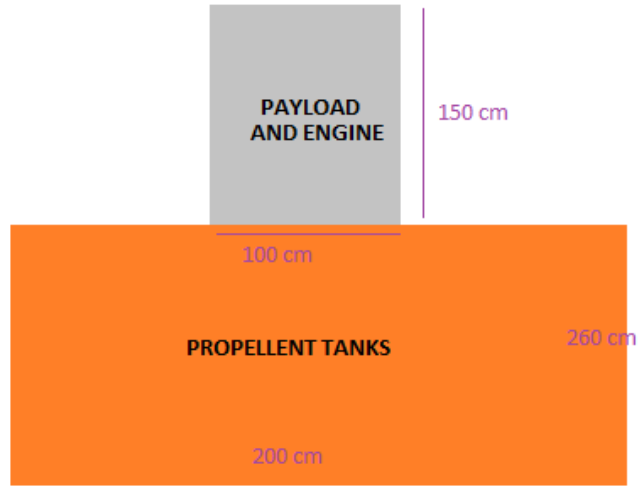


Figure 41: S/C propellant and payload map.

The total volume and mass of propellant tanks is equal to 13936 kg and 12 m³ in addition to payload.

11.5 Radiation Shielding

Radiation from the natural space environment can damage and reduce mission lifetime. In particular, Single Event Effects due to ionizing sources in the Solar System or in the galaxy can pass through external material of the S/C and reach payload with scientific instruments. To avoid this, it is necessary to have one or more solutions to shield our components. A good way to insulate the S/C is a set of layers with different materials to avoid radiation entering inside. A preliminary list of the layers is below:

- **OUTER LAYER:** an outer layer able to resist to shedding and flaking, and, if necessary, with additionally aluminized to increase reflection of UV radiation. Common materials are Beta Cloth, Kapton, Teflon and Tedlar.
- **REFLECTORS:** multiple reflectors layer to avoid radiation penetrating inside. Common materials are Kapton, Mylar, Polyester and Teflon (usually these layers are ventilated to avoid ballooning in the ascension phase).
- **SEPARATORS:** additional layers, very thin, to separate different layers listed before.
- **INNER LAYER:** inner cover in metal and laminated layer, usually selected with low inflammability due to proximity with electrical and thermal subsystems.

We made a comparison and two trade-offs, one for the outer layer and one for reflectors, considering the weight and absorbance of each material (**Tables 53** and **54**).

Table 53: Comparison between different materials of the outer layer.

MATERIAL OUTER LAYER	Teflon	Beta Cloth	Kapton	Tedlar
Thickness	9	7	9	7
Weight	9	7	9	7
Radiation absorbance	9	8	7	6
TOTAL	8.4	7.4	8.1	6.5

Table 54: Comparison between different materials of the reflectors.

MATERIAL REFLECTORS	Teflon	Mylar	Kapton	Polyester
Thickness	9	8	9	10
Weight	9	9	9	10
Radiation absorbance	9	6	7	5
TOTAL	8.4	7.4	8.1	7.7

The trade-off is a weighted mean in which different importance was given to each parameter (weight from 0 to 5): thickness 2, weight 3, radiation absorbance 4. We selected the highest absorbance when possible, to reduce the amount of layers needed.

It is clear Teflon is the most convenient choice for the outer layer, and it is also one of the most used in flight missions (ISS). In the reflectors, also polyester should be considered in pair with Teflon to reduce the weight of the substrates.

11.6 Selection of a S/C

A preliminary draft of the spacecraft design is shown in **Figure 42**.

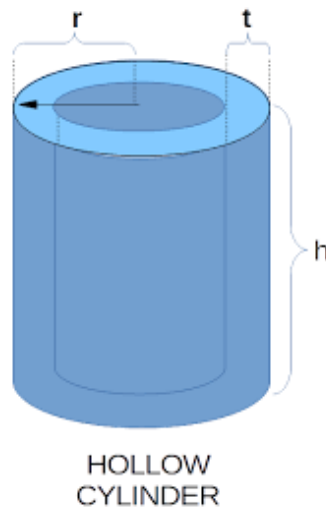


Figure 42: Design of S/C as a hollow cylinder.

Table 55: Dimensions of the hollow cylinder we used to model our spacecraft.

Volume (m³)	14.1
Radius (m)	1.0
Area (m²)	3.4
Height (m)	4.2

We considered a higher total volume with respect to payload requirements, to avoid crowding inside the structure (**Table 55**) and meet structure integrity requirements (stiffness, critical stress, etc); also, center of mass stability requires particular disposition of weights and empty space is required (in the future, it could be filled with dividing layers of isolating material to avoid voids). With respect to the material, aluminium is cheaper than to magnesium (2.38€/kg respect to 3.31€/kg) and has a trustworthy history in space missions design. Considering both cost and mechanical properties, we made a final trade-off, shown in **Table 56**.

Table 56: Trade-off between different materials.

Material	Aluminium6061	Aluminium7075	MagnesiumA2	MagnesiumZK
Weight	9	9	10	10
Axial Stiffness	8	8	6	6
Lat Stiffness	8	8	7	7
Critical Stress	9	9	10	10
Cost	10	10	9	9
TOTAL	8.7	8.7	8.2	8.2

In this trade-off, to each parameter we assigned: weight 4, stiffness 2, critical stress 3, cost 2. We highlighted weight and critical stress over cost and stiffness.

It is easier for the mission to obtain a completely custom structure design: it will be necessary to build it from our indications, and not select one on the market.

Looking at the requirements, we can show if the design actually satisfies the constraints (**Table 57**).

Table 57: List of the structure requirements that have been satisfied.

REQUIREMENT	Satisfied	Comment
ST.1	Yes	Stiffness, natural frequencies and critical buckling stress parameters are enough to avoid structure failure.
ST.2	Yes	Only aluminium thickness alone cannot prevent damage from radiation. Additional shielding required, as described in Radiation Shielding paragraph
ST.3	No	Center of Mass is slightly dislocated with respect to the centre of the S/C: this can lead to issues during orbital manoeuvres, and must be fixed with extra weights
ST.4	Yes	The position of the components allows maintenance inside the S/C
ST.5	/	Future improvements will consider launcher-spacecraft connection.

12 Propulsion

The propulsion subsystem is responsible for finding a proper launcher for our mission and developing a suitable propulsion system for our spacecraft, which will need to be modelled in a way such that it can both perform interplanetary manoeuvres (corresponding to high boosts) and trajectory maintenance and correction manoeuvres (corresponding to small boosts). In the following sections, at first we fix the requirements differentiating between the ones we need for the launcher and the ones needed for the spacecraft, while later we analyze in detail the spacecraft we want to choose and eventually we develop a proper propulsion system for our spacecraft.

12.1 Requirements

12.1.1 Launcher

We start defining some requirements for the launcher. The launcher we will choose will have to be capable of taking our payload up to the target orbit that has an altitude $h_{coast} = 6564$ km from Earth's surface: this means it will have to provide a total velocity boost of at least 12.5 km/s (according to Orbits design subsystem, see **Table 18**). Moreover, it will have to be suitable to safely release the spacecraft in the target orbit when it will reach it, after having protected it during the whole launch procedure.

The requirements for the launcher are summarized in **Table 58**.

Table 58: List of the requirements for the launcher.

ID	REQUIREMENTS
LA.01	The launcher should be able to bring the payload up to a target orbit with an altitude $h_{coast} = 6564$ km.
LA.02	The launcher needs to provide a total $\Delta v_{launcher,2} = 12.5$ km/s.
LA.03	The launcher should be capable of reaching the target orbit and release the payload consisting in the SPES spacecraft.
LA.04	The launch vehicle shall provide protection to the spacecraft during the entire launch.

12.1.2 Spacecraft

For what concerns the spacecraft, we will need it to be capable of reaching the scientific orbit of the mission, which consists in an orbit around Jupiter during which it performs flybys of Europa, but it also will have to maintain and correct this orbit if needed. To do all this, it will need to provide a total velocity boost of 9.64 km/s: this means that it will also have to be able to carry a quantity of propellant sufficient to perform all the manoeuvres from the beginning up to the End Of Life (EOL).

The requirements for the spacecraft are summarized in **Table 59**.

Table 59: List of the requirements for the spacecraft.

ID	REQUIREMENTS
SC.01	SPES has to reach as a target orbit a Jupiter orbit that performs flybys of Europa.
SC.02	SPES must provide a total $\Delta v_{spacecraft} = 9.64 \text{ km/s}$ (without EOL).
SC.03	SPES is required to maintain the flyby orbit.
SC.04	SPES needs enough fuel to perform all the maneuvers for the whole mission duration, including the EOL.

12.2 Launcher

In order to understand which launcher we should use, we took as a reference the Europa Clipper mission, because of all the similarities that our mission has with it. In the paper in which they illustrate the Europa Clipper preliminary design [62], they show how the best solution for that kind of mission is using the Space Launch System (SLS) as a launcher.

Starting from this, for our mission we decided to take into consideration the SLS option, but we also wanted to compare it with SpaceX's Falcon Heavy: these two are in fact the most powerful launchers that are available nowadays and we wanted to understand which one of the two could be more convenient for our scopes. To do this we selected different criteria for the comparison: all the info reported below was taken from the user's manuals of the two launchers [19], [20].

- Maximum thrust: SLS is the most powerful of the two, with a maximum thrust of $\sim 3.7 \cdot 10^7 \text{ N}$, but also Falcon Heavy confirms to be a valid alternative since its maximum thrust is $\sim 2.3 \cdot 10^7 \text{ N}$.
- Payload mass to a given orbit: this gives an idea of how much mass our launcher is capable to take at different altitudes from Earth's surface, and it is a very useful criterion to understand if a certain launcher can match our requirements. In the case of SLS, we were able to obtain only a value for the payload mass to LEO (Low Earth Orbit, $h_{LEO} > 1000 \text{ km}$) that is 95t. For Falcon Heavy instead we were able to collect more information: the payload mass to LEO was less than the one for SLS (63.8t), but we also found a value for the payload mass to GEO (Geosynchronous Equatorial Orbit, $h_{GEO} = 36000 \text{ km}$), of the order of 26.7t, and also a value for the payload mass to Mars, approximately 16.8t. In this way, we arrived to the conclusion that both our launchers would be suitable for our mission: in fact our requirement LA.01 states that our launcher should be able to take us to an orbit $h_{coast} = 6564 \text{ km}$, which is exactly within the range $h_{LEO} < h_{coast} < h_{GEO}$; if we add to this the fact that our payload mass is $m_{payload} = 12.935\text{t}$, that is less than all the masses reported above, we can say that both launchers effectively match the requirement.
- Cost per launch: the cost per launch of SLS is not exactly defined but, referring to different sources, we could find that it is likely larger than 2.2 billion dollars, that makes it the most expensive launcher available today; oppositely, Falcon Heavy has

a much lower cost per launch, around 97 million dollars, because of his reusability. This could potentially have a strong impact on the choice of our launcher.

- Propellant: both launchers are provided with liquid propellant in the first stage (liquid oxygen and liquid hydrogen for SLS, only liquid oxygen for Falcon Heavy) and with solid propellant in the boosters (Polybutadiene acrylonitrile (PBAN) for SLS and kerosene (RP-1) combined with liquid oxygen for Falcon Heavy).
- Success rate: up to now SLS has done only one launch, that resulted in a complete success, but of course is not enough to provide an effective estimate of the launcher reliability; Falcon Heavy, instead has performed a lot of successful launches, with a success rate of almost 99%, thanks to the high number of tests done on the Falcon 9 (recalling that Falcon Heavy is basically composed by three Falcon 9 put together).

Taking into account all this information (that we summarized in **Table 60**), we can conclude that both launchers could represent a valid option in the choice of the launcher we want to use for our mission, because they share similar performances and reliability. The great difference lies in the cost per launch: in fact, a mission to Europa will require huge expenses and the cost of the mission itself will be already very high; in this framework, having the possibility to spare some funds while choosing the launcher, without losing anything in reliability, makes Falcon Heavy a more convenient option to opt for.

Table 60: Comparison between NASA's Space Launch System (SLS) and SpaceX's Falcon Heavy. Values are taken from the user's manuals of both of them [19], [20]. Pay attention: the success rate of SLS is given as 100%, but only one successful launch was performed.

Launcher	Max thrust (kN)	Payload to LEO (t) (h<1000 km)	Payload to GEO (t) (h=36000 km)	Cost per launch (M\$)	Propellant	% of success
Space Launch System (SLS)	36786	95	-	>2200	Lox, LH ₂ PBAN	100% (just 1 launch)
Falcon Heavy	22819	63.8	26.7	97	Lox/RP-1 / Lox	99%

12.3 Spacecraft

Starting from the total Δv required for the spacecraft that the Orbital Design subsystem provided us (see **Table 25**), we tried to give an estimate of the amount of propellant we would require to perform all the maneuvers, obtaining different results for different choices of the propellant and comparing them.

12.3.1 Tsiolkovsky Equation

Starting from classical mechanic assumption, we can find a relation that allows to give a first estimate of the propellant mass needed to perform a certain Δv with a rocket/spaceship.

We can start considering the definition of thrust for our spacecraft, given by Eq. 50, where M is the spacecraft mass while v_{ex} is the so-called *exhaust velocity*. The exhaust velocity is the velocity at which a certain type of propellant is ejected by the spacecraft, and is defined as $v_{ex} = I_{sp} g_0$, where I_{sp} is the specific impulse of the engine, while $g_0 = 9.807 \text{ m s}^{-2}$ is Earth's gravitational acceleration at sea level.

$$T = M \frac{dV}{dt} = - \frac{dM}{dt} v_{ex} \quad (50)$$

Starting from this we can see that the instantaneous infinitesimal velocity variation is $dV = -dM/M v_{ex}$, so we can proceed in calculating a finite value of velocity increment Δv_{boost} , integrating between the initial mass of the spacecraft M_f (fueled mass, including both spacecraft and propellant) and the final mass $M_d = M_f - M_{propellant}(t)$ (dry mass, obtained from M_f subtracting the mass of the propellant consumed up to the time t):

$$\Delta v_{boost} = - \int_{M_f}^{M_d} \frac{dM}{M} v_{ex} \quad (51)$$

In this way, we finally obtain the Tsiolkovsky equation, also known as the rocket equation, expressed as in Eq. 52, that gives the velocity boost that a rocket experiments when ejecting part of the propellant or also all of it. Depending on how much propellant is used, the value of M_d can change, but we are interested in the total boost, that is when all the propellant has been consumed, and so we used $M_d = M_{spacecraft}$.

$$\Delta v_{boost} = v_{ex} \ln \left(\frac{M_f}{M_d} \right) = I_{sp} g_0 \ln \left(\frac{M_d + M_{propellant}}{M_d} \right) \quad (52)$$

Inverting Eq. 52, we eventually find a relation that allows us to directly obtain a value for the propellant mass needed to perform a velocity increment Δv_{boost} , given a certain specific impulse I_{sp} :

$$M_{propellant} = M_d \exp \left(\frac{\Delta v_{boost}}{I_{sp} g_0} \right) - M_d. \quad (53)$$

This is the equation that we used in the following to give a first estimate of the propellant mass needed for different choices of propellant.

12.3.2 Propulsion System Selection

There is a variety of possible propellants for space crafts. Our selection was made on a series of parameters:

- TLR value (Technology Readiness Level) over 8;
- Specific Impulse over 150 N to reduce propellant mass (in case of chemical propellants);
- Low dimensions and mass of the engine.

Our choice was chemical propellant, which both satisfies the parameters above and also SC.02 (required Δv of 9.64 km/s). We selected the options with higher TLR levels: hydrazine and two green alternatives (1NHPGP and EPSSC1K).

Using Eq. 53, the calculation of the required propellant mass was done for each case. For each of them, a proposal for an engine is added. In **Table 61** a trade-off between the different propellants and related engines is shown.

It is clear that EPSSC1K has a great advantage in our mission with respect to the total propellant mass of the S/C. It will guarantee that requirements are satisfied: total Δv is reached, and we will be able to complete all orbital manoeuvres for the mission. The power consumption is limited to 15 Vdc. Also the cost is much lower for green alternatives with respect to hydrazine. On the other hand, these kinds of thrusters are small and each of them can provide only 0.3 N of thrust: we need a set of multiple components in the engine. This will increase the total cost of the propulsion system.

Table 61: Types of propellant and associated engine, with the specifics for each case.

TYPE	Green alternative	Green alternative	Hydrazine system
ENGINE	1NHPGP	EPSSC1K	LEROS1b
PROPELLENT	ADN	ADN	Hydrazine
COMPANY	Bradford Engineering	NanoAvionics	NAMMO
ENGINE MASS (kg)	1.52	3.74	4.5
THRUST (N)	0.25-1	0.3	0.5-30.7
SPECIFIC IMPULSE (s)	204-235	252	200-235
EXHAUST VELOCITY (km/s)	1.9	2.4	1.9
ENGINE DIMENSIONS (m)	0.17x0.1x0.1	0.1x0.1x0.2	0.64x0.25x0.25
PROPELLENT MASS (kg)	11652.16	4593.92	12841.42
TLR	9	9	9



(a) 1NHPGP thruster (ADN, green propellant).



(b) EPSSC1K thruster (ADN, green propellant).



(c) LEROS1b thruster (hydrazine).

Figure 43: Images of the three engines taken into consideration for the trade-off.

The 1NHPGP is less efficient in terms of exhaust velocity, and the total mass is higher. Moreover, its power consumption is around 40 Vdc, more than double with respect to EPSSC1K. However, the thrust of a single engine is 1 N: this will reduce the cost of the system, even if multiple thrusters will be required. LEROS1b was used in the mission Juno: it was chosen between the alternatives also because of its past missions history and its high reliability.

Even if the cost of hydrazine is higher per unit mass with respect to other propellants, it has a thrust per single engine up to 30 N: this will translate in a lower number of thrusters to operate in orbit. The total mass of propellant is higher with respect to other choices, and power consumption is around 35 Vdc.

A final trade-off on the engine is shown in **Table 62**.

Table 62: Trade-off between different engines.

ENGINE SYSTEM	1NHPGP	EPSSC1K	LEROS1b
Reliability	8	8	10
Mass/Volume	9	9	7
Thrust/Impulse	8	10	9
Design complexity	7	7	9
Operating Voltage	6	9	6
Cost	7	7	9
TOTAL	7.6	8.4	8.6

The trade-off is a weighted average with different importance for each parameter (weight from 0 to 5): reliability 5, mass and volume 3, thrust and impulse 3, complexity 2, power consumption 3 and cost 2. We wanted an engine as reliable as possible due to the long mission travel; also, mass and thrust were considered as first priorities in our selection. The best option appears to be LEROS1b, equipped with hydrazine. At the same time, if we consider a higher cost of the propellant, it is also possible to select a greener option, ADN: in this case, the EPSSC1K is a good solution with nearly the same properties as LEROS1b.

12.3.3 Propellant Tank Selection

Considering LEROS1b, fueled by hydrazine, we selected a 177 litres tank Model OST 31-1 already used by Ariane S/C, shown in **Figure 44**. Its properties are listed in **Figure 45**.



Figure 44: Hydrazine tank Model OST 31-1.

177 Litre Hydrazine Tank	
Volume (net)	177 litres
Propellant volume	132 litres (Blow down 4:1)
Propellants	Hydrazine (N2H4)
MEOP	24 bar
Proof pressure	36 bar (1.5 x MEOP)
Burst pressure	48 bar (2 x MEOP)
Mass	15 kg
Pressurant gas	Helium or nitrogen
Geometry	Spherical, elliptical domes with or without variable length cylindrical intersections
Interface fixation	Pole mounting, rigidly fixed at propellant port boss.
Materials	
- pressure vessel	Ti6Al4V STA (Hemisphere and Rings 3.7164.7)
- fluid ports	Ti6Al4V annealed (3.7164.1)
- PMD	All titanium
Heritage	Aeolus

Figure 45: Specifics of the hydrazine tank Model OST 31-1.

12.4 Results

The selected propulsion system is LEROS1b with multiple 177 liters tanks for hydrazine. The total amount of hydrazine required is 12481 kg, for a volume of 12 m³. This results in a total of nearly 73 tanks. In this case, we are not considering EOL: due to the additional amount of propellant for disposal, tanks will increase considering EOL.

The system selected can satisfy the initial requirements (**Table 63**).

Table 63: List of the requirements that will be satisfied.

REQUIREMENT	Satisfied	Comment
SC.1	Yes	The selected engine can perform all the manoeuvres required.
SC.2	Yes	Δv is reached by the engine.
SC.3	Yes	Orbit is maintained by the engine.
SC.4	No	Fuel required is high due to disposal: it is necessary to change disposal manoeuvre to solve the problem.

13 Conclusions

13.1 Final Mass and Power budget

In **Tables 64** and **65** we provide the total mass budget and power budget for the SPES mission, divided for each subsystem.

Table 64: Total mass budget for all subsystems, with the relative uncertainties. Propellant is not considered in the total.

Subsystem	Mass budget (kg)	Uncertainty (kg)	
PAYLOAD	21.966	± 0.046	Only preliminary design for XAO
ADCS	6.9	± 2.1	Low TRL of thrusters
THERMAL	1.24	± 0.37	30% of the value TRL not high for all components
CDHS	1.2	± 0.12	10% of the value of GR-VPX-GR740-SX
EPS	43.057	± 19.376	45% of the value Low TRL for RTG
COMMS	2.32	± 0.23	10% of the value High TRL
STRUCTURES	16.92	± 6.75	40% of the value
PROPELLUTION	4.5 (propellant: 12481)	± 1.8 (propellant: ± 5136)	40% of the value
TOTAL	98.103	± 30.792	

Table 65: Total power budget for all subsystems, with the relative uncertainties.

Subsystem	Power budget (W)	Uncertainty (W)	
PAYLOAD	70	± 24	Observation and Reading mode of the camera, low TRL of XAO
ADCS	23.4	<6	Low TRL of thrusters
THERMAL	-	-	No power consumption
CDHS	30	± 9	30% of the value of GR-VPX-GR740-SX
EPS	0.165	± 0.050	30% of the value PDU might be rescaled or not
COMMS	25	± 2.5	10% of the value High TRL
STRUCTURES	-	-	No power consumption
PROPELLUTION	-	-	No power consumption
TOTAL	148.565	± 41.550	

13.2 Compliance Check

The mission requirements were achieved as a combination of efficient choice of instruments, mission design and references for the respective subsystems. In this section, the compliance check of SPES is discussed based on overall scientific requirements explained in Section 4, and particularly focusing on how the payload accomplishes those scientific goals, thanks to the support of other subsystems.

The main objective of the payload is to use different instruments covering the main electromagnetic wave bands (radio, infrared, optical and ultraviolet) to achieve a comprehensive study of various components on Europa. The overall scientific requirements,

based on the objectives discussed in Section 2, are mostly satisfied by the design. Structures and activities on the surface, such as streaks and plumes, will be directly imaged by DragonEye Imager and/or traced by the spectra taken from SPUR, while the underneath ocean will be characterized with the measurements of XAO. Moreover, SPUR is designed as well for the detection of biological signals from the atmosphere, as discussed in Section 4.

The scientific instruments are supported by all other subsystems. Thanks to Orbital Design subsystem, the 4 days flyby period allows the s/c to acquire adequate science data. The Nadir duration is about 4 hours, during which SPUR and DragonEye Imager are able to make observations under different operation modes. In particular, even though the closest approach (a two-minute flyby between 25 km and 1043 km) is slightly lower than the expectations, since the exposure time can be significantly short and can be adjusted according to the altitudes as discussed in Section 4.3, it is possible for DragonEye to obtain sufficient high-resolution images focused on Europa’s surface. But in terms of SPUR, since the atmospheric components in which we are interested are more abundant at heights lower than 150 km, it could be problematic to provide high-significance spectral signals in such a short closest approach period.

ADCs also plays an important role in attitude control of all three scientific instruments. Because of the precise selection of reaction wheels, it is possible to stabilize all three axes even in the worst scenario of disturbance within Europa’s space environments, and therefore the blurring problems could be probably avoided. In addition, the thruster could be useful to change the orientation in a fast way.

Other subsystems will also be able to satisfy some of the fundamental mission requirements. For example, in CDHs, the state-to-art OBC will permit a strong computation capability in the data processing. The design of various operation modes will provide the best data collection strategy in different situations and will allow the RTG (proposed by EPS subsystem) to be always able to sustain the power requirements of the spacecraft. Propulsion and Orbital Design subsystems were able to produce a strategy adapt to reach Europa and perform the scientific phase as discussed before. Moreover, thanks to the high-level radiation shielding designed by the Structure subsystem and to the coating proposed by the Thermal Control subsystem, all instruments will be able to work within the harsh Jovian Magnetospheric environment in an optimal range of temperatures.

13.3 Future Improvements

In the next couple of years, further improvements could be made to SPES mission design:

- Our actual payload consists of a single narrow-angle camera, which is able to reach an extremely high spatial resolution, at the expense of a smaller field of view; one idea could be to include also a wide-angle camera to solve this issue, like many other missions have done in the past, including Europa Clipper. Clearly, this will add mass to our payload, so a trade-off between scientific return and mass and power budget will be needed. In addition, new technologies may arise in the next couple of years, from which our mission could benefit. For example, the development of a low-mass spectrometer with less stringent requirements on altitude may allow for a more flexible observational strategy;
- The use of star trackers instead of sun sensors as the main attitude sensors would bring some advancements. Star trackers are able to reach a pointing accuracy in the order of a few arcseconds, and they might be necessary if we decided, for

example, to increase the gain of the communication antenna. Clearly, they are more expensive than Sun sensors, but we think the benefits will be larger than the downside of increasing the cost budget;

- Even though a flyby approach was carried out to reduce the Δv budget to the minimum, a future improvement could be done by exploring pork chop plots to reduce uncertainties in launch opportunities, rather than relying only on JPL website. Moreover, we saw that the propellant requirement increases extensively due to the Δv needed for spacecraft disposal. As a future prospect, designing a more accurate End Of Life manoeuvre would have a massive influence on the Propulsion subsystem, giving the possibility to consider a much lower amount of fuel that would also lead to a strong redefinition of the final Structure design;
- We could adopt an Advanced Stirling Radioisotope Generator (ASRG) instead of the chosen e-MMRTG, even though it would be possible only after the release of such an RTG model in the market (refer to Section 10.3.4). By using an ASRG, the generated power degradation would decrease (since the efficiency would be around 25%) and the power source would be able to sustain the full operations of the payload for more years, without needing to use the Nominal sub-modes;
- In the process of choosing the microprocessor for SPES we could search for other less costly possibilities and less power demanding. Describing a more detailed architecture of how OBC is connected to other subsystems, Data storage, and Memory could be some further improvements;
- Since they have the same astronomical target and considering the small dimension of our spacecraft, SPES could be coupled to Europa Clipper mission for the launch and the interplanetary journey to reach Europa, making SPES payload a sort of "auxiliary payload" for Europa Clipper. This would allow this mission to spare more or less ~ 6 km/s from the total Δv budget (**Table 25**) and it would reduce a lot the propellant requirements for the SPES mission, making also less problematic the high value of Δv found for the End Of Life maneuver;
- Last but not least, we must mention the fact that some subsystems were not taken into account in the scope of this project but they have their own importance for the SPES mission to be considered a complete mission. One example is the navigation subsystem, which is very important to tell how the spacecraft is going to be oriented to the desired destination and it would also be needed to describe the changes in velocity, obtained through the manipulation of the forces, needed to arrive at our target. Additionally, it would also give information on the position of the spacecraft as a function of time. Navigation to and around Europa is a challenging task for several reasons and all of them should be taken into account while design the Navigation subsystem.

Creating a ground station architecture with telemetry, tracking, and command interface with the spacecraft is another important aspect missing in this mission design.

All in all, the proposed solutions must be worked on more in detail to see if they are actually feasible and how the performances of SPES would change in each of those cases, but this could be done in the future steps of the mission design.

13.4 Considerations on the Design Process

Excellent teamwork was carried out between the subsystems, as well as the division of work within each subsystem itself.

However, one of the main difficulties of the mission design was related in particular to Propulsion and Structures subsystems: in fact, for these two the time constraints were very strict, and this necessarily led to a first-order analysis and to results that are mainly strong approximations with respect to what would be needed for the mission. Even if having more time could have led to more precise results, both subsystems were nonetheless able to provide the main elements needed for a complete mission proposal. Another important problem that was encountered was instead related to the total dry mass of the SPES mission, a fundamental value needed by Structures team to be able to carry on a satisfying design. Since every subsystem was clearly able to provide its mass budget only at a later stage of the work, Structures team had at its disposal a limited time to create a proper structure design for the spacecraft.

In a similar way, also CDHs subsystem faced some difficulties in calculating the Housekeeping Data and Data Rate for the downlink which needed information on the data rate from other subsystems and it wasn't a priority for each one of them so couldn't provide, so we decided to take the 10 percent of the Payload Data as the Housekeeping Data.

In general, the conceptual design process was unclear at first to most of the subsystems. There was a time delay in exchanging information and requirements between different subsystems due to the focus on searching for precise values and many tedious trial-and-error strategies.

In the process of learning, considerations about error margin and references aided the mission design and its further development. Indeed, after this initial stall, all subsystems started developing their design considering error margins and looking for values taken from references from previous (or future) missions that had similar objectives. In this way, we were able to move forward with the development of each subsystem, providing gradually more and more accurate values, that brought us to the current state of design.

14 References

- [1] Nasa's europa clipper, Jun 2014.
- [2] Europa-UVS in Instruments. <https://europa.nasa.gov/spacecraft/europa-uvs>.
- [3] Michael J. Russell, Alison E. Murray, and Kevin P. Hand. The Possible Emergence of Life and Differentiation of a Shallow Biosphere on Irradiated Icy Worlds: The Example of Europa. *Astrobiology*, 17(12):1265–1273, December 2017.
- [4] Blue Canyon reaction wheels. <https://www.bluecanyontech.com/datasheet/>.
- [5] 1N HPGP thruster datasheet. <https://www.ecaps.space/products-1n.php>.
- [6] NSS sun sensors. <https://www.newspacesystems.com/NewSpace-Sun-Sensor>.
- [7] IMU datasheet. <https://satsearch.co/products/GS-IMU3000TA>.
- [8] W.J. Larson and A.V. Wertz. *Space Mission Analysis and Design*. Springer, 2013.
- [9] S.W. Angrist. *Direct Energy Conversion: 4th edition*. Allyn & Bacon, 1982.
- [10] NSS reaction wheels. <https://www.newspacesystems.com/Reaction-Wheel>.
- [11] RedWire sun sensor. <https://redwirespace.com/CSS-pyramid>.
- [12] CubeSpace sun sensor. <https://www.cubespace.co.za/sensors/cubesense/>.
- [13] Bradford Engineering sun sensor. <https://squarespace.com/be-datasheet-fss>.
- [14] Theresa Kowalkowski, Jennie Johannessen, and Try Lam. Launch period development for the juno mission to jupiter, 08 2008.
- [15] Brent Buffington, Stefano Campagnola, and Anastassios Petropoulos. EUROPA multiple-flyby trajectory design. <https://hdl.handle.net/ec2012>, 2012.
- [16] Miniature Satellite Energy-Regulating datasheet. <https://satsearch.co/MiSER>.
- [17] Series 44 Temperature Probes. <https://www.scinstruments.com/series-44>.
- [18] Power Distribution Unit for large nanosatellites. <https://gomspace.com/shop/subsystems/power/nanopower-p60.aspx>.
- [19] Jennifer Harbaugh. Space launch system reference guide, Mar 2022.
- [20] SpaceX. Falcon user's guide - spacex, 2021.
- [21] Galileo - jupiter missions - nasa jet propulsion laboratory.
- [22] Information@eso.org. Esa/hubble space telescope.
- [23] B.D. Teolis, D.Y. Wyrrick, A. Bouquet, B.A. Magee, and J.H. Waite. Plume and surface feature structure and compositional effects on europa's global exosphere: Preliminary europa mission predictions. *Icarus*, 284:18–29, 2017.

- [24] Christopher F. Chyba and Cynthia B. Phillips. Possible ecosystems and the search for life on europa. *Proceedings of the National Academy of Sciences*, 98(3):801–804, 2001.
- [25] Mark A. Sephton, Jack Hunter Waite, and Tim G. Brockwell. How to detect life on icy moons. *Astrobiology*, 18(7):843–855, 2018. PMID: 30035638.
- [26] Ronald Greeley, Robert Sullivan, James Klemaszewski, Kim Homan, James W. Head, Robert T. Pappalardo, Joseph Veverka, Beth E. Clark, Torrence V. Johnson, Kenneth P. Klaasen, Michael Belton, Jeffrey Moore, Erik Asphaug, Michael H. Carr, Gerhard Neukum, Tilmann Denk, Clark R. Chapman, Carl B. Pilcher, Paul E. Geissler, R. Greenberg, and R. Tufts. Europa: Initial galileo geological observations. *Icarus*, 135(1):4–24, 1998.
- [27] Ronald Greeley. Geology of europa - laboratory for atmospheric and space physics, Aug 2015.
- [28] Brent Buffington. Trajectory design for the europa clipper mission concept. *AIAA/AAS Astrodynamics Specialist Conference 2014*, 01 2014.
- [29] Louise M. Prockter, James W. Head, Robert T. Pappalardo, Robert J. Sullivan, Amy E. Clifton, Bernd Giese, Roland Wagner, and Gerhard Neukum. Morphology of Europan bands at high resolution: A mid-ocean ridge-type rift mechanism. *Journal of Geophysical Research (Planets)*, 107(E5):5028, May 2002.
- [30] Are Water Plumes Spraying from Europa? NASA’s Europa Clipper is on the Case. <https://www.nasa.gov/feature/goddard/2021>.
- [31] T. A. Cassidy, R. E. Johnson, and O. J. Tucker. Trace constituents of Europa’s atmosphere. *Icarus*, 201(1):182–190, May 2009.
- [32] M. Volwerk, M. G. Kivelson, and K. K. Khurana. Wave activity in Europa’s wake: Implications for ion pickup. *JGR*, 106(A11):26033–26048, November 2001.
- [33] Gravity and Radio Science on Europa Clipper. <https://gravity-radio-science/>.
- [34] Dragoneye Imager datasheet. <https://dragonflyaerospace.com/dragoneye/>.
- [35] Raptor Imager datasheet. <https://dragonflyaerospace.com//raptor/>.
- [36] M. Blton, J. W. Head, C. Chapman, K. Klasen, C. Anger, M. Carr, A. McEwen, C. Pieters, M. Davies, R. Greeley, R. Greenberg, G. Neukum, C. Pilcher, J. Veverka, F. Fanale, A. Ingersoll, J. Pollack, P. Gierash, and Mo. The Galileo Solid State Imaging Experiment and Performance of the Camera at Earth-Moon Encounter. In *Lunar and Planetary Science Conference*, volume 22 of *Lunar and Planetary Science Conference*, page 83, March 1991.
- [37] Jean-Loup Bertaux, Oleg Korablev, Séverine Perrier, Eric Quémerais, Franck Montmessin, F. Leblanc, S. Lebonnois, P. Rannou, F. Lefèvre, F. Forget, A. Fedorova, E. Dimarellis, A. Reberac, D. Fonteyn, J. Y. Chaufray, and S. Guibert. SPICAM on Mars Express: Observing modes and overview of UV spectrometer data and scientific results. *Journal of Geophysical Research: Planets*, 111, October 2006.

- [38] Instruments | Spacecraft. <https://europa.nasa.gov/spacecraft/instruments>.
- [39] Archive information of SPICAM. <https://archives.esac.esa.int/psa/ftp/MARS-EXPRESS/SPICAM/MEX-M-SPI-2-IREDR-RAWXMARS-EXT1-V2.0/CATALOG/INST.CAT>.
- [40] Todd Bayer, Molly Bittner, Brent Buffington, Gregory Dubos, Eric Ferguson, Ian Harris, Maddalena Jackson, Gene Lee, Kari Lewis, Jason Kastner, Ron Morillo, Ramiro Perez, Mana Salami, Joel Signorelli, Oleg Sindiy, Brett Smith, Melissa Soriano, Karen Kirby, and Nori Laslo. Europa Clipper Mission: Preliminary Design Report. In *2019 IEEE Aerospace Conference*, pages 1–24, Big Sky, MT, USA, March 2019. IEEE.
- [41] L. Iorio. A possible new test of general relativity with Juno. *Classical and Quantum Gravity*, 30(19):195011, October 2013.
- [42] Juno Status Report. <https://www.nasa.gov/mission-pages/juno/news/>.
- [43] Yuto Takei, Tomoaki Toda, Atsushi Fujii, Hiroshi Takeuchi, Takahiro Yamada, Tadateru Takahashi, Takanao Saiki, and Yuichi Tsuda. Utilization of Ka-band Communication for Hayabusa2 Asteroid Proximity Operation. *Transactions of the Japan Society of Aeronautical and Space Sciences, Aerospace Technology Japan*, 18(3):116–122, January 2020.
- [44] Mark Hughes. An Introduction to Antenna Basics. *All About Circuits*, 2016.
- [45] Arif Karabeyoglu. Aa284a advanced rocket propulsion - lecture 7: Launch trajectories. <https://web.stanford.edu/cantwell/advanced-rocket-propulsion-2019>, Oct 2019.
- [46] Hirokawa Jiro. Honeycomb-structured weight-saving high gain planar antennas installed on hayabusa2, 2014.
- [47] David D Morabito. Deep-space ka-band flight experience. *The Interplanetary Network Progress Report*, 42:211, 2017.
- [48] Stephen D Slobin. Atmospheric and environmental effects. *DSN Telecommunications Link Design Handbook*, pages 810–005, 2002.
- [49] Stephen D Slobin and T Pham. 34-m bwg stations telecommunications interfaces,”. *DSN Telecommunications Link Design Handbook*, pages 810–005, 2010.
- [50] Todd J Bayer. In-flight anomalies and lessons learned from the mars reconnaissance orbiter mission. In *2008 IEEE Aerospace Conference*, pages 1–13. IEEE, 2008.
- [51] Yuto Takei, Tomoaki Toda, Atsushi Fujii, Hiroshi Takeuchi, Takahiro Yamada, Tadateru Takahashi, Takanao Saiki, and Yuichi Tsuda. Utilization of ka-band communication for hayabusa2 asteroid proximity operation. *TRANSACTIONS OF THE JAPAN SOCIETY FOR AERONAUTICAL AND SPACE SCIENCES, AEROSPACE TECHNOLOGY JAPAN*, 18(3):116–122, 2020.
- [52] Thermal Control. <https://www.nasa.gov/thermal-control>.
- [53] Earth fact sheet. <https://nssdc.gsfc.nasa.gov/earthfact>.

- [54] Jupiter fact sheet. <https://nssdc.gsfc.nasa.gov/jupiterfact>.
- [55] Solar system temperatures. <https://solarsystem.nasa.gov/temperatures/>.
- [56] Europa fact sheet. <https://www2.jpl.nasa.gov/galileo/europa/>.
- [57] Yosef Ashkenazy. The surface temperature of Europa. *Heliyon*, 5(6), 2019.
- [58] John H. Henninger. Solar Absorptance and Thermal Emittance of Some Common Spacecraft Thermal-Control Coatings. <https://www.nasa.gov/19840015630/>.
- [59] Kuan-Lin Lee, Calin Tarau, William G. Anderson, and Derek Beard. Titanium-Water Heat Pipe Radiators for Space Fission Power System Thermal Management. *Microgravity Science and Technology*, 32(3):453–464, March 2020.
- [60] Jan Andersson, Magnus Hjorth, Fredrik Johansson, and Sandi Habinc. LEON Processor Devices for Space Missions: First 20 Years of LEON in Space. In *2017 6th International Conference on Space Mission Challenges for Information Technology (SMC-IT)*, pages 136–141, Alcala de Henares, September 2017. IEEE.
- [61] GR740 Development Board GR-VPX-GR740. <https://www.gaisler.com/index.php/products/boards/gr-vpx-gr740>.
- [62] Todd Bayer, Molly Bittner, Brent Buffington, Gregory Dubos, Eric Ferguson, Ian Harris, M. Jackson, Gene Lee, Kari Lewis, Jason Kastner, Ron Morillo, Ramiro Perez, Mana Salami, Joel Signorelli, Oleg Sindiy, Brett Smith, Melissa Soriano, Karen Kirby, and Nori Laslo. Europa clipper mission: Preliminary design report, 03 2019.
- [63] Lucas Antunes Tambara. GR740 Radiation Summary.
- [64] John E. Westfall. Timing the eclipses of Jupiter’s Galilean satellites. <https://alpo-astronomy.org/jupiter/GaliInstr.pdf>.
- [65] Multi-Mission Radioisotope Thermoelectric Generator (MMRTG). https://mars.nasa.gov/internal_resources/788/.
- [66] June F. Zakrajsek, Dave F. Woerner, Dirk Cairns-Gallimore, Stephen G. Johnson, and Louis Qualls. Nasa’s radioisotope power systems planning and potential future systems overview. In *2016 IEEE Aerospace Conference*, pages 1–10, 2016.
- [67] Advanced Stirling Radioisotope Generator (ASRG). https://rps.nasa.gov/system/downloadable_items/36_APP_ASRG_Fact_Sheet_v3_9-3-13.pdf.
- [68] Enhanced Multi-Mission Radioisotope Thermoelectric Generator (e-MMRTG). <https://rps.nasa.gov/resources/enhanced-MMRTG>.
- [69] Alexandra Witze. Europa’s peek-a-boo plumes confirmed. *Nature*, September 2016.
- [70] Mars Express orbiter instruments. https://www.esa.int/Science_Exploration/Space_Science/Mars_Express/Mars_Express_orbiter_instruments.
- [71] F Leblanc, T A Cassidy, R E Johnson, M Marconi, A Hendrix, and M Wong. Atmospheres of Europa and Ganymede.

- [72] S. Cervantes and J. Saur. Constraining Europa’s Subsolar Atmosphere With a Joint Analysis of HST Spectral Images and Galileo Magnetic Field Data. *Journal of Geophysical Research: Space Physics*, 127(9):e2022JA030472, 2022. _eprint: <https://onlinelibrary.wiley.com/doi/pdf/10.1029/2022JA030472>.
- [73] SPICAM on Mars Express: A 10 year in-depth survey of the Martian atmosphere | Elsevier Enhanced Reader.
- [74] Magnus Själander, Sandi Habinc, and Jiri Gaisler. LEON4: Fourth Generation of the LEON Processor.
- [75] H. U. Keller, C. Barbieri, P. Lamy, H. Rickman, R. Rodrigo, K.-P. Wenzel, H. Sierks, M. F. A’Hearn, F. Angrilli, M. Angulo, M. E. Bailey, P. Barthol, M. A. Barucci, J.-L. Bertaux, G. Bianchini, J.-L. Boit, V. Brown, J. A. Burns, I. Büttner, J. M. Castro, G. Cremonese, W. Curdt, V. Da Deppo, S. Debei, M. De Cecco, K. Dohlen, S. Fornasier, M. Fulle, D. Germerott, F. Gliem, G. P. Guizzo, S. F. Hviid, W.-H. Ip, L. Jorda, D. Koschny, J. R. Kramm, E. Kührt, M. Küppers, L. M. Lara, A. Llebaria, A. López, A. López-Jimenez, J. López-Moreno, R. Meller, H. Michalik, M. D. Michelena, R. Müller, G. Naletto, A. Origné, G. Parzianello, M. Pertile, C. Quintana, R. Ragazzoni, P. Ramous, K.-U. Reiche, M. Reina, J. Rodríguez, G. Rousset, L. Sabau, A. Sanz, J.-P. Sivan, K. Stöckner, J. Tabero, U. Telljohann, N. Thomas, V. Timon, G. Tomasch, T. Wittrock, and M. Zaccariotto. OSIRIS – The Scientific Camera System Onboard Rosetta. *Space Science Reviews*, 128(1-4):433–506, February 2007.
- [76] Christina Plainaki. The Jovian Energetic Ion Environment of Ganymede: Planetary Space Weather Considerations in View of the JUICE Mission. *The Astrophysical Journal*, 2022.
- [77] D. Blaney, The MISE Science Team, and The MISE Engineering Team. The Mapping Imaging Spectrometer for Europa: Science and Instrument Status. *Bulletin of the AAS*, 52(6), oct 26 2020. <https://baas.aas.org/pub/2020n6i106p04>.
- [78] SD Slobin. 101, rev. c. 70-m subnet telecommunications interfaces [r/ol]. dsn telecommunications link design handbook, california. *CIT*, pages 810–005, 2009.
- [79] Stephen D Slobin and TT Phan. 34-m hef subnet telecommunications interfaces. *DSN Telecommunications Link Design Handbook*, pages 810–005, 2008.